UNIVERSITÄT KONSTANZ
UNIVERSITY OF UTAH

Fachbereich Biologie
Department of Biology

DIPLOMA THESIS

Genetic Structure and Function Analysis of the Conserved Integral Membrane Components (FliOPQR) of the Flagellar Type III Secretion Apparatus of *Salmonella enterica*

MARC ERHARDT

20th December, 2006

Supervisors
Prof. Dr. WINFRIED BOOS
Prof. KELLY T. HUGHES, Ph.D.

UNIVERSITÄT KONSTANZ
Fachbereich Biologie
78457 Konstanz

TABLE OF CONTENTS

LIST OF FIGURES

LIST OF TABLES

ABSTRACT

Bacteria swim in liquid environment by rotation of an unique nanomachine, the flagellum. For assembly of the flagellum, a flagellar-specific type III secretion apparatus is essential. The conserved integral membrane components FliOPQR of *Salmonella enterica* serovar Typhimurium were previously proposed to be part of the type III secretion apparatus. It has been previously shown that FliOPQR are essential for export of flagellar substrates. However, virtually nothing is known about the function and localization of the proteins.

The first part of this work reports the growth and purification of the bacteriophage χ, who only attacks motile bacteria. Furthermore, the virulence of phage χ in *S. typhimurium* strains expressing antigenically distinct flagellin variants is examined. Afterwards, the construction of tetracycline resistance cassette insertions, as well as the construction of clean deletions of *fliOPQR* is described. It is shown in this chapter that *fliO, fliP, fliQ* and *fliR* are required for motility and that a clean deletion of each gene can be complemented by introduction of the respective wildtype gene.

The next part of this work reports conserved domains and topology predictions of FliOPQR based on a homology search. Afterwards, the topology prediction is confirmed by construction of C-terminal β-galactosidase and alkaline phosphatase fusion proteins. Non-motile *fliO* and *fliP* mutants are examined by DNA sequencing analysis and subsequently motile revertant mutants of the revealed *fliO* point mutations (V72G and L91R) are isolated and characterized. In addition, a C-terminal YPF (yellow fluorescent protein) fusion to FliO is constructed and the localization of the FliO-YFP fusion construct is analyzed by fluorescence microscopy. It is found that FliO is probably not localized within the flagellar basal body structure, contrary to previous suggestions. The construction of a *S. typhimurium* strain, chromosomally expressing FliM-CFP (cyan fluorescent protein) as well as FliO-YFP constructs, confirms this finding by the observation that FliM-CFP and FliO-YFP are not co-

localized.

In the last part of this work the energization of flagellar type III secretion is analyzed. The flagellar type III secretion apparatus transports most proteins necessary for the assembly of the flagellum across the inner membrane in an ATP-dependent manner. This work shows that flagellar type III secretion is also dependent on the proton motive force. Abolishment of both the proton gradient ΔpH and the membrane potential $\Delta\Psi$ using the ionophore carbonyl cyanide m-chlorophenylhydrazone (CCCP), prevented secretion of the anti-σ^{28} factor FlgM. Secretion of FlgM could be restored by growth in medium lacking CCCP. Furthermore, it is shown that the secretion of FlgM is inhibited at pH 5 in the presence of 34 mM acetate, indicating an important role of the proton gradient ΔpH and/or the intracellular proton concentration. Addition of the ionophore CCCP resulted in an immediate growth arrest, but not in a significant decrease of cytoplasmic ATP levels, thus demonstrating that both the flagellar type III secretion ATPase FliI and the proton motive force are necessary for the export of flagellar type III secretion substrates.

DEUTSCHE ZUSAMMENFASSUNG

Bakterien schwimmen in wässriger Umgebung durch Rotation einer einzigartigen Nanomaschine, dem Flagellum. Für den Aufbau des Flagellums ist ein Flagellum-spezifischer Typ III Sekretionsapparat notwendig. Als Bestandteil dieses Typ III Sekretionssystems von *Salmonella enterica* serovar Typhimurium, wurden die konservierten Membranproteine FliOPQR vorgeschlagen. Es wurde von anderen Arbeitsgruppen gezeigt, dass die Proteine FliOPQR in der Tat für den Export von Bausteinen des Flagellums notwendig sind. Über die Funktion, Arbeitsweise und zelluläre Lokalisation der Proteine ist aber fast nichts bekannt.

Diese Arbeit beschreibt im ersten Teil die Aufzucht und die Reinigung des Bakteriophagen χ, welcher nur motile Bakterien befällt. Des Weiteren wird die Virulenz des Phagen χ bei *S. typhimurium* Stämmen untersucht, die unterschiedliche Varianten des Flagellin-Proteins exprimieren. Im Nachfolgenden Abschnitt wird einerseits die Konstruktion von FliOPQR Mutanten, die eine Tetrazyklin-Resistenzkassette inseriert haben, und ausserdem die Konstruktion von chromosomalen Deletionsmutanten von FliOPQR, beschrieben. In diesem Abschnitt wird gezeigt, dass jedes der Gene, *fliO, fliP, fliQ* als auch *fliR*, für die Motilität von *S. typhimurium* nötig ist und dass die chromosomalen Deletionsmutanten von den jeweiligen Wildtyp-Genen komplementiert werden können.

Im nächsten Teil dieser Arbeit werden konservierte Domänen und Topologie-Vorhersagen der Proteine FliOPQR, basierend auf einer Homologiesuche, besprochen. Anschließend wird die Topologie-Vorhersage durch die Konstruktion C-terminaler Fusionen von β-Galaktosidase, als auch alkalischer Phosphatase, an FliOPQR bestätigt. Des weiteren wird die DNA-Sequenz von nicht motilen *fliO* und *fliP* Mutanten ermittelt. Nachfolgend werden motile Suppressionsmutanten

zweier gefundener Punktmutationen von *fliO* (V72G und L91R) isoliert und charakterisiert. Im darauf folgenden Abschnitt wird die Konstruktion von YFP (gelbes, fluoreszierendes Protein) an den C-Terminus von FliO beschrieben und die zelluläre Lokalisation von FliO-YFP wird mit Hilfe von Fluoreszenzmikroskopie untersucht. Es wird gezeigt, dass FliO wahrscheinlich nicht innerhalb des flagellaren Basalkörpers lokalisiert ist. Zur Bestätigung dieses Ergebnisses wird ein *S. typhimurium* Stamms konstruiert, welcher die Fusionsproteine FliM-CFP (blaues, fluoreszierendes Protein) und FliO-YFP auf chromosomaler Ebene exprimiert. Durch fluoreszenzmirkoskopische Experimente wird in diesem Stamm gezeigt, dass die Fusionsproteine nicht kolokalisiert sind.

Der letzte Teil dieser Arbeit beschäftigt sich mit der Energetisierung der Sekretion von Proteinen durch den Flagellum-spezifischen Typ III Sekretionsapparat. Das Typ III Sekretionssystem des Flagellums transportiert die meisten Proteine, die für den Aufbau des Flagellums benötigt werden, über die innere Bakterienmembran in einer von der Hydrolyse von ATP abhängigen Art- und Weise. Diese Arbeit zeigt, dass das Typ III Sekretionssystem des Flagellums zusätzlich von dem Protonengradienten ΔpH und dem Membranpotential $\Delta\Psi$ abhängig ist. Sowohl der Protonengradient als auch das Membranpotential wird durch Carbonylcyanid m-Chlorphenylhydrazon (CCCP) abgebaut, worauf die Sekretion des anti-σ^{28} Faktors FlgM gehemmt wird. Es wird gezeigt, dass die Sekretion von FlgM durch Wachstum in Medium ohne CCCP wiederhergestellt werden kann. Ausserdem wird die Sekretion von FlgM durch Zugabe von 34 mM Acetat bei pH 5 gehemmt. Dieses Ergebnis deutet darauf hin, dass der Protonengradienten ΔpH und / oder die cytoplasmatische Protonenkonzentration eine herausragende Role bei der Energetisierung der Typ III Sekretion spielt. Die Zugabe von CCCP führte zu einem augenblicklichen Wachstumsarrest, allerdings wurde keine signifikante Abnahme des cytoplasmatischen ATP Spiegels festgestellt. Diese Ergebnisse demonstrieren, dass sowohl die ATPase FliI des Typ III Sekretionssystems des Flagellum als auch der Protonengradient und das Membranpotential, für den Transport von Substraten durch das Typ III Sekretionssystems des bakteriellen Flagellums notwendig sind.

ACKNOWLEDGMENTS

Most of all I would like to express my gratitude to my research advisors and collegues, Professor Kelly T. Hughes and Fabienne F. C. Chevance of the University of Utah in Salt Lake City. They are not only great scientists, but also and most importantly wonderful persons, and I am most grateful for having had the opportunity to meet and work with them.

I am also deeply indebted to my supervisor Professor Dr. Winfried Boos of the Universität Konstanz, who helped me in numerous questions throughout my studies and provided me with the unique opportunity to do my diploma thesis at Kelly Hughes' lab at the University of Utah.

I warmly thank Koushik Paul, Mayukh Sarkar and Professor David F. Blair, our collaborators in the "world of FliOPQR", for valuable advice and help. The interesting discussions have been very helpful for my research.

I also thank Professor Stan Williams for his help and kind permission for using the luminometer.

Many thanks to the members of the Hughes' lab, Kelly Winterberg, Chris Wozniak, Takanori Hirano, Hee-Jung Lee and Yichu Su for introducing me in the lab and everything else, and also to Lory Mattucci for her kind help with all my questions and for organizing my visa for the United States.

Special thanks to Stefanie Bürger and Hanna Singer for critically reading the manuscript.

I also gratefully acknowledge fellowship support from the "Studienstiftung des deutschen Volkes", who supported my studies in Germany and my stay at the University of Utah in Salt Lake City.

I dedicate this work to Hanna Singer, who loves me like I am, and to my parents Roland and Brigitte Erhardt, who always supported me in every aspect of my studies.

"I must say, for my part, that no more pleasant sight has ever yet come before my eye than these many thousands of living creatures, seen all alive in a little drop of water, moving among one another, each several creature having its own proper motion." [a]

[a] Antony van Leeuwenhoek, 1676

1 INTRODUCTION

Bacteria swim in their environment by rotating a rigid, helical filament, the flagellum (Berg and Anderson (11)). The flagellum is a sophisticated molecular nanomachine made of about 25 different proteins (Berg (10), Kojima and Blair (37), Macnab (43), Namba and Vonderviszt (60)). The structure of the flagellum can be divided in three parts: a basal body as the rotary motor (Berg and Anderson (11), Silverman and Simon (73)); a flexible hook that couples the rotary motor to the third component, the rigid filament (DePamphilis and Adler (20, 21)). The filament is about 10 to 15 μm long, yet only 120 - 200 nm in diameter and the rotary machine turns at hundreds of revolutions per second, utilizing both the membrane potential $\Delta\Psi$ and the proton gradient ΔpH (Manson *et al.* (50), Matsuura *et al.* (51)).

The enteric bacteria *Salmonella enterica* serovar Typhimurium (*S. typhimurium*) and *Escherichia coli* (*E. coli*) possess essentially identical chemotaxis systems, which enable the cells to detect and respond to chemical attractants and repellents in their environment (Adler and Templeton (1)). For swimming up or down a concentration gradient of attractants or repellents respectively, *S. typhimurium* and *E. coli* alternate their swimming pattern between "run" and "tumble" phases by changing the rotational direction of the flagellum (Larsen *et al.* (39), Silverman and Simon (73)). Rotation of the flagellum in a counter-clockwise direction results in the formation of a bundle of several flagellar filaments with a left-handed helical shape, which propels the cell during the "run" phase in a constant direction. The reversal of the rotational direction of the flagellum during the "tumble" phase produces a twisting force that changes the left-handed helical shape of the filament to a right-handed helical shape, which causes the bundle to fall apart. During the "tumble" phase the cell stays in place, while changing its spatial orientation (Larsen *et al.* (39)). It is important to note that the chemotaxis system of bacteria sense spatial attractant

or repellent gradients as a temporal gradient by using periodic comparisons of the concentrations of the respective chemical stimulus (Macnab and Koshland (46)).

1.1 Structure and assembly of the bacterial flagellum

Salmonella typhimurium produces approximately 6 to 10 peritrichous flagella per cell (Macnab (44)). As mentioned above, the structure of the bacterial flagellum can be divided in three parts; a basal body spanning from the cytoplasm to the outer membrane, a flexible hook and the filament. An overview of the flagellum structure is given in Figure 1.1.

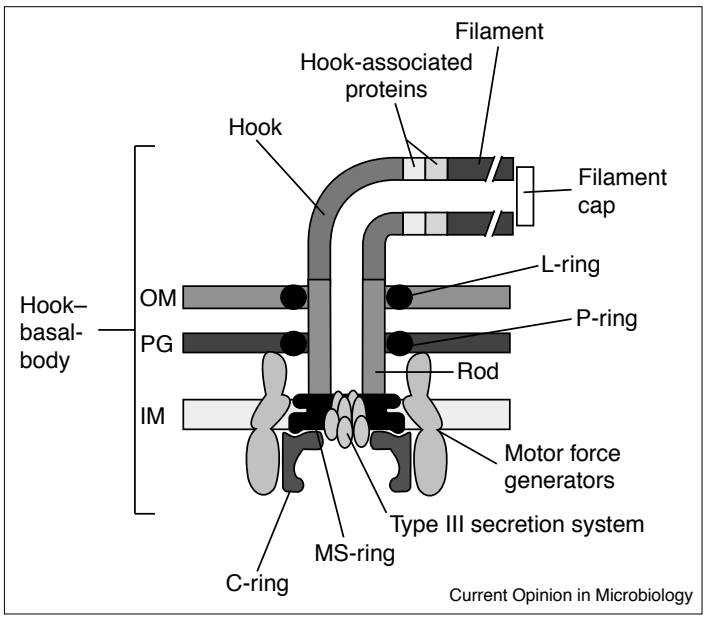

FIGURE 1.1: Schematic overview of the bacterial flagellum (figure adapted from Aldridge and Hughes (3)). The flagellum structure can be divided in three parts: 1) a basal body with the MS-ring in the inner membrane (IM), the cytoplasmic C-ring, the P-ring in the peptidoglycan layer (PG), the L-ring in the outer membrane (OM), the rod spanning the periplasmic space and the type III secretion apparatus attached to the cytoplasmic face of the MS-ring; 2) a flexible hook with hook-associated proteins (HAPs); 3) the rigid filament and the filament cap. The basal body and the hook can be combined to the hook-basal-body complex (HBB) as displayed in the figure. The HBB structure interacts with the motor force generators, which enables the rotation of the flagellum by utilizing the proton motive force.

Flagellum assembly initiates with the formation of the MS-ring (consisting of FliF) in the inner membrane, followed by attachment of the rotor/switch complex (FliG and C-ring proteins FliM and FliN) at the cytoplasmic face of the MS-ring. Upon completion of the C-ring, the motor proteins MotA and MotB are assembled in the inner membrane. The motor proteins MotA and MotB form the stator and attach non-covalently to the peptidoglycan layer, whereas the rotor (FliG) is non-covalently attached to the MS-ring. Together the stator and the rotor form the flagellar motor, whose rotation is energized by the proton motive force (Macnab (43)). Afterwards, the flagellar-specific type III secretion (T3S) apparatus (FlhA, FlhB, FliH, FliI, FliJ, FliO, FliP, FliQ, FliR) assembles within the MS-ring at the basis of the basal body (Aizawa (2)), facilitating the export of most extra cytoplasmic components of the flagellum. Subsequently the rod components FlgB, FlgC, FlgF, FliE (proximal rod) and FlgG (distal rod) are secreted by the type III secretion apparatus and progressively assembled (Minamino *et al.* (58)). The P-ring protein FlgI and the L-ring lipoprotein FlgH are probably exported by the Sec-dependent pathway (Homma *et al.* (32)) and therefore the assembly of the periplasmic P-ring and the L-ring in the outer membrane is independent of the construction of preceding flagellar components. Upon completion of the rings and the rod, the hook (consisting of FlgE) is assembled to an approximate length of 55 nm (Hirano *et al.* (30)). The last steps of flagellum assembly include secretion of the anti-σ^{28} factor FlgM (Hughes *et al.* (34)), which results in σ^{28}-dependent expression of flagellar genes that are under Class III promotor regulation, and the assembly of the hook-associated proteins FlgK, FlgL and FliD (Homma *et al.* (31)). Subsequently, the filament is constructed as the last structural component of the flagellum, whereas the subunits FliC and FljB (flagellin) are assembled at the distal end of the growing filament. A single filament can be constructed of as many as 20,000 flagellin subunits (Macnab (43)), which represents a significant amount of the total protein mass of the cell.

1.2 The flagellar type III secretion apparatus

The flagellar-specific type III secretion (T3S) apparatus is believed to assemble within the MS-ring at the basis of the flagellar basal body and consists of six integral membrane proteins (FlhA, FlhB, FliO, FliP, FliQ, FliR) and three cytoplasmic proteins (FliH, FliI, FliJ) (Minamino and Macnab (56)), which are essential for the export of rod-type, hook-type and filament-type secretion substrates (Minamino and Macnab (56)). A schematic of the flagellar-specific type III secretion apparatus is displayed in Figure 1.2.

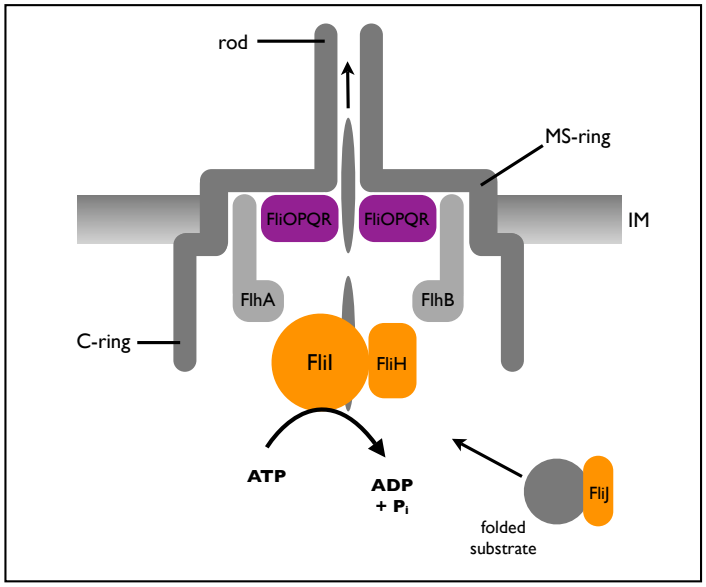

FIGURE 1.2: Schematic of the flagellar type III secretion apparatus. FlhA, FlhB, FliO, FliP, FliQ and FliR are integral membrane components. FliI, the flagellar-specific ATPase, FliH, the regulator of FliI and FliJ, a general chaperone, are soluble proteins. The flagellar type III secretion apparatus is believed to assemble within the MS-ring at the cytoplasmic face of the flagellar basal body. The secretion is ATP dependent and the substrates have to be secreted in an unfolded state through a narrow channel of about 2.0 nm in diameter (Fan and Macnab (22), Yonekura *et al.* (87)). ATP = adenosine 5'-triphosphate; ADP = adenosine 5'-diphosphate; P_i = inorganic phosphate; IM = inner membrane.

The integral membrane components FliOPQR are relatively small (FliO = 13.08 kDa; FliP = 26.79 kDa; FliQ = 9.60 kDa; FliR = 28.93 kDa) and are predicted to have 1

to 8 membrane spanning helices. Nothing is known about possible functions of FliO, FliP, FliQ and FliR respectively. FlhA and FlhB are much larger integral membrane proteins (75 kDa and 42 kDa respectively) and also have large cytoplasmic domains, where the proteins interact with the soluble components of the type III secretion apparatus, FliH, FliI and FliJ (Minamino and MacNab (57)). FlhB is furthermore controlling the switch of substrate specificity to export late structural subunits upon completion of early flagellar structures (Ferris and Minamino (25)).

The secretion of flagellar substrates is dependent on ATP (adenosine triphosphate) hydrolysis, which is catalyzed by the ATPase FliI as shown by Fan and Macnab (22). The catalytically active C-terminal domain of FliI shows high sequence homology to the catalytic β-subunit of the F_0F_1 ATPase (Fan *et al.* (23), Vogler *et al.* (85)). The recent analysis of Lupas and Martin (42) furthermore suggests that T3S system ATPases belong to the group of unfoldases, which indicates another function of FliI in addition to the energization of the export of flagellar substrates. The two remaining soluble components of the T3S apparatus are FliH, the regulator of FliI, which is important for efficient flagellar assembly and FliJ, a general chaperone for flagellar secretion substrates (Macnab (43)). It is important to note that the flagellar secretion substrates are translocated by the flagellar T3S apparatus across the cytoplasmic membrane through a narrow channel of about 2.0 nm in diameter (Yonekura *et al.* (87)), therefore the proteins are most likely exported in an unfolded or partially folded state.

Another interesting fact is that the flagellar type III secretion apparatus is believed to be the ancestor of all type III secretion systems. Accordingly, most of the T3S components are conserved in both flagellar type III secretion and virulence-associated type III secretion systems (Hueck (33), Macnab (45)), and therefore unravelling common principles and functions of flagellar T3S and virulence-associated T3S systems may lead to new important medical applications.

1.3 Chromosomal location and known functions of FliOPQR

As displayed in Figure 1.3, the genes encoding for the putative flagellar type III secretion components FliOPQR of *S. typhimurium*, are contiguous within the *fliLMNOPQR* operon under control of a flagellar Class II promotor (Chilcott and Hughes (16)).

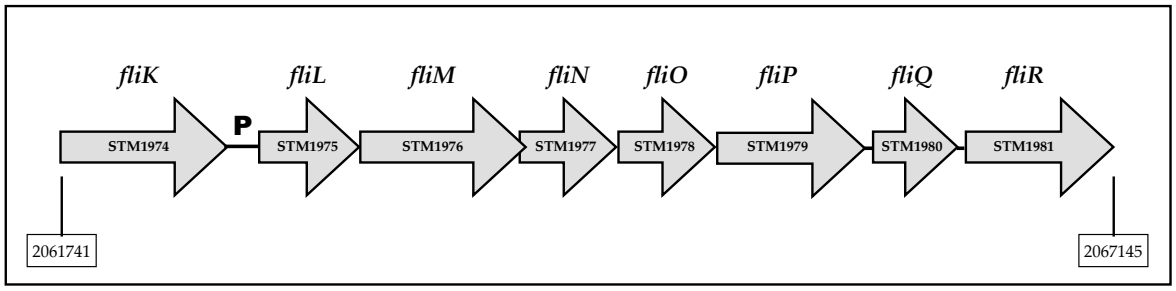

FIGURE 1.3: Chromosomal location and orientation of *fliOPQR* of *S. typhimurium*. *fliO* (locus tag: STM1978), *fliP* (locus tag: STM1979), *fliQ* (locus tag: STM1980) and *fliR* (locus tag: STM1981) are under the control of the flagellar Class II promotor $P_{fliLMNOPQR}$ (P). *fliK* = coding for flagellar hook-length control protein; *fliL* = unknown function; *fliM* and *fliN* = coding for flagellar motor/switch proteins; *fliOPQR* = unknown function.

The genes *fliO*, *fliP*, *fliQ* and *fliR* were first cloned and characterized by Ohnishi *et al.* (61), who experimentally identified FliOPQR in the membrane fraction, which is consistent with the large hydrophobic residue content of the proteins. The topology prediction of FliOPQR by the same authors is discussed later in this work. It has been furthermore shown by Ohnishi *et al.* (61) that FliP undergoes N-terminal signal peptide cleavage, which is important but not essential for FliP function. In addition, Ohnishi *et al.* (61) suggested first that FliP, FliQ, FliR and possibly FliO are components of the flagellar - specific type III secretion apparatus and putatively located within the flagellar basal body. It is important to note that only FliP, FliQ and FliR, but not FliO, have homologs in the virulence-associated type III secretion systems of pathogenic bacteria.

As noted above, FliOPQR are proposed to be located in a patch of membrane in the central pore of the MS ring. However, only FliP and FliR have been detected in

the basal body as discussed in the study of Fan *et al.* (23). Stoichiometries of FliP and FliR respectively, were estimated by immunoblotting and quantitative radiolabelling analysis to be about 4 or 5 subunits of FliP and fewer than 3 (around 1) subunits of FliR per basal body. In a later study, Schoenhals *et al.* (69) showed that functional FliO can be translated from two start codons, resulting in a long ($FliO_L$) and a short version ($FliO_S$) of FliO. However, translation of the second start only occurred in cases where the first start was attenuated.

The proteins FliOPQR were also proposed by Minamino and Macnab (56) to be components of the flagellar-specific type III secretion apparatus. The authors indeed showed that FliO, FliP, FliQ and FliR are essential for secretion of rod-type, hook-type and filament-type secretion substrates. Recently, Van Arnam *et al.* (81) showed that a FliR-FlhB fusion construct in *Salmonella*, which does exist in *Clostridium*, is able to complement *fliR*, *flhB* and *fliR* + *flhB* null strains. The authors accordingly suggest that wildtype FliR and FlhB are physically associated in a 1:1 ratio in the flagellar basal body.

As discussed above, virtually nothing is known about the function of FliO, FliP. FliQ and FliR respectively. It seemed intriguing to examine the function and localization of the putative flagellar type III secretion apparatus components FliOPQR. Therefore the proteins were intensively studied in this work.

2 MATERIALS AND METHODS

2.1 Materials and chemicals

Standard chemicals were purchased in analytical quality from established commercial suppliers, in most cases Sigma-Aldrich and Fluka. The ionophore carbonyl cyanide m-chlorophenylhydrazone (CCCP) was purchased from Sigma-Aldrich and freshly disolved in dimethyl sulfoxide (DMSO). Potassium acetate was purchased from J. T. Baker and the pH was adjusted to the desired final pH by addition of HCl or NaOH. Antibodies used in this study are displayed in Table 2.1.

TABLE 2.1: List of antibodies used in this study. The primary target, brief description, used dilution and references are given. The polyclonal anti-GFP antibody was a kind gift of M. Babst.

TARGET	DESCRIPTION	DILUTION	REFERENCE
anti-FlgM	polyclonal (rabbit)	1:10,000	Hughes *et al.* (34)
anti-GFP	polyclonal (rabbit)	1:2,000	Invitrogen
anti-rabbit-HRP	polyclonal, horseradish-peroxidase conjugated (goat)	1:10,000	Biorad

2.2 Bacterial culture and growth media conditions

LB (Luria-Bertani) medium (Davis *et al.* (19)) was used for liquid cultures of bacterial strains. For solid medium, Bacto-agar was added to a final concentration of

1.5 %. MacConkey-lactose agar was purchased from Difco and used as indicator medium for assay of Lac^+ and Lac^- phenotypes. LB medium supplemented with E salts (Vogel and Bonner (84)) and 0.2% glucose was used as P22 broth for growth of phage stocks. Minimal medium (NZE) was used as described in (Maloy and Roth (48)) and supplemented with 0.2 % lactose as sole carbon source. Motility plates (Silverman and Simon (72)) contained tryptone (10 g/l), NaCl (5 g/l) and 0.3 % Bacto-agar. For growth of bacteriophage χ, tryptone broth (TB) containing tryptone (10 g/l), NaCl (5 g/l), 1% Bacto-agar, 10 mM $MgSO_4$ and 5 mM $CaCl_2$ was used. For titering of phage χ, TB top agar containing tryptone (10 g/l), NaCl (5 g/l) and 0.4 % Bacto-agar was used. Selection for tetracycline sensitivity was performed using Tet-sensitive plates as described previously (Bochner *et al.* (12), Maloy and Nunn (47)). Tet-sensitive plates contained 1.5 % Bacto-agar, 0.5 % tryptone, 0.5 % yeast extract, 0.17 M NaCl, 0.07 M $NaH_2PO_4 \cdot H_2O$, 10 mM $ZnCl_2$, 50 mg/ml chlortetracycline, 12 mg/ml fusaric acid and were incubated at 42 °C.

Bacterial strains were cultured in Luria-Bertani (LB) medium with aeration at 37 °C, and at 30 °C for growth of strains harboring the plasmid pKD46 (Datsenko and Wanner (18)). Concentrations of antibiotics and additives are displayed in Table 2.2.

TABLE 2.2: Concentrations of antibiotics and additives used in LB liquid cultures and agar plates

Ampicillin	100 μg/ml
Tetracycline	15 μg/ml
Chloramphenicol	12.5 μg/ml
Kanamycin	50 μg/ml
X-Pho (5-bromo-4-chloro-3-indolylphosphat-*p*-toluidine)	40 μg/ml
X-Gal (5-bromo-4-chloro-3-indolyl-13-D-galactopyranoside)	40 μg/ml

2.3 Standard methods used for DNA preparation

Chromosomal DNA of *S. typhimurium* LT2, TH2788 and *E. coli* K12 was extracted using the QIAampDNA blood minikit (Qiagen). Plasmids DNA was purified from *E. coli* DH5α and JM-109 strains using the Mini-Plasmid kit (Qiagen). Restriction digestions using restriction endonucleases (New England Biolabs, Fermentas), ligations using T4 DNA ligase (Fermentas), dephosphorylation of plasmid DNA using calf intestinal phosphorylase (New England Biolabs) and polymerase chain reaction (PCR) using DNA polymerases (*Taq* polymerase, Promega and Accuzyme polymerase, Gentaur) were performed by standard procedures as described in Sambrook *et al.* (64). Correct cloning was confirmed by sequencing analysis at the University of Utah HSC Core DNA Sequencing Facility.

Transformation of *S. typhimurium* was performed using electroporation (Bio-Rad Gene Pulser). *E. coli* DH5α and JM-109 were transformed using the SEM-transformation method as described in Inoue *et al.* (35), or the TSS-transformation as described in Chung *et al.* (17). Chemically competent *E. coli* were prepared for SEM-transformation as follows. An overnight culture was grown from a frozen stock of *E. coli* DH5α. The overnight culture was diluted 1:100 in 20 ml LB and grown to an optical density OD_{600} of 0.6 at 37 °C. Afterwards, the cells were pelleted, resuspended in 0.1 M $CaCl_2$ and incubated on ice for 30 minutes. The preceding step was repeated, the cells were resuspended in 1.5 ml 0.1 M $CaCl_2$ 20 % glycerol and subsequently stored at -70 °C until further use.

2.4 Bacterial strain construction and list of constructed strains

The generalized transducing Bacteriophage P22 HT105/1 int-201 (Sanderson and Roth (66)) was used for transducing experiments with *S. typhimurium*. Briefly, 100 μl of serial dilutions of phage P22 were mixed with 100 μl recipient cells grown to

saturation. After incubation for about 30 minutes at 37 °C, 100 μl of the phage/cell mixture was plated on appropriate selection plates. Subsequently, transduced cells were made phage-free by purification on green-indicatior plates (Chan *et al.* (14)) and phage P22 sensitivity was tested by cross-streaking against phage P22 H2 on green-indicator plates. The bacterial strains used and constructed in this study are shown in Table 2.3.

TABLE 2.3: List of strains used and constructed in this study. Strain nomenclature as used in K. T. Hughes' laboratory, relevant genotype as far as known and references are displayed in the table.

STRAIN	**GENOTYPE**	**SOURCE**
TH434	*Escherichia coli* K12 λ-	J. Roth
TH437	*Salmonella enterica serovar Typhimurium* LT2	lab stock
TH470	*leuA414 supE attA::[P22 sieA44 16-amH1455 tpfr49] Fels-*	lab stock
TH471	*leuA414 hsdSB(r-m+) Fels-*	lab stock
TH473	*leuA414 supE hsdSB(r-m+) Fels-*	lab stock
TH1042	*zea-3525::*Tn*10*dCm (cw of *fliC)*	lab stock
TH1317	*pJS28(ApR P22 9+)/hisG10085::*Tn*phoA his(HA)9556::*Mu*d*P22	lab stock
TH1721	*fla-1191(*Δ*flgA-J1191) fljBenx vh2*	lab stock
TH1722	*fla-2157(*Δ*flgG-L2157) fljBenx vh2*	lab stock
TH1723	*fla-2039(*Δ*tar-flhDC2039) fljBenx vh2*	lab stock
TH1724	*fla-2018(*Δ*flhA-cheA2018) fljBenx vh2*	lab stock
TH1725	*fla-2050(*Δ*fliA-D2050) fljBenx vh2*	lab stock
TH1726	*fla-2211(*Δ*fliE-K2211) fljBenx vh2*	lab stock
TH1727	*fla-2195(*Δ*fliJ-R2195) fljBenx vh2*	lab stock
TH1756	*fliO2008 fljBenx vh2*	lab stock
TH1757	*fliP2041 fljBenx vh2*	lab stock
TH1758	*fliQ1180 fljBenx vh2*	lab stock
TH1759	*fliR1161 fljBenx vh2*	lab stock
TH1788	*E. coli* DH5α	lab stock
TH2788	*fliY5221::*Tn*10*dTc	lab stock
TH3022	*fli(L-R)5254::*Mu*d*K	lab stock
TH3062	*fli(L-R)5281::*Mu*d*K	lab stock
TH3067	*fli(L-R)5286::*Mu*d*K	lab stock

STRAIN	GENOTYPE	SOURCE
TH3069	*fli(E-R)5288::*Mu*d*K	lab stock
TH3073	*fliM5292::*Mu*d*K	lab stock
TH3171	*fliO5343::*Mu*d*K	lab stock
TH3172	*fliP5344::*Mu*d*K	lab stock
TH3173	*fli(K-R)5345::*Mu*d*K	lab stock
TH3187	*E. coli* CC118 Δ*phoA*	lab stock
TH3264	*zec-7080::*Tn*10*dTc *fljBenx vh2*	lab stock
TH3357	*E. coli* CC191 Δ*lac* Δ*phoA*	lab stock
TH3374	Δ*fli(L-R)2574*	lab stock
TH3672	DH5α / p322KS	lab stock
TH3730	*P(flhDC)5451::*Tn*10*dTc[del-25] (Tc-induced Mot+)	lab stock
TH3933	*motA5461::*Mu*d*J (>95%-*motA*::Tn*10*)	lab stock
TH4236	CC160 Δ*(ara-leu)7697 araD139* Δ*(lac)X74*	lab stock
TH4237	CC245 *F- supF supE hsdR galK trpR mctB lacY tonA dam::Km*	lab stock
TH4238	λTn*lacZ*/in 7x10+9 pfu/ml propagate CC245	lab stock
TH4239	λ*phoA*/in 6.5x10+9 pfu/ml propagate CC245	lab stock
TH4522	*DUP1731[(leuA1179)*MudJ*(nadC220)] recA644::*Tn*10*dCm	lab stock
TH4702	LT2 / pKD46 (Red recombinase plasmid)	lab stock
TH4885	*fliF5629::frt-Km-frt (*Δ*bp40fliF-bp1fliG)*	lab stock
TH5139	Δ*flgM5628::FRT*	lab stock
TH6232	Δ*hin-5717::FRT (fljBA-OFF)*	lab stock
TH6233	Δ*hin-5718::FRT (fljBA-ON)*	lab stock
TH6706	Δ*araBAD925::tetRA* / pKD46	lab stock
TH7503	*fliM5980* (FliM-GAGAGA-CFP)	lab stock
TH7568	Δ*hin-5717::FRT fliC5050::*Mu*d*J Δ*araBAD923::flgM-FKF ParaB934*	lab stock
TH8518	*fliQ6206::*Mu*d*J	lab stock
TH8519	*fliR6207::*Mu*d*J	lab stock
TH8537	Δ*araBAD949::YFP*	lab stock
TH10106	Δ*[Fels-2,Gifsy-1,Gifsy-2]*	lab stock
TH10216	Δ*araBAD6608::fliR* Δ*fliR2368 fljBenx vh2*	lab stock
TH10411	*fliO6650::tetRA (after aa5)*	this study
TH10412	*fliO6651::tetRA (after aa121)*	this study

STRAIN	GENOTYPE	SOURCE
TH10413	*fliP6652::tetRA (after aa5)*	this study
TH10414	*fliP6653::tetRA (after aa241)*	this study
TH10415	*fliQ6654::tetRA (after aa5)*	this study
TH10416	*fliQ6655::tetRA (after aa85)*	this study
TH10417	*fliR6656::tetRA (after aa5)*	this study
TH10418	*fliR6657::tetRA (after aa260)*	this study
TH10419	Δ*fliO6658::tetRA (Δaa6-121)*	this study
TH10420	Δ*fliP6659::tetRA (Δaa6-241)*	this study
TH10421	Δ*fliQ6660::tetRA (Δaa6-85)*	this study
TH10422	Δ*fliR6661::tetRA (Δaa6-260)*	this study
TH10445	*fliO6650::tetRA (after aa5)* / pKD46	this study
TH10446	*fliO6651::tetRA (after aa121)* / pKD46	this study
TH10447	*fliP6652::tetRA (after aa5)* / pKD46	this study
TH10448	*fliP6653::tetRA (after aa241)* / pKD46	this study
TH10449	*fliQ6654::tetRA (after aa5)* / pKD46	this study
TH10450	*fliQ6655::tetRA (after aa85)* / pKD46	this study
TH10451	*fliR6656::tetRA (after aa5)* / pKD46	this study
TH10452	*fliR6657::tetRA (after aa260)* / pKD46	this study
TH10453	Δ*fliO6658::tetRA (Δaa6-121)* / pKD46	this study
TH10454	Δ*fliP6659::tetRA (Δaa6-241)* / pKD46	this study
TH10455	Δ*fliQ6660::tetRA (Δaa6-85)* / pKD46	this study
TH10456	Δ*fliR6661::tetRA (Δaa6-260)* / pKD46	this study
TH10498	*zec-8469::*Tn*10*dTc (92% to *fliR*)	this study
TH10548	Δ*fliO6708 (Δaa6-121)*	this study
TH10549	Δ*fliP6709 (Δaa6-241)*	this study
TH10550	Δ*fliQ6710 (Δaa6-85)*	this study
TH10551	Δ*fliR6711 (Δaa6-260)*	this study
TH10552	*fliQ6712-yfp* (FliQ-GAGAGA-YFP)	this study
TH10553	DH5α / pCS2	lab stock
TH10571	Δ*araBAD6608::fliR* Δ*fliR6661::tetRA fljBenx vh2*	this study
TH10572	CC160 / pMS5 (*fliO*) derived from pDB3	this study
TH10573	CC160 / pMS6 (*fliP*) derived from pDB3	this study

STRAIN	GENOTYPE	SOURCE
TH10574	CC160 / pMS7 (*fliQ*) derived from pDB3	this study
TH10575	CC160 / pMS8 (*fliR*) derived from pDB3	this study
TH10585	Δ*araBAD925::tetRA* Δ*fliO6708*	this study
TH10586	Δ*araBAD925::tetRA* Δ*fliP6709*	this study
TH10587	Δ*araBAD925::tetRA* Δ*fliQ6710*	this study
TH10588	Δ*araBAD925::tetRA* Δ*fliR6711*	this study
TH10589	Δ*araBAD6608::fliR* Δ*fliR6661::tetRA* / pKD46	this study
TH10590	Δ*araBAD925::tetRA* Δ*fliO6708* / pKD46	this study
TH10591	Δ*araBAD925::tetRA* Δ*fliP6709* / pKD46	this study
TH10592	Δ*araBAD925::tetRA* Δ*fliQ6710* / pKD46	this study
TH10593	Δ*araBAD925::tetRA* Δ*fliR6711* / pKD46	this study
TH10594	*fliR6720-yfp* (FliR-GAGAGA-YFP)	this study
TH10595	*fliO6721-yfp* (FliO-GAGAGA-YFP)	this study
TH10596	Δ*fliP6722 (*Δ*aa6-241) fliO6723 (aa1 = ATG -> ATT)*	this study
TH10602	*fliO1077 fljBenx vh2*	this study
TH10603	*fliO1084 fljBenx vh2*	this study
TH10604	*fliO1086 fljBenx vh2*	this study
TH10605	*fliO1087 fljBenx vh2*	this study
TH10606	*fliO1088 fljBenx vh2*	this study
TH10607	*fliO1089 fljBenx vh2*	this study
TH10608	*fliO1431 fljBenx vh2*	this study
TH10609	*fliO1485 fljBenx vh2*	this study
TH10610	*fliP1191 fljBenx vh2*	this study
TH10611	*fliP1193 fljBenx vh2*	this study
TH10612	*fliP1544 fljBenx vh2*	this study
TH10613	*fliP1628 fljBenx vh2*	this study
TH10614	*fliQ167 fljBenx vh2*	this study
TH10615	*fliQ184 fljBenx vh2*	this study
TH10616	*fliQ188 fljBenx vh2*	this study
TH10617	*fliQ1648 fljBenx vh2*	this study
TH10618	*fliR189 fljBenx vh2*	this study
TH10619	*fliR1218 fljBenx vh2*	this study

STRAIN	GENOTYPE	SOURCE
TH10620	*fliR1219 fljBenx vh2*	this study
TH10621	*fliR1220 fljBenx vh2*	this study
TH10622	*fliR1221 fljBenx vh2*	this study
TH10623	*fliR1719 fljBenx vh2*	this study
TH10630	Δ*fliO6658::tetRA (aa6-121) fliF5629::FKF*	this study
TH10633	JM-109 / pMS9 (*fliO*) derived from pKG116	this study
TH10634	JM-109 / pMS10 (*fliP*) derived from pKG116	this study
TH10635	JM-109 / pMS11(*fliQ*) derived from pKG116	this study
TH10636	JM-109 / pMS12 (*fliR*) derived from pKG116	this study
TH10637	JM-109 / pUC4K	K. Paul
TH10644	pKD45 / SY327 CS161	A. Böhm
TH10668	*fliF5629::frt-Kan-frt fliQ6712* (FliQ-GAGAGA-YFP)	this study
TH10669	*fliF5629::frt-Kan-frt fliR6720* (FliR-GAGAGA-YFP)	this study
TH10670	*fliF5629::frt-Kan-frt fliO6721* (FliO-GAGAGA-YFP)	this study
TH10671	*fliP6735-yfp* (FliP-GAGAGA-YFP)	this study
TH10672	JM-109 / pEM3 (*fliO*, KanR)	this study
TH10673	JM-109 / pEM4 (*fliP*, KanR)	this study
TH10674	JM-109 / pEM5 (*fliQ*, KanR)	this study
TH10675	JM-109 / pEM6 (*fliR*, KanR)	this study
TH10676	Δ*fliO6708* / pEM3 (*fliO*, KanR)	this study
TH10677	Δ*fliP6709* / pEM4 (*fliP*, KanR)	this study
TH10678	Δ*fliQ6710* / pEM5 (*fliQ*, KanR)	this study
TH10679	Δ*fliR6711* / pEM6 (*fliR*, KanR)	this study
TH10680	CC160 / pEM3 (*fliO*, KanR)	this study
TH10681	CC160 / pEM4 (*fliP*, KanR)	this study
TH10682	CC160 / pEM5 (*fliQ*, KanR)	this study
TH10683	CC160 / pEM6 (*fliR*, KanR)	this study
TH10731	*fliO1087 zec-8469::*Tn*10*Tc (79% to *fliO1087) fljBenx vh2*	this study
TH10732	*fliO1089 zec-8469::*Tn*10*Tc (75% to *fliO1089) fljBenx vh2*	this study
TH10733	JM-109 / pKG116	K. Paul
TH10736	*zea-3525::*Tn*10*dCm Δ*fliO6658::tetRA*	this study
TH10737	*fliM5292::*Mu*d*K Δ*fliO6658::tetRA*	this study

STRAIN	GENOTYPE	SOURCE
TH10738	*motA5461::*Mu*d*J *fliO1087 zec-8469::*Tn*10*Tc *fljBenx vh2*	this study
TH10739	*motA5461::*Mu*d*J *fliO1089 zec-8469::*Tn*10*Tc *fljBenx vh2*	this study
TH10759	*zea-3525::*Tn*10*dCm *fliO6721* (FliO-GAGAGA-YFP)	this study
TH10760	*fliM5980* (FliM-GAGAGA-CFP) Δ*fliO6658::tetRA*	this study
TH10764	Δ*araBAD6608::fliR fliR6776 (stop after aa88) fljBenx vh2*	this study
TH10765	Δ*araBAD6608::fliR fliR6777 (W72R, aa109 out-of-frame)*	this study
TH10766	Δ*fliO6708* / pEM7 (FliO-GAGAGA-YFP)	this study
TH10820	*fliO1087 zec7080::*Tn*10*dTc (46% to *fliO1087) fljBenx vh2*	this study
TH10821	*fliO1089 zec7080::*Tn*10*dTc (36% to *fliO1089) fljBenx vh2*	this study
TH10822	*fliM5292::*Mu*d*K *fliO6721 zea3525::*Tn*10*dCm	this study
TH10823	*recA644::*Tn*10*dCm *fliO6721* (FliO-GAGAGA-YFP)	this study
TH10825	*recA644::*Tn*10*dCm *fliO6721* (FliO-GAGAGA-YFP) / pKD46	this study
TH10827	SM10λpir / pCM665	C. Manoil
TH10828	SM10λpir / pCre1	C. Manoil
TH10836	*fliM5980 fliO6721 zea3525::*Tn*10*dCm	this study
TH10874	Δ*flgM5628::FRT* Δ*araBAD923::flgM-FKF ParaB934*	this study
TH10897	Δ*fliOP6811::tetRA (*Δ*fliO-aa5 to fliP-aa241)*	this study
TH10898	Δ*fliOP6811::tetRA (*Δ*fliO-aa5 to fliP-aa241) / pKD46*	this study
TH11112	Δ*fliO6708 motA5461::*Mu*d*J	this study
TH11113	Δ*fliP6709 motA5461::*Mu*d*J	this study
TH11183	*DUP1150[(flgE5315)**Mu*d*K**(putA1017)]* / pKD46	this study
TH11219	DH5α / pEM8 *(fliO)*	this study
TH11220	DH5α / pEM9 *(fliP)*	this study
TH11221	DH5α / pEM10 *(fliQ)*	this study
TH11222	DH5α / pEM11 *(fliR)*	this study
TH11227	Δ*fliOP6856 (*Δ*fliO-aa5 to fliP-aa241)*	this study
TH11516	*fliO1087 (L91R) fli7125 mot+*	this study
TH11517	*fliO1087 (L91R) fli7126 mot+*	this study
TH11518	*fliO1087 (L91R) fli7127 mot+*	this study
TH11519	*fliO1087 (L91R) fli7128 mot+*	this study
TH11520	*fliO1087 (L91R) fli7129 mot+*	this study
TH11521	*fliO1087 (L91R) fli7130 mot+*	this study

STRAIN	GENOTYPE	SOURCE
TH11522	*fliO1089 (V72G) fli7131 mot+*	this study
TH11523	*fliO1089 (V72G) fli7132 mot+*	this study
TH11524	*fliO1089 (V72G) fli7133 mot+*	this study
TH11525	*fliO1089 (V72G) fli7134 mot+*	this study
TH11526	*fliO1089 (V72G) fli7135 mot+*	this study
TH11527	*fliO1089 (V72G) fli7136 mot+*	this study
TH11528	*fliO1087 (L91R) fli7137 mot+*	this study
TH11531	*fliO1087 (L91R) fli7125 mot+ motA5461::*Mu*d*J (lac+)	this study
TH11532	*fliO1087 (L91R) fli7126 mot+ motA5461::*Mu*d*J (lac+)	this study
TH11533	*fliO1087 (L91R) fli7127 mot+ motA5461::*Mu*d*J (lac-)	this study
TH11534	*fliO1087 (L91R) fli7128 mot+ motA5461::*Mu*d*J (lac+)	this study
TH11535	*fliO1087 (L91R) fli7129 mot+ motA5461::*Mu*d*J (lac+)	this study
TH11536	*fliO1087 (L91R) fli7130 mot+ motA5461::*Mu*d*J (lac+)	this study
TH11537	*fliO1089 (V72G) fli7131 mot+ motA5461::*Mu*d*J (lac+)	this study
TH11538	*fliO1089 (V72G) fli7132 mot+ motA5461::*Mu*d*J (lac+)	this study
TH11539	*fliO1089 (V72G) fli7133 mot+ motA5461::*Mu*d*J (lac+)	this study
TH11540	*fliO1089 (V72G) fli7134 mot+ motA5461::*Mu*d*J (lac+)	this study
TH11541	*fliO1089 (V72G) fli7135 mot+ motA5461::*Mu*d*J (lac+)	this study
TH11542	*fliO1089 (V72G) fli7136 mot+ motA5461::*Mu*d*J (lac+)	this study
TH11543	*fliO1089 (V72G) fli7137 mot+ motA5461::*Mu*d*J (lac+)	this study
TH11544	*zec-8469::*Tn*10*dTc *fla7138::*Tn*5phoA*	this study
TH11545	*zec-8469::*Tn*10*dTc *fla7139::*Tn*5phoA*	this study
TH11546	*zec-8469::*Tn*10*dTc *fla7140::*Tn*5phoA*	this study
TH11547	*zec-8469::*Tn*10*dTc *flhA-cheA7141::*Tn*5phoA*	this study
TH11548	*zec-8469::*Tn*10*dTc *fliJ-R7142::*Tn*5phoA*	this study
TH11549	*zec-8469::*Tn*10*dTc *fliE-K7143::*Tn*5phoA*	this study
TH11550	*zec-8469::*Tn*10*dTc *fla7144::*Tn*5phoA*	this study
TH11551	*zec-8469::*Tn*10*dTc *fla7145::*Tn*5phoA*	this study
TH11552	*zec-8469::*Tn*10*dTc *fla7146::*Tn*5phoA*	this study
TH11553	*zec-8469::*Tn*10*dTc *fla7147::*Tn*5phoA*	this study
TH11554	*zec-8469::*Tn*10*dTc *fla7148::*Tn*5phoA*	this study
TH11555	*zec-8469::*Tn*10*dTc *fla7149::*Tn*5phoA*	this study

STRAIN	GENOTYPE	SOURCE
TH11556	*zec-8469::*Tn*10*dTc *fla7150::*Tn*5phoA*	this study
TH11557	DH5α / pEM12-1 *(fliO-BamHI-lacZ)*	this study
TH11558	DH5α / pEM13-1 *(fliP-BamHI-lacZ)*	this study
TH11559	DH5α / pEM14-1 *(fliQ-BamHI-lacZ)*	this study
TH11560	DH5α / pEM15-1 *(fliR-BamHI-lacZ)*	this study
TH11561	DH5α / pEM16-1 *(fliO-BamHI-phoA)*	this study
TH11562	DH5α / pEM16-2 *(fliO-BamHI-phoA)*	this study
TH11563	DH5α / pEM16-3 *(fliO-BamHI-phoA)*	this study
TH11564	DH5α / pEM17-1 *(fliP-BamHI-lacZ)*	this study
TH11565	DH5α / pEM18-1 *(fliR-BamHI-lacZ)*	this study
TH11566	DH5α / pEM18-2 *(fliR-BamHI-lacZ)*	this study
TH11567	DH5α / pEM18-3 *(fliR-BamHI-lacZ)*	this study
TH11568	DH5α / pEM18-4 *(fliR-BamHI-lacZ)*	this study
TH11569	DH5α / pEM18-5 *(fliR-BamHI-lacZ)*	this study
TH11570	CC191 *(*Δ*lac* Δ*phoA)* / pEM12 (lac+)	this study
TH11571	CC191 *(*Δ*lac* Δ*phoA)* / pEM13 (lac-)	this study
TH11572	CC191 *(*Δ*lac* Δ*phoA)* / pEM14 (lac+)	this study
TH11573	CC191 *(*Δ*lac* Δ*phoA)* / pEM15 (lac+)	this study
TH11574	CC191 *(*Δ*lac* Δ*phoA)* / pEM18 (Xpho-)	this study

2.5 List of oligoprimers used in this study

TABLE 2.4: List of oligoprimers used in this study. Primer number as used in K. T. Hughes' laboratory, primer name and 5′ - 3′ DNA sequence are displayed in the table. Primers MS19 and MS20 were a kind gift of K. Paul.

PRIMER	NAME	SEQUENCE (5′ - 3′)
140	3′fliL	GGCCAAGCTTACCGCAGAATAAAAGC
270	T1test	TGCAGGAGAGATTTCACCGC
458	FLINBSPHI5′	GGAGCTCATGAGTGACATGAATAATCC
656	tetTOUT	TATTACGACAAGCTATCG
767	FLIMENDOUT	CAGCCAATATGGCACCGTAAAC
985	LacZ-1kb-OUT	CATTTTCAATCCGCACCTC
1114	FlgK-del-B	CGTGGAAAAGACGCGGATAAT
1255	fliJstopF	GAATTTGCTCAGCGTGCAGC
1852	pTrc5′seq	GCAAATATTCTGAAATGAGC
1994	fliO-tetRstart	AGCGTATGCGTCGTTTGAGTCGTTAATGATGAA GACAGAATTAAGACCCACTTTCACATT
1995	fliO-tetAstart	GCGGCGATCCGGCTGGCGCGGTGGGCTGAGAAA CCGTGGCCTAAGCACTTGTCTCCTG
1996	fliO-tetRend	ACCGGCGGATTTCCAGAACATGATGAAGAGCTT ACTCAAGTTAAGACCCACTTTCACATT
1997	fliO-tetAend	GAAAGGAATAACAAACGGCGCATCAGGATCTCC CGGAACGCTAAGCACTTGTCTCCTG
1998	fliP-tetRstart	TACTCAAGCGTTCCGGGAGATCCTGATGCGCCG TTTGTTATTAAGACCCACTTTCACATT
1999	fliP-tetAstart	CGGCGGGACTAAAAAGCCACAGACCCGCCAGAG AAAGGAACTAAGCACTTGTCTCCTG
2000	fliP-tetRend	GCTGGTCGATGGTTGGCAATTGCTTATGGGGTC GCTGGCCTTAAGACCCACTTTCACATT
2001	fliP-tetAend	ATTCAGGAGTCATTTTGCGCCTCTAACTGTAAA AGCTTTGCTAAGCACTTGTCTCCTG

PRIMER	NAME	SEQUENCE (5′ - 3′)
2002	fliQ-tetRstart	AAGCTTTTACAGTTAGAGGCGCAAAATGACTCC
		TGAATCCTTAAGACCCACTTTCACATT
2003	fliQ-tetAstart	CGAGAGCGACTTTCATCGCCTCGGTGCCCATCA
		TCATGACCTAAGCACTTGTCTCCTG
2004	fliQ-tetRend	CCTGCTGCTGGATTACGTGCGCACTCTGTTCAG
		CAATTTATTAAGACCCACTTTCACATT
2005	fliQ-tetAend	GTAACCTGGATCATCGTTCTGTTTATCCGATGA
		TATAAGGCTAAGCACTTGTCTCCTG
2006	fliR-tetRstart	CTTATATCATCGGATAAACAGAACGATGATCCA
		GGTTACATTAAGACCCACTTTCACATT
2007	fliR-tetAstart	GCCAGAAATAGAGATGCAGCCAGTATAGCCATT
		GCTCGCTCTAAGCACTTGTCTCCTG
2008	fliR-tetRend	AATTTTCAATTTGCTTGCTGATATTGTTAGCGA
		GATGCCGTTAAGACCCACTTTCACATT
2009	fliR-tetAend	CCTTAGTAAAACAGGATAAAAATTATGGGTTAT
		TATTTATCTAAGCACTTGTCTCCTG
2010	fliO-DeleteFor	CGATATTATTACGCCATC
2011	fliO-DeleteRev	AGAAAGGAATAACAAACGGCGCATCAGGATCTC
		CCGGAACGTTCTGTCTTCATCATTAAC
2012	fliP-DeleteFor	ATGAAGAGCTTACTCAAGCG
2013	fliP-DeleteRev	GGATTCAGGAGTCATTTTGCGCCTCTAACTGTA
		AAAGCTTTGTAACAAACGGCGCATCAG
2014	fliQ-DeleteFor	CTGGCCCAAAGCTTTTA
2015	fliQ-DeleteRev	TTGTAACCTGGATCATCGTTCTGTTTATCCGAT
		GATATAAGGGGATTCAGGAGTCATTTT
2016	fliR-DeleteFor	CAGCAATTTACCTTATATCA
2017	fliR-DeleteRev	AACCTTAGTAAAACAGGATAAAAATTATGGGTT
		ATTATTTATTGTAACCTGGATCATCGT
2018	fliO-PCR-for	TCACCGATATTATTACGCCA
2019	fliO-PCR-rev	CGGGACTAAAAAGCCACAGA
2020	fliP-PCR-for	ACCGGCGGATTTCCAGAAC
2021	fliP-PCR-rev	AGGGCGAGAGCGACTTTCAT

PRIMER	NAME	SEQUENCE (5′ - 3′)
2022	fliQ-PCR-for	CAATTGCTTATGGGGTCGCT
2023	fliQ-PCR-rev	GATGCAGCCAGTATAGCCATT
2024	fliR-PCR-for	GTGCGCACTCTGTTCAGCAA
2025	fliR-PCR-rev	GGCAGTGGATATATCCTGGTG
2026	fliQ-Venus-	AACCTGCTGCTGGATTACGTGCGCACTCTGTTC
	End-for	AGCAATTTAGGCGCAGGCGCAGGCGCAATGGTG
		AGCAAGGGCGAG
2027	fliQ-Venus-	TTGTAACCTGGATCATCGTTCTGTTTATCCGAT
	End-Rev	GATATAAGGTTACTTGTACAGCTCGTC
2049	fliO-Venus-	CCACCGGCGGATTTCCAGAACATGATGAAGAGC
	End-for	TTACTCAAGGGCGCAGGCGCAGGCGCAGTGAGC
		AAGGGCGAGGAG
2050	fliO-Venus-	GAGAAAGGAATAACAAACGGCGCATCAGGATCT
	End-Rev	CCCGGAACGTTACTTGTACAGCTCGTC
2051	fliP-Venus-	GTGCTGGTCGATGGTTGGCAATTGCTTATGGGG
	End-for	TCGCTGGCCGGCGCAGGCGCAGGCGCAGTGAGC
		AAGGGCGAGGAG
2052	fliP-Venus-	GGATTCAGGAGTCATTTTGCGCCTCTAACTGTA
	End-Rev	AAAGCTTTGTTACTTGTACAGCTCGTC
2053	fliR-Venus-	GAAATTTTCAATTTGCTTGCTGATATTGTTAGC
	End-for	GAGATGCCGGGCGCAGGCGCAGGCGCAGTGAGC
		AAGGGCGAGGAG
2054	fliR-Venus-	AACCTTAGTAAAACAGGATAAAAATTATGGGTT
	End-Rev	ATTATTTATTTACTTGTACAGCTCGTC
2055	FliQ-seq-for	TACCGATGCGTATCCTCC
2056	FliR-seq-rev	CCATAATAATCGTTGACA
2148	pKG116-seq-	CCGGAATTCAAGTCATCAATAATGCCATAAGGA
	for	GTAC
2149	pKG116-seq-	TTTATCCGCGGATCCTCGAGGAGCTCG
	rev	
2165	fliOstart-tox-	GCGTATGCGTCGTTTGAGTCGTTAATGATGAAG
	for	ACAGAATCAGAAGAACTCGTCAAGAAG

PRIMER	NAME	SEQUENCE (5′ - 3′)
2166	fliO-YFP-tox-rev	ACAGCTCCTCGCCCTTGCTCACTGCGCCTGCGC CTGCGCCCGGATATTATCGTGAGGATG
2167	YFPstart-rev	GATGGGCACCACCCCGGTG
2168	fliO-NcoI-for	CATGCCATGGCATGATGAAGACAGAAGCCACGG
2169	fliR-XbaI-rev	GCTCTAGAGCTTATTATGGGTTATTATTTATCG GCATCTCG
2170	fliOend-lacZ-for	CCGGCGGATTTCCAGAACATGATGAAGAGCTTA CTCAAGACCATGATTACGGATTCACTG
2171	fliOend-lacZ-rev	AAGGAATAACAAACGGCGCATCAGGATCTCCCG GAACGTTATTTTTGACACCAGACCAAC
2172	fliOend-phoA-for	CCGGCGGATTTCCAGAACATGATGAAGAGCTTA CTCAAGAAACAAAGCACTATTGCACTG
2173	fliOend-phoA-rev	GAAAGGAATAACAAACGGCGCATCAGGATCTCC CGGAACGTTATTTCAGCCCCAGAGCGG
2220	ISphoA-flgN-for	TCTAATCATTGCCGGATGCGACGTTGCGCCTTT CCGGCCTGACTGTCTCTTGATCAGATC
2221	ISphoA-flgN-rev	CAGTGCCTGATAGCGCTGTGCTATCAGGCCTA CAAGGCATCTGACTCTTATACACAAGTA
2222	fliOP-delete-rev	ATTCAGGAGTCATTTTGCGCCTCTAACTGTAAA AGCTTTGTTCTGTCTTCATCATTAACG
2223	fliO-BamHI-rev	CGCGGATCCCCGGATCTCCCGGAACGCTTGA
2224	fliP-NcoI-for	CATGCCATGGCATGCGCCGTTTGTTATTCCTTT CTC
2225	fliP-BamHI-rev	CGCGGATCCCCACTGTAAAAGCTTTGGGCCAGC
2226	fliQ-NcoI-for	CATGCCATGGCATGACTCCTGAATCCGTCATGA TG
2227	fliQ-BamHI-rev	CGCGGATCCCCTCCGATGATATAAGGTAAATTG CTGAAC
2228	fliR-NcoI-for	CATGCCATGGCATGATCCAGGTTACAAGCGAGCA
2229	fliR-BamHI-rev	CGCGGATCCCCTGGGTTATTATTTATCGGCATC TCGC
2230	TM6Y-BamHI-	CTAGTCTAGACTAGTTACGCTGGATCCGTTTTG

PRIMER	NAME	SEQUENCE (5′ - 3′)
	XbaI-rev	GCGAAAAAGAG
2396	fliM-seq-for	GCCGGACAACCAAAACAG
2397	phoA-1kB-OUT	CGTCTCGCCAATTTGCCC
MS19	FliO.F.NdeI	GGGATATCCATATGATGATGAAGACAGAAGCCACG
MS20	FliO.rev. KpnI	CGGGGTACCTCATTAGGATCTCCCGGAA

2.6 Motility assay

Motility of *S. typhimurium* was assayed on motility plates containing 0.3 % agar and incubation at 37 °C for 4-5 hours. Motile cells swim from areas with limited nutrient content to areas with rich nutrient content depending on functional flagella. Single colonies of *S. typhimurium*, stabbed into a motility plate, will swarm in a circular wave outwards, while the nutrients in the center are exhausted. Cells defective in swarming, due to defects in the flagellum or chemotaxis apparatus, are said to be non-motile.

2.7 Phage complementation assay

For complementation of *fliO*, *fliP*, *fliQ* and *fliR* non-motile mutants, phage P22 was grown on TH1756 (*fliO2008*), TH1757 (*fliP2041*), TH1758 (*fliQ1180*) and TH1759 (*fliR1161*) respectively. The phage stock was diluted 1:100 and 100 μl of the diluted phage solution was added to 100 μl of the respective *S. typhimurium* overnight culture. A line of the phage/cell mixture was streaked on motility plates and after overnight incubation at 37 °C complementation was assayed.

2.8 Cloning of a kanamycin resistance cassette in pMS9 - 12

For the insertion of a kanamycin resistance cassette (Kan^R) into the reading frame of the *cat* (coding for chloramphenicol acetyl transferase) gene of pMS9, pMS10, pMS11 and pMS12 (pKG116 expressing *fliO, fliP, fliQ* and *fliR* respectively), an *Eco*RI-fragment containing *neo* (coding for neomycin phosphotransferase, which confers for Kan^R) was cut out of pUC4K. After gel purification, the *Eco*RI-fragment was ligated into dephosphorylated and *Eco*RI-cut pMS9 - 12 respectively. Subsequently, 2 μl of the ligation mixture were electroporated in competent *E. coli* JM-109 and selected for kanamycin resistance, resulting in pEM3, pEM4, pEM5 and pEM6 (pKG116, Kan^R, expressing *fliO, P, Q* and *fliR* respectively). Correct insertion of the Kan^R-cassette was confirmed by restriction digestion, testing for chloramphenicol sensitivity and complementation of TH10548 (Δ*fliO6708*) with pEM3, TH10549 (Δ*fliP6709*) with pEM4, TH10550 (Δ*fliQ6710*) with pEM5 and TH10551 (Δ*fliR6711*) with pEM6 respectively.

TABLE 2.5: List of plasmids used and constructed in this study. Name of the used plasmid, derivative used for construction of the displayed vector, resistance marker of the respective plasmid, overall characteristics and references are given in the table.

PLASMID	DERIVATIVE	RESISTANCE	CHARACTERISTICS	REF.
pDB3	pJH120	Amp^R	P_{araB}; L-ara ind.	K. Paul
pMS5	pDB3	Amp^R	*fliO* under P_{araB}	K. Paul
pMS6	pDB3	Amp^R	*fliP* under P_{araB}	K. Paul
pMS7	pDB3	Amp^R	*fliQ* under P_{araB}	K. Paul
pMS8	pDB3	Amp^R	*fliR* under P_{araB}	K. Paul
pUC4K	pUC7	Kan^R, Amp^R	-	(83)
pKG116	pKG110	Cm^R	P_{nahG}; Na-salicylate-ind.	K. Paul
pMS9	pKG116	Cm^R	*fliO* under P_{nahG}	K. Paul
pMS10	pKG116	Cm^R	*fliP* under P_{nahG}	K. Paul
pMS11	pKG116	Cm^R	*fliQ* under P_{nahG}	K. Paul

PLASMID	DERIVATIVE	RESISTANCE	CHARACTERISTICS	REF.
pMS12	pKG116	Cm^R	*fliR* under P_{nahG}	K. Paul
pEM3	pKG116	Kan^R	*fliO* under P_{nahG}	this study
pEM4	pKG116	Kan^R	*fliP* under P_{nahG}	this study
pEM5	pKG116	Kan^R	*fliQ* under P_{nahG}	this study
pEM6	pKG116	Kan^R	*fliR* under P_{nahG}	this study
pCS2	-	Amp^R	*yfp* under $P_{sCMV\ IE94}$	(59)
pEM7	pKG116	Cm^R	*fliO-yfp* under P_{nahG}	this study
pTrc99A	pKK233-2	Amp^R	P_{trc}, IPTG-ind.	(6)
pEM8	pTrc99A	Amp^R	*fliO* w/o stop under P_{trc}	this study
pEM9	pTrc99A	Amp^R	*fliP* w/o stop under P_{trc}	this study
pEM10	pTrc99A	Amp^R	*fliQ* w/o stop under P_{trc}	this study
pEM11	pTrc99A	Amp^R	*fliR* w/o stop under P_{trc}	this study
pEM12	pTrc99A	Amp^R	*fliO-lacZ* under P_{trc}	this study
pEM13	pTrc99A	Amp^R	*fliP-lacZ* under P_{trc}	this study
pEM14	pTrc99A	Amp^R	*fliQ-lacZ* under P_{trc}	this study
pEM15	pTrc99A	Amp^R	*fliR-lacZ* under P_{trc}	this study
pEM16	pTrc99A	Amp^R	*fliO-phoA* under P_{trc}	this study
pEM17	pTrc99A	Amp^R	*fliP-phoA* under P_{trc}	this study
pEM18	pTrc99A	Amp^R	*fliR-phoA* under P_{trc}	this study
pKD46	pBAD	Amp^R	λ - γ, β, *exo* under P_{araB}	(18)
pCM400	pBR322	Kan^R, Cm^R	Tn*lacZ*/in	(49)
pCM1000	pBR322	Kan^R, Cm^R, Tet^R, Amp^R	Tn*phoA*/in	(49)
pJK409	pBR322	Amp^R	*flk-Bam*HI-*lacZ*	lab stock

2.9 Cloning of *fliO-yfp* fusion construct in pKG116

For the construction of plasmid-expressed FliO-YFP fusion protein, genomic DNA of TH10595 (*fliO6721-yfp* (FliO-GAGAGA-YFP)) was prepared using the Qiagen Blood Minikit and subsequently used as the template for PCR amplification with forward primer #MS19 (FliO.F.NdeI) and reverse primer #MS20 (FliO.rev.KpnI) by the proofreading Accuzyme DNA polymerase. The resulting *Nde*I-*fliO-yfp-Kpn*I PCR product was afterwards digested with *Kpn*I and *Nde*I respectively, and ligated in digested pKG116. Competent *E. coli* JM-109 were electroporated with 2 μl of the ligation mixture, followed by selection for chloramphenicol resistance. The resulting plasmid pEM7 carries *fliO-yfp* under the control of the Na-salicylate inducible P_{nahG} promotor. Correct cloning of *fliO-yfp* was confirmed by restriction digestion, sequencing analysis and complementation of TH10548 (Δ*fliO6708*).

2.10 Cloning of *fliO, fliP, fliQ* and *fliR* in pTrc99A

The genes *fliO, fliP, fliQ* and *fliR*, lacking the respective 3' stop codon, were cloned in pTrc99A for subsequent construction of in-frame, 3'- *lacZ* and *phoA* fusions respectively. For the amplification of a PCR product with 5'-*Nco*I and 3'-*Bam*HI restriction sites by the proofreading Accuzyme polymerase, *S. typhimurium* LT2 genomic DNA was used as the PCR template, together with primers #2168 (fliO-*Nco*I-for) and #2223 (fliO-*Bam*HI-rev) for *Nco*I-*fliO-Bam*HI, primers #2224 (fliP-*Nco*I-for) and #2225 (fliP-*Bam*HI-rev) for *Nco*I-*fliP-Bam*HI, primers #2226 (fliQ-*Nco*I-for) and #2227 (fliQ-*Bam*HI-rev) for *Nco*I-*fliQ-Bam*HI and primers #2228 (fliR-*Nco*I-for) and #2229 (fliR-*Bam*HI-rev) for *Nco*I-*fliR-Bam*HI . Subsequently, the PCR product was purified, digested with *Nco*I and *Bam*HI respectively, and ligated in pTrc99A, resulting in pEM8, pEM9, pEM10 and pEM11(pTrc99A expressing *fliO, P, Q* and *fliR* respectively, under the control of the IPTG-inducible P_{trc} promotor). After TSS-transformation

of *E. coli* DH5α with 20 μl ligation mixture, transformants were selected for ampicillin resistance. Correct cloning of the genes was confirmed by restriction digestion, sequencing analysis and complementation of TH10548 (Δ*fliO6708*) with pEM8, TH10549 (Δ*fliP6709*) with pEM9, TH10550 (Δ*fliQ6710*) with pEM10 and TH10551 (Δ*fliR6711*) with pEM11 respectively. The use of the 5'-*Nco*I restriction site introduced an additional, out-of-frame 5'-ATG, which may affect the correct expression of *fliP* and *fliQ* as discussed later in the chapter "Determination of FliOPQR topology".

2.11 Construction of plasmid-based *fliO, fliP, fliQ* and *fliR-phoA* and *lacZ* fusions

For the construction of in-frame, 3'-*lacZ* fusions to *fliO, fliP, fliQ* and *fliR* respectively, pCM400 or pJK409 were digested with *Bam*HI, in order to obtain a *Bam*HI-*lacZ*-*Bam*HI fragment, which is necessary for subsequent cloning of the 3'-*lacZ* fusion construct. After purification, the *Bam*HI-*lacZ* fragment was ligated in dephosphorylated pEM8, pEM9, pEM10 and pEM11 respectively, transformed in chemically competent *E. coli* DH5α and selected for ampicillin resistance. Correct orientation of the *lacZ* insertion was tested by restriction digestion of putative *lacZ* insertions with *Nco*I and *Eco*RI restriction enzymes. Alternatively, correct orientation was checked by colony PCR, using a single colony of the transformant harboring a putative *lacZ*-insertion as the PCR template, and forward primer #1852 (pTrc5'seq) and reverse primer #985 (LacZ-1kb-OUT; reading out of *lacZ*).

For the construction of in-frame, 3'-*phoA* fusions to *fliO, fliP, fliQ* and *fliR* respectively, pCM1000 was digested with *Bam*HI, in order to obtain a *Bam*HI-*phoA*-*Bam*HI fragment, which was subsequently cloned in dephosphorylated pEM8, pEM9, pEM10 and pEM11 respectively, according to the cloning protocol of the 3'-*lacZ* fusion construct as described above. Correct orientation of the *phoA* insertion was checked by colony PCR with forward primer #1852 (pTrc5'seq) and reverse primer #2397 (phoA-1kB-OUT; reading out of *phoA*).

2.12 Insertion of a tetracycline resistance cassette using λ-RED mediated recombination

The tetracycline resistance cassette, derived from *Tn*10 and consisting of the genes *tetR* and *tetA*, was inserted using λ-RED mediated recombination, according to the method of Datsenko and Wanner (18). *tetRA*-cassettes were inserted 15 bases after the start codon (for subsequent construction of N-terminal fusions) or 15 bases before the stop codon (for subsequent construction of C-terminal fusions) of *fliO*, *fliP*, *fliQ* and *fliR* respectively. In addition, each of the four genes was replaced with a *tetRA*-cassette, starting 15 base pairs after the start codon and ending 15 base pairs before the stop codon, for the subsequent construction of clean deletion mutants. A schematic of the *tetRA*-insertion process is displayed in Figure 4.1. The genes *tetR* and *tetA* were PCR amplified by the proofreading polymerase Accuzyme using TH2722 genomic DNA as the PCR template and forward primer 5'-40Bp + TTA AGA CCC ACT TTC ACA TT-3' and reverse primer 5'-42Bp + CTA AGC ACT TGT CTC CTG-3'. The resulting PCR fragment of about 2 kB length consisted of the genes *tetRA* and 5' and 3' flanking regions of 40-42 base pairs homology to the downstream or upstream target gene region respectively. Afterwards, the PCR product was purified using the Qiagen PCR purification kit (or gel extraction kit, depending on the purity of the product) and eluted in 20 μ elution buffer (Qiagen). A list of insertion strains, which were constructed in this study and primers used for amplification of the *tetRA*-cassette, is shown in Table 2.6.

Electro-competent cells of TH4702 (LT2 harboring pKD46) were prepared as follows. TH4702 were grown in LB containing 100 μg/ml ampicillin overnight at 30 °C, diluted 1:100 in 25 ml LB Amp^{100} and grown 1 hour at 30 °C. Subsequently, the λ-RED genes were induced by addition of 0.2 % L-arabinose and the cells were grown to OD_{600} of 0.6 - 0.8 at 30 °C. The cells were pelleted and washed twice with ice-cold water and resuspended in 100 μl water. Afterwards, 1 μl of the PCR product was electroporated into 40 μl of competent cells. Immediately after electroporation, 1 ml

TABLE 2.6: List of *tetRA*-insertion strains constructed in this study and used primer for PCR amplification of the *tetRA* cassette with 5′ and 3′ flanking regions of 40-42 base pairs homology to the downstream or upstream target gene region respectively.

STRAINS AND GENOTYPE	**FORW PRIMER #**	**REV PRIMER #**
TH10411 *fliO6650::tetRA (after aa5)*	#1994 (fliO-tetRstart)	#1995 (fliO-tetAstart)
TH10412 *fliO6651::tetRA (after aa121)*	#1996 (fliO-tetRend)	#1997 (fliO-tetAend)
TH10413 *fliP6652::tetRA (after aa5)*	#1998 (fliP-tetRstart)	#1999 (fliP-tetAstart)
TH10414 *fliP6653::tetRA (after aa241)*	#2000 (fliP-tetRend)	#2001 (fliP-tetAend)
TH10415 *fliQ6654::tetRA (after aa5)*	#2002 (fliQ-tetRstart)	#2003 (fliQ-tetAstart)
TH10416 *fliQ6655::tetRA (after aa85)*	#2004 (fliQ-tetRend)	#2005 (fliQ-tetAend)
TH10417 *fliR6656::tetRA (after aa5)*	#2006 (fliR-tetRstart)	#2007 (fliR-tetAstart)
TH10418 *fliR6657::tetRA (after aa260)*	#2008 (fliR-tetRend)	#2009 (fliR-tetAend)
TH10419 Δ*fliO6658::tetRA (Δaa6-121)*	#1994 (fliO-tetRstart)	#1997 (fliO-tetAend)
TH10420 Δ*fliP6659::tetRA (Δaa6-241)*	#1998 (fliP-tetRstart)	#2001 (fliP-tetAend)
TH10421 Δ*fliQ6660::tetRA (Δaa6-85)*	#2002 (fliQ-tetRstart)	#2005 (fliQ-tetAend)
TH10422 Δ*fliR6661::tetRA (Δaa6-260)*	#2006 (fliR-tetRstart)	#2009 (fliR-tetAend)
TH10897 Δ*fliOP::tetRA*	#1994 (fliO-tetRstart)	#2001 (fliP-tetAend)

LB was added and the cells were incubated for 1 hour at 37 °C. 300 μl of the cells were plated on plates containing 15 μg/ml tetracycline and incubated overnight at 37 °C. About 16 Tet^R colonies were tested for tetracycline sensitivity and the most Tet^S transformants were kept for further use. Correct insertions of the *tetRA* cassette was confirmed by PCR using primer #270 (reads out of *tetA*, 753 bp upstream of stop codon) or #656 (reads out of *tetR*, 118 bp upstream of stop codon) to read out of the *tetRA* cassette, and primers up- or downstream of the region, where the *tetRA* cassette was inserted.

2.13 Construction of clean-deletion mutants

Clean (in-frame) deletion mutants of *fliO*, *fliP*, *fliQ*, *fliR* and *fliOP* respectively, were constructed using λ-RED mediated recombination and tetracycline-sensitive selection for the loss of the tetracycline resistance cassette. For PCR amplification of the replacement DNA fragment, a short oligoprimer (about 18mer) with homology to downstream parts of the gene to be deleted, was used together with a longer oligoprimer (about 60mer) with homology to both downstream and upstream parts of the gene to be deleted. A schematic of the replacement process is displayed in Figure 4.2. The resulting PCR fragment of about 100 - 150 bp length was gel purified using the Qiagen gel purification kit and subsequently eluted in 20 μl elution buffer (Qiagen). A list of clean-deletion strains, which were constructed in this study and primers used for amplification of the replacement DNA fragment, is given in Table 2.7.

TABLE 2.7: List of clean-deletion strains constructed in this study and primers used for PCR amplification of the replacement DNA fragment.

STRAINS AND GENOTYPE	**FORW PRIMER #**	**REV PRIMER #**
TH10548 Δ*fliO6708 (Δaa6-121)*	#2010 (fliO-DeleteFor)	#2011 (fliO-DeleteRev)
TH10549 Δ*fliP6709 (Δaa6-241)*	#2012 (fliP-DeleteFor)	#2013 (fliP-DeleteRev)
TH10550 Δ*fliQ6710 (Δaa6-85)*	#2014 (fliQ-DeleteFor)	#2015 (fliQ-DeleteRev)
TH10551 Δ*fliR6711 (Δaa6-260)*	#2016 (fliR-DeleteFor)	#2017 (fliR-DeleteRev)
TH11227 Δ*fliOP*	#2018 (fliO-PCR-for)	#2222 (fliOP-delete-rev)

For the replacement of the *tetRA*-cassette by λ-RED mediated recombination, *S. typhimurium* strains containing the *tetRA* cassette to be replaced and harboring pKD46, were grown overnight at 30 °C. Electro-competent cells expressing λ-RED recombinases were prepared as described above. Subsequently, 1 μl of the replacement DNA fragment was electroporated into 40 μl competent cells. Immediately after electroporation, 1 ml LB was added and the cells were incubated for 1 hour at

37 °C. 100 μl of serial dilutions (10^0, 10^{-1}, 10^{-2}) of the electroporated cells were plated on tetracycline-sensitive plates and incubated overnight at 42 °C. Subsequently, about 12 Tet^S colonies were picked and single-streaked on LB plates. At least 2 single colonies of each Tet^S transformants were picked and patched on LB and Tet^R plates to confirm the loss of the tetracycline resistance cassette. Additionally, the clean, in-frame deletion was confirmed by PCR and sequencing analysis.

2.14 Construction of chromosomally expressed *fliO, fliP, fliQ* and *fliR-yfp* fusions

Electro-competent cells of *S. typhimurium* strains TH10446 (*fliO6651::tetRA (after aa121)* / pKD46), TH10448 (*fliP6653::tetRA (after aa241)* / pKD46), TH10450 (*fliQ6655::tetRA (after aa85)* / pKD46) and TH10452 (*fliR6657::tetRA (after aa260)* / pKD46) respectively, were used for subsequent replacement of the *tetRA* resistance cassette with *yfp* (coding for Venus, a yellow-fluorescent protein derivative by Nagai *et al.* (59)). The *yfp* gene was PCR amplified by the proofreading polymerase Accuzyme using pCS2 (Nagai *et al.* (59)) as the PCR template and forward primer 5'-42Bp + ATG GTG AGC AAG GGC GAG-3' and reverse primer 5'-42Bp + TTA CTT GTA CAG CTC GTC-3'. The resulting PCR fragment of about 0.8 kB length consisted of the *yfp* gene and 5' and 3' flanking regions of 42 base pairs homology to the downstream or upstream target gene region respectively. Afterwards the PCR product was gel purified using the Qiagen gel purification kit and subsequently eluted in 20 μl elution buffer (Qiagen).

The tetracycline resistance cassette at the 3'-end of *fliO*, *fliP*, *fliQ* and *fliR* respectively, was replaced using λ-RED mediated recombination and tetracycline-sensitive selection for the loss of the *tetRA*-cassette, as described above for the construction of clean deletion mutants of *fliO*, *fliP*, *fliQ* and *fliR*. Following the tetracycline-sensitive selection, the correct fusion construct was confirmed by sequencing analysis. A list of strains, chromosomally expressing C-terminal YFP fu-

TABLE 2.8: List of strains, chromosomally expressing FliO, FliP, FliQ and FliR-GA_3-YFP fusions, genotype and primers used for PCR amplification of the replacement *yfp* fragment are displayed in the table.

STRAINS AND GENOTYPE	**FORW PRIMER #**	**REV PRIMER #**
TH10595 *fliO6721-yfp*	#2049 (fliO-VenusEnd-for)	#2050 (fliO-VenusEnd-Rev)
TH10671 *fliP6735-yfp*	#2051 (fliP-VenusEnd-for)	#2052 (fliP-VenusEnd-Rev)
TH10552 *fliQ6712-yfp*	#2026 (fliQ-VenusEnd-for)	#2027 (fliQ-VenusEnd-Rev)
TH10594 *fliR6720-yfp*	#2053 (fliR-VenusEnd-for)	#2054 (fliR-VenusEnd-Rev)

sions to FliOPQR and primers used for PCR amplification of the *yfp* gene, is given in Table 2.8.

2.15 Fluorescence microscopy and image analysis

Cells expressing YFP and CFP fusions were analyzed using a Delta Vision optical sectioning microscope (Applied Precision) as described afterwards. An overnight culture was diluted 1:100 in 1 ml LB and grown to mid-logarithmic stage for 1 and 2 hours respectively. The cells were washed with 1 ml PBS (phosphate-buffered saline) and resuspended in 100 μl PBS. About 1 μl of cells were applied to a glass slide and the cells immobilized using poly L-lysine treated coverslips (18 x 18 mm, thickness 1 1/2). The cells were visualized using the Delta Vision optical microscope with appropriate excitation and emission wavelengths for YFP and CFP respectively. Subsequently images were aquired using Delta Vision SoftWorkX software (Applied Precision) and figures were assembled using iWork 06 (Apple Computer).

2.16 Isolation of chromosomal Tn*5phoA* fusions

Phage P22 harboring Tn*5phoA* was grown on *S. typhimurium* strain TH1317 using lysogen induction of phage P22 by mitomycin C (Benson and Goldman (9)). Subsequently, 0.5 ml of an overnight culture of TH10498 (*zec-8469::*Tn*10*dTc) was infected with 0.5 ml phage P22 (Tn*5phoA*) followed by incubation for 30 minutes at room temperature. Afterwards, 4.5 ml LB broth was added and the phage/cell mixture was incubated for 30 minutes at 37 °C. Phage χ was added to 1 ml of the mixture with a multiplicity of infection (moi) of 5. Subsequently, molten top agar was added and the mixture poured on selection plates containing 50 μg/ml kanamycin and 40 μg/ml XPho (5-bromo-4-chloro-3-indolylphosphat-*p*-toluidine). Kan^R, XPho$^+$ and phage χ^R colonies were subsequently made phage-free by streaking for single colonies on green plates. After screening for motility, the Tn*5phoA* insertion was mapped using phage complementation with phage P22 grown on TH1721 (*fla-1191(*Δ*flgA-J1191*)), TH1722 (*fla-2157(*Δ*flgG-L2157*)), TH1723 (*fla-2039(*Δ*tar-flhDC2039*)), TH1724 (*fla-2018(*Δ*flhA-cheA2018*)), TH1725 (*fla-2050(*Δ*fliA-D2050*)), TH1726 (*fla-2211(*Δ*fliE-K2211*)) and TH1727 (*fla-2195 (*Δ*fliJ-R2195*)) respectively.

2.17 FlgM-secretion assay

FlgM-secretion assays were performed as described previously (Karlinsey *et al.* (36)) with the following adaptions. Briefly, overnight cultures of *S. typhimurium* strains LT2, TH3730 and TH10874 respectively were diluted 1:100 in 3 ml LB and in the case of TH3730, the culture was grown to OD_{600} of 0.5 and transcription of *flhDC* was induced by addition of tetracycline (15 μg/ml) with further incubation for 1 hour at 37 °C. Afterwards, the cells were pelleted and washed twice with 3 ml LB containing appropriate CCCP dilutions and tetracycline. To control for DMSO-

induced effects, 0.5% DMSO was added to samples not treated with CCCP. After resuspension in fresh media, the cells were incubated for 30 minutes at 37 °C and immediately kept on ice until further treatment. *S. typhimurium* LT2 cultures were grown to OD_{600} of 0.8 and washed twice with 3 ml LB containing appropriate CCCP dilutions. After resuspension in fresh media, the cells were incubated at 37 °C for 30 minutes and kept on ice until further treatment. TH10874 cultures were grown in LB supplemented with 0.2% L-arabinose and treated as described for *S. typhimurium* LT2. For detection of secreted FlgM, 2 ml samples were pelleted for 5 minutes at 13,000 rpm in a tabletop centrifuge and 1.8 ml of the supernatant was saved and filtered through a 0.45 μm pore-size cellulose acetate filter (Nagene) to remove remaining bacterial cells. 1.6 ml of the filtrate was then filtered through a prewetted 0.45 μm pore-size BA85 nitrocellulose filter (Schleicher & Schuell) for protein binding. Afterwards, the proteins were eluted by addition of 40 μl of 2x SDS sample buffer (Laemmli and Favre (38)) and heat treatment for 30 minutes at 65 °C. For detection of intracellular FlgM, the pelleted cells were resuspended in 50 μl of 1x SDS sample buffer and boiled for 10 minutes. Pellet and supernatant fractions were adjusted to 20 OD_{600} LT2 equivalents per μl, and 200 OD_{600} equivalents were loaded onto a 16.5% glycerine sodium dodecyl sulfate-polyacrylamide glycerine gel and analyzed by immunoblotting using anti-FlgM antibodies as described below.

2.18 Quantitative immunoblotting

Intra- and extracellular levels of FlgM protein were determined by quantitative immunoblotting. After separation by sodium dodecyl sulfate-polyacrylamide gel electrophoresis (SDS-PAGE) on 16.5 % glycerine gels, the proteins were electrotransferred to a Hybond-P PVDF transfer membrane. FlgM protein was detected using serum-purified anti-FlgM rabbit polyclonal antibodies (dilution 1 : 10,000; Hughes *et al.* (34)) and immunostained with horseradish-peroxidase conjugated anti-rabbit polyclonal antibodies (dilution 1 : 10,000; Biorad) using the enhanced-

chemiluminescence ECL Plus detection kit (Amersham Biosciences). Densitometric measurements of FlgM bands were performed by analysing the scanned blots with the software ImageJ 1.36b for Mac OSX (Rasband (63)).

2.19 Determination of cytoplasmic ATP levels

Cytoplasmic ATP was detected using the firefly luziferase assay (time-stable ATP determination kit; Biaffin, Germany). Overnight cultures of *S. typhimurium* LT2 were diluted 1:50 in LB and grown to an optical density OD_{600} of about 0.8. The cells were pelleted and resuspended in LB supplemented with 10 and 30 μM CCCP respectively, or in LB supplemented with 0.5% DMSO for samples not treated with CCCP. The resuspended cells were incubated at 37 °C and samples were taken at time points 0, 15, 30 and 60 minutes after addition of CCCP. 0.5 ml of the samples were centrifuged and the resulting pellets washed twice with resuspension buffer (100 mM Tris-HCl (pH 7.75), 2 mM EDTA). Afterwards the cell suspension was adjusted to OD_{600} of 1.0. For the release of cytoplasmic ATP, the samples were boiled for 2 minutes (Lundin and Thore (41)) and centrifuged to remove cell debris. 50 μl of the resulting supernatant was added to 50 μl of luziferase reagent in a 96-well plate and the luminescence at 560 nm was read with a TopCount NXT Microplate scintillation and luminescence counter (Packard).

2.20 Random mutagenesis of *fliR* using error-prone polymerase chain reaction

Error-prone polymerase chain reaction of *fliR* was accomplished using different amounts (1, 2 and 5 U respectively) of *Taq* DNA polymerase (Promega) and primers # 2024 fliR-PCR-for and # 2025 fliR-PCR-rev. The purified PCR product was electroporated in competent TH10589 (Δ*araBAD6608::fliR* Δ*fliR6661::tetRA* / pKD46) cells

and subsequently selected for the loss of the *tetRA*-cassette by tetracycline-sensitive selection as described above. Tet^S transformants were streaked for single colonies on LB-plates and tested for motility on motility plates. Replacement of the tetracycline resistance cassette was confirmed by PCR and subsequently, non-motile *fliR* mutants were examined by sequencing analysis.

2.21 Isolation and characterization of motile revertants of strain TH10605 (*fliO1087*) and TH10607 (*fliO1089*)

Motile revertants of *S. typhimurium* strains TH10605 (*fliO1087* (L91R)) and TH10607 (*fliO1089* (V72G)) respectively, were isolated by poking single colonies of TH10605 and TH10607 respectively into motility plates followed by incubation at 30 °C, 37 °C as well as 42 °C. Motile revertants appeared after about one day incubation and were further isolated for single colonies on LB plates. Subsequently, isolated motile revertants were again tested for motility and 6 motile revertants of TH10605 (*fliO1087*) and 7 motile revertants of TH10607 (*fliO1089*) were kept for further examination.

For mapping of the suppressor mutation two different approaches were used. TH10605 and TH10607 were transduced with phage P22 grown on TH3264 (*zec-7080::*Tn*10*dTc), resulting in TH10820 (*fliO1087 zec7080::*Tn*10*dTc (Tet^R linked 46% to *fliO1087*)) and TH10821 (*fliO1089 zec7080::*Tn*10*dTc (Tet^R linked 36% to *fliO1089*)) respectively. Phage P22 grown on TH10820 and TH10821 was used for infection of the motile revertants, followed by selection on tetracycline resistance and screening for motility. Alternatively, phage P22 grown on TH3933 (*motA5461::*Mu*d*J) was crossed with motile revertants followed by selection for Kan^R, resulting in TH11531 - TH11543. For subsequent mapping of the *fliO1087* suppressor mutation, phage P22 grown on TH10738 (*motA5461::*Mu*d*J *fliO1087 zec-8469::*Tn*10*Tc) was used for infection of TH11531 - TH11536 followed by selection on Tet^R and screening for Lac$^+$ and Lac$^-$ phenotypes respectively on MacConkey-lactose plates. Likewise

for mapping of the *fliO1089* suppressor mutation, phage P22 grown on TH10739 (*motA5461*::Mu*d*J *fliO1089 zec-8469*::Tn*10*Tc) was crossed with TH11537 - TH11543 followed by selection for tetracycline resistance and screening for Lac^+ and Lac^- phenotypes respectively on MacConkey-lactose plates. About 400 to 600 transductants of each suppressor mutation were screened for Lac phenotypes.

2.22 Computational programs used for homology search, sequence alignment and topology prediction.

DNA and protein sequences of the genes *fliO* (locus tag: STM1978; GeneID: 1253499), *fliP* (locus tag: STM1979; GeneID: 1253500), *fliQ* (locus tag: STM1980; GeneID: 1253501) and *fliR* (locus tag: STM1981; GeneID: 1253502) were retrieved from the *Salmonella typhimurium* LT2 genome (GenBank: AE006468; McClelland *et al.* (52)). Protein sequences of FliO, FliP, FliQ and FliR respectively were subsequently used for homology search at the Swiss Institute of Bioinformatics (Gasteiger *et al.* (28)) using the NCBI BLAST2 service. Afterwards, a selection of homologous proteins was aligned for sequence similarity using the multiple sequence alignment program ClustalW (Chenna *et al.* (15)) at the European Bioinformatics Institute (European Molecular Biology Laboratory). For the prediction of transmembrane helices, the HMMTOP v.2.0 server was used (Tusnady and Simon (79, 80)). Alignment and topology prediction data was subsequently visualized using the alignment shading software TEXshade for LATEX2e (Beitz (7, 8)).

3 BACTERIOPHAGE χ (CHI)

3.1 Introduction

Bacteriophage χ is a phage that only attacks flagellated and motile strains of enteric bacteria. It was first discovered by Sertic and Boulgakov (70, 71) and Meynell (54) described that phage χ needs rotating flagella for its infection. Electron microscopy pictures, presented by Meynell (54), show phage χ attached to flagella.

It has been shown that phage χ translocates along the rotating filament "like a nut on a bolt" (Samuel *et al.* (65), Berg and Anderson (11), Schade *et al.* (68)), until it injects its DNA into the cell at the base of the flagellum. However, the direction of rotation of the filament is important, since only counter-clockwise (CCW) rotation of the flagellum allows phage χ to travel along the filament towards the flagellum base (Samuel *et al.* (65)).

In this study, different protocols for purification of phage χ were compared in order to obtain sufficient plaque forming units (pfu) for genome sequencing analysis. Since the direction of rotation of the flagellum is important for phage χ translocation towards the flagellum base, the question whether phage χ is also sensitive for two different flagellin variants, FliC and FljB respectively, was examined. Although FliC and FljB are identical for the first 171 amino acids and last 48 amino acids and show a overall identity of 73 %, about 180 surface-exposed amino acids in the middle domain of FliC and FljB respectively vary in a much higher degree (37 % identities), therefore resulting in distinct antigenic properties (Bonifield and Hughes (13)).

3.2 Results

3.2.1 Growth and purification of bacteriophage χ

For growth of bacteriophage χ several different approaches were compared.

1. Phage χ was grown on log-phase cultures of *S. typhimurium* LT2 in tryptone broth (TB) as described by Schade and Adler (67). Briefly, an overnight culture of *S. typhimurium* LT2 was diluted 1:100 in TB and grown to about 10^8 cells/ml. About $6 \cdot 10^6$/ml cells were added to about $6 \cdot 10^5$ pfu/ml of phage χ and grown for 8 hours at 37 °C. Growth of phage χ on *S. typhimurium* LT2 in TB resulted in phage χ titers of about $2 - 9 \cdot 10^9$ pfu/ml. Addition of $MgSO_4$ and $CaCl_2$ showed no significant increase in phage titers.

2. Phage χ was grown on saturated cultures of *S. typhimurium* strain TH3730 (tetracycline - induced flagellar gene expression). *S. typhimurium* TH3730 was grown to saturation (about 10^9 cells/ml) in medium containing 15 μg/ml tetracycline. About 10^9 pfu/ml of phage χ (moi = 1) was added and incubated for 4 hours for a single burst at 37 °C. Growth of phage χ on *S. typhimurium* TH3730 resulted in phage χ titers of about $10^8 - 10^9$ pfu/ml.

3. Phage χ was grown on log-phase cultures of *S. typhimurium* LT2 in LB medium supplemented with E salts (Vogel and Bonner (84)) and 0.2% glucose. *S. typhimurium* LT2 was grown to OD_{600} of about 0.5 and phage χ was added in a multiplicity of infection (moi) of about 3 - 4 and incubated overnight at 37 °C. Growth of phage χ on *S. typhimurium* LT2 in LB medium resulted in phage χ titers of about $3 - 5 \cdot 10^{10}$ pfu/ml.

For growth of phage χ in concentrations sufficient for genome sequencing, several *S. typhimurium Fels*$^-$ strains were examined for motility and phage χ sensitivity. *S. typhimurium* strains TH470 (*leuA414 supE attA::[P22 sieA44 16-amH1455 tpfr49] Fels-*), TH473 (*leuA414 supE hsdSB(r-m+) Fels-*) and TH10106 (Δ*[Fels2,Gifsy1,Gifsy2]*)

showed reduced motility, whereas TH471 (*leuA414 hsdSB(r-m+) Fels-*) showed motility comparable to *S. typhimurium* wildtype strain LT2 and was subsequently used for growth of phage χ. *S. typhimurium* strain TH471 was grown to OD_{600} of 0.6 and a single plague of phage χ was added. After overnight incubation at 37 °C, the remaining cells and debris were pelleted and the supernatant containing phage χ used for large-scale growth of phage χ. Titers of phage χ of about $9 \cdot 10^9$ pfu/ml were obtained and purified phage χ was used by Prof. Roger Hendrix (Pittsburgh Bacteriophage Institute) for genome sequencing analysis.

3.2.2 Virulence of bacteriophage χ is independent of expression of flagellin variants FliC and FljB respectively

In order to examine, whether virulence of phage χ is dependent on the expression of either one of the two distinct flagellin proteins FliC and FljB respectively, phage χ was grown on both *S. typhimurium* strain TH6232 (Δ*hin-5717::FRT (fljBA-OFF)*) and TH6233 (Δ*hin-5718::FRT (fljBA-ON)*).

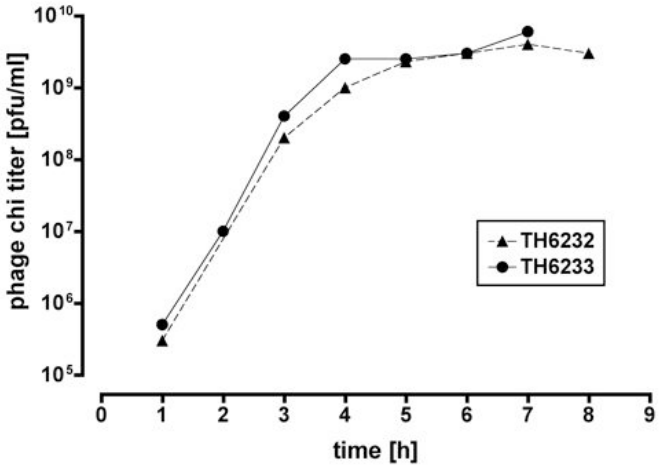

FIGURE 3.1: Plaque forming units (pfu) per ml of bacteriophage χ grown on *S. typhimurium* strain TH6232 (fljBC OFF) and TH6233 (fljBC ON) respectively. *S. typhimurium* TH6232 and TH6233 express the antigenically distinct flagellin proteins FliC and FljB respectively. (■) TH6232 (fliC ON); (●) TH6233 (fljB ON).

An overnight culture of TH6232 (fliC ON) and TH6233 (fljB ON) was diluted 1:100 in tryptone broth and grown for 1 hour at 37 °C. Subsequently, $6 \cdot 10^5$ pfu/ml of phage χ was added and samples were taken every hour for measurement of the op-

tical density OD_{600} and for titering of phage χ. As displayed in Figure 3.1, phage χ does not distinguish between the antigenically distinct flagellin proteins FliC and FljB.

3.3 Discussion

Bacteriophage χ, which only attacks motile enteric bacteria expressing functional flagella, is a very interesting object to study. This work shows that the highest titers of phage χ can be obtained by growth of highly motile *S. typhimurium* strains in LB medium supplemented with E salts and 0.2 % glucose. In this study we purified phage χ to concentrations sufficient for DNA sequencing analysis of the phage χ genome, which should reveal interesting features of the genetic mechanism and abilities of a phage attacking only motile, flagellated bacteria.

Furthermore, this work shows that virulence sensitivity of phage χ is independent of the expression of the distinct flagellar filament proteins FliC and FljB respectively. As shown in Figure 3.1, phage χ grows equally well on *S. typhimurium* strain TH6232 expressing FliC and TH6233 expressing FljB. Based on our results, it is obvious that surface-exposed amino acids of the flagellin proteins are not important for phage χ attachment to the filament. This result may be explained by the findings of Samuel *et al.* (65), who showed that both the CCW rotation and the structure of the helical grooves of the filament are essential for infection by phage χ. Therefore one can speculate that only the mechanical and overall structural conditions and attributes of the flagellum are important for attachment and translocation of phage χ to the filament and not direct protein-protein interactions. The fact that phage χ infects only motile bacterial strains provides a useful tool for genetic studies. For instance, phage χ can be used for positive selection for the loss of motility. In addition, phage χ might be interesting in terms of the recently re-discovered bacteriophage therapy, a new approach where bacteriophages are used for specific targeting of multi-resistant, pathogenic bacteria (Stone (75), Summers (76)).

4 CONSTRUCTION OF *tetRA*-INSERTIONS AND DELETION MUTANTS

4.1 Introduction

It has been shown before that the gene products of *fliO*, *fliP*, *fliQ* and *fliR* are essential for the export of flagellar secretion substrates (Minamino and Macnab (56)). In this study we constructed several strains harboring a tetracycline resistance cassette (consisting of the genes *tetR* and *tetA*) 15 base pairs after the ATG start codon and 15 base pairs before the stop codon, using λ-RED mediated recombination and selection for tetracycline resistance. The chromosomal *tetRA*-insertion strains at the 3'-end of *fliO*, *fliP*, *fliQ* and *fliR* respectively were subsequently used for construction of C-terminal in-frame fusions of the yellow fluorescent protein YFP, as described in Materials and Methods.

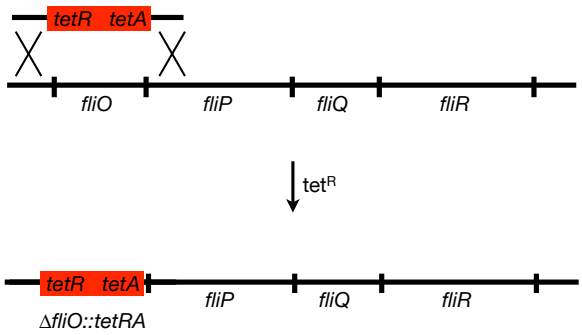

FIGURE 4.1: Schematic construction of a Δ*fliO-tetRA* deletion strain. Using λ-RED mediated recombination and selection for tetracycline resistance, *fliO* was replaced by insertion of a tetracycline resistance cassette.

Additionally, we constructed deletion strains of *fliO*, *fliP*, *fliQ* and *fliR*, whereas the inserted *tetRA*-cassette replaced the respective gene starting 15 base pairs after the ATG start codon to 15 base pairs before the stop codon, using λ-RED mediated recombination and selection for tetracycline resistance, as shown in Figure 4.1.

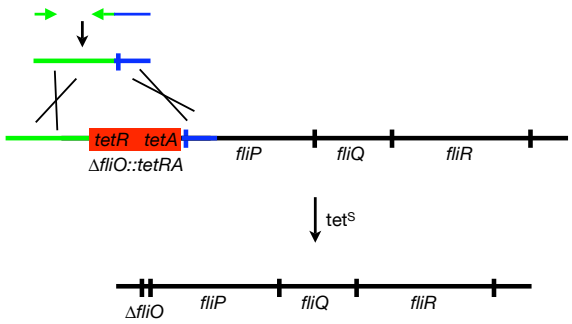

FIGURE 4.2: Schematic construction of a Δ*fliO* clean deletion strain. A small DNA fragment harboring a clean deletion of *fliO* was PCR amplified using a small upstream primer and a large, 60-nt primer with homologies as indicated by the colors. The resulting PCR fragment of about 100 bp length was electroporated in a Δ*fliO-tetRA* deletion strain, followed by subsequent selection for the loss of the *tetRA* resistance cassette using tetracycline-sensitive selection.

The chromosomal *tetRA*-deletion strains were subsequently used for construction of clean, in-frame deletion mutants of *fliO*, *fliP*, *fliQ* and *fliR* respectively. As displayed in Figure 4.2, the *tetRA*-cassette was replaced by a small DNA fragment harboring the clean deletion, using λ-RED mediated recombination and selection for tetracycline sensitivity as described in Materials and Methods.

4.2 Results

4.2.1 Motility of *tetRA*-insertion mutants

We constructed *S. typhimurium* strains harboring a tetracycline resistance cassette insertion at the 5'-start and 3'-end of *fliO*, *fliP*, *fliQ* and *fliR* respectively as described in Materials and Methods. As displayed in Figure 4.3, only strain TH10418 harboring a *tetRA*-cassette at the end of *fliR* showed normal motility on motility plates in the absence of tetracycline. All other *tetRA*-insertion strains were non-motile under these conditions.

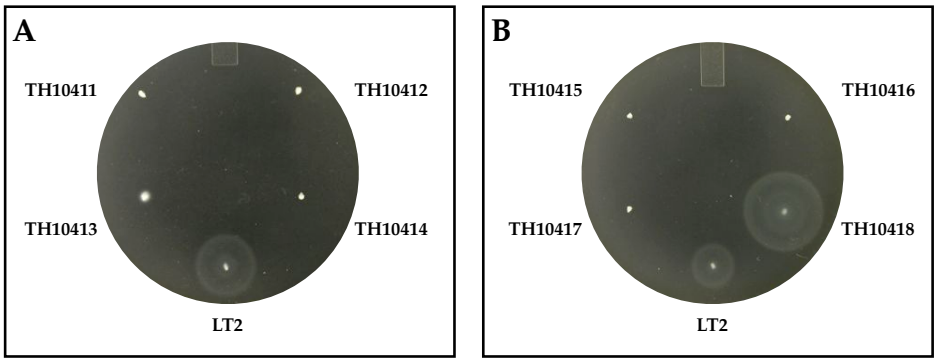

FIGURE 4.3: Motility of *tetRA*-insertions strains in absence of tetracycline. A single colony of the respective *tetRA*-insertion strains was poked in motility plates lacking tetracycline and incubated for about 5 hours at 37 °C.
Left panel (A): Motility of TH10411(*fliO6650::tetRA (after aa5)*), TH10412 (*fliO6651::tetRA (after aa121)*), TH10413 (*fliP6652::tetRA (after aa5)*) and TH10414 (*fliP6653::tetRA (after aa241)*) compared to wildtype *S. typhimurium* LT2.
Right panel (B): Motility of TH10415 (*fliQ6654::tetRA (after aa5)*), TH10416 (*fliQ6655::tetRA (after aa85)*), TH10417 (*fliR6656::tetRA (after aa5)*) and TH10418 (*fliR6657::tetRA (after aa260)*) compared to wildtype *S. typhimurium* LT2.

In presence of tetracycline (induction of the *tetRA* genes), the *tetRA*-insertion strains TH10412 (*tetRA*-insertion at the 5'-end of *fliO*) and TH10418 (*tetRA*-insertion at the 5'-end of *fliR*) showed weak motility, as displayed in Figure 4.4.
A summary of all constructed strains harboring a *tetRA* insertion, deletion or a clean

deletion, as well as the observed motility on motility plates in the presence and absence of tetracycline, is displayed in Table 4.1.

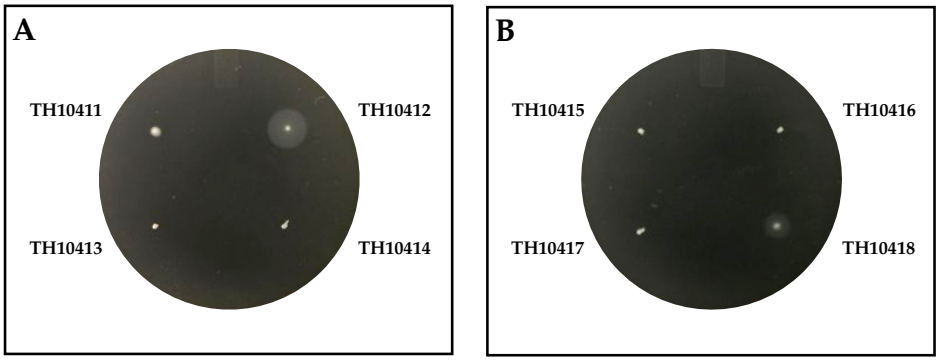

FIGURE 4.4: Motility of *tetRA*-insertions strains in presence of tetracycline. A single colony of the respective *tetRA*-insertion strains was poked in motility plates containing 15 μg/ml tetracycline and incubated for about 5 hours at 37 °C.
Left panel (A): Motility of TH10411(*fliO6650::tetRA (after aa5)*), TH10412 (*fliO6651::tetRA (after aa121)*), TH10413 (*fliP6652::tetRA (after aa5)*) and TH10414 (*fliP6653::tetRA (after aa241)*).
Right panel (B): Motility of TH10415 (*fliQ6654::tetRA (after aa5)*), TH10416 (*fliQ6655::tetRA (after aa85)*), TH10417 (*fliR6656::tetRA (after aa5)*) and TH10418 (*fliR6657::tetRA (after aa260)*).

4.2.2 Motility of clean-deletion mutants

Clean deletion strains of *fliO*, *fliP*, *fliQ* and *fliR* respectively were constructed by replacement of the tetracycline resistance cassette, using λ-RED mediated recombination and selection for the loss of the *tetRA*-cassette as described in Materials and Methods. The clean deletion strains TH10548, TH10549, TH10550 and TH10551 showed no motility on motility plates incubated for 5 hours or overnight at 37 °C as displayed in Table 4.1.

4.2.3 Phage-complementation of clean-deletion mutants

Phage complementation was used in order to show that Δ*fliO*, Δ*fliP*, Δ*fliQ* and Δ*fliR* clean-deletion strains can be complemented by introduction of the respective wild-type genes. Phage P22 grown on *fliO*$^-$, *fliP*$^-$, *fliQ*$^-$ and *fliR*$^-$ strains respectively, was used for infection of Δ*fliO*, Δ*fliP*, Δ*fliQ* as well as Δ*fliR* clean-deletion strains as described in Materials and Methods.

TABLE 4.1: List of *fliO*, *fliP*, *fliQ* and *fliR tetRA*-insertion and clean-deletion strains constructed in this study. The table compares the motility of the different strains in presence and absence of tetracycline (Tc).

STRAIN	**GENOTYPE**	**MOTILITY -Tc**	**MOTILITY +Tc**
TH10411	*fliO6650::tetRA (after aa5)*	non-motile	non-motile
TH10412	*fliO6651::tetRA (after aa121)*	non-motile	++
TH10413	*fliP6652::tetRA (after aa5)*	non-motile	non-motile
TH10414	*fliP6653::tetRA (after aa241)*	non-motile	non-motile
TH10415	*fliQ6654::tetRA (after aa5)*	non-motile	non-motile
TH10416	*fliQ6655::tetRA (after aa85)*	non-motile	non-motile
TH10417	*fliR6656::tetRA (after aa5)*	non-motile	non-motile
TH10418	*fliR6657::tetRA (after aa260)*	+++	+
TH10419	Δ*fliO6658::tetRA (*Δ*aa6-121)*	non-motile	non-motile
TH10420	Δ*fliP6659::tetRA (*Δ*aa6-241)*	non-motile	non-motile
TH10421	Δ*fliQ6660::tetRA (*Δ*aa6-85)*	non-motile	non-motile
TH10422	Δ*fliR6661::tetRA (*Δ*aa6-260)*	non-motile	non-motile
TH10548	Δ*fliO6708 (*Δ*aa6-121)*	non-motile	N/A
TH10549	Δ*fliP6709 (*Δ*aa6-241)*	non-motile	N/A
TH10550	Δ*fliQ6710 (*Δ*aa6-85)*	non-motile	N/A
TH10551	Δ*fliR6711 (*Δ*aa6-260)*	non-motile	N/A

As an example, the phage complementation assay of clean-deletion strain TH10548 (Δ*fliO*) is displayed in Figure 4.5. Briefly, TH10548 was infected with phage P22 grown on $fliO^-$, $fliP^-$, $fliQ^-$ and $fliR^-$ strains respectively and incubated overnight at 37 °C. When the phage introduced wildtype *fliO* in TH10548 (Δ*fliO*) cells, the particular infected cell regained motility. Since the phage, that introduced the wildtype *fliO* cannot insert in the bacterial chromosome and thus cannot replicate, only the originally infected mother cell is motile and swarms outwards, while leaving a trail of non-motile daugher cells behind. The non-motile daughter cells of this particular cell form visible colonies. As displayed in Figure 4.5, the clean deletion strain TH10548 (Δ*fliO*) could be complemented by phage P22 grown on strains harboring wildtype *fliO*. The phage grown on the $fliO^-$ strain could not comple-

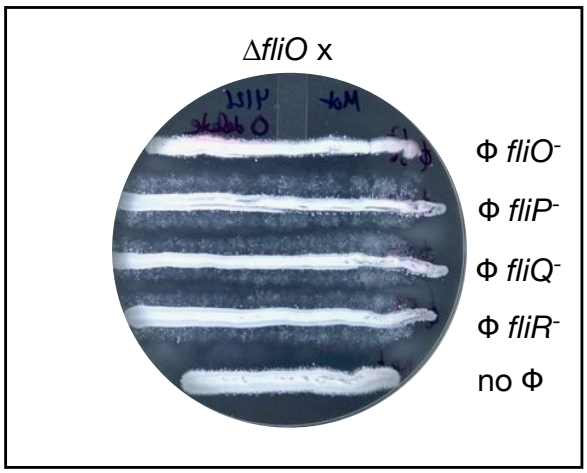

FIGURE 4.5: TH10548 (Δ*fliO*) phage complementation assay. TH10548 (Δ*fliO*) was infected with phage P22 grown on *fliO*$^{-}$, *fliP*$^{-}$, *fliQ*$^{-}$ and *fliR*$^{-}$ strains respectively, and streaked on motility plates. After overnight incubation, regained motility of TH10548 (Δ*fliO*) cells could be observed as trails of non-motile daughter cells. Details of the process are discussed in the text.

ment the Δ*fliO* strain for obvious reasons. Furthermore, one can see that the clean deletion of *fliO* is non-polar on downstream genes, since even the phages grown on *fliP*$^{-}$, *fliQ*$^{-}$ and *fliR*$^{-}$ strains respectively, were able to complement the Δ*fliO* clean deletion as shown in Figure 4.5. The same results were obtained by phage complementation with TH10549 (Δ*fliP6709*), TH10550 (Δ*fliQ6710*) and TH10551 (Δ*fliR6711*), showing that the clean deletion mutations of Δ*fliO*, Δ*fliP*, Δ*fliQ* and Δ*fliR* respectively, are non-polar and can be complemented by introduction of the respective wildtype genes (data not shown).

4.3 Discussion

In this study several strains, harboring *tetRA* insertions in *fliO*, *fliP*, *fliQ* and *fliR* were constructed. The *tetRA* insertions at the 5'-start and 3'-end of *fliO*, *fliP*, *fliQ* and *fliR* respectively, provide a useful tool for the subsequent construction of chromosomally expressed N-terminal or C-terminal fusion proteins, as shown later in this work. For instance, the 3'-end *tetRA*-insertion strains were used for construction of C-terminal YFP fusions.

We showed that the *tetRA*-insertions at the 5'-start and 3'-end of *fliO*, *fliP*, *fliQ* and *fliR* respectively, were non-motile in the absence of tetracycline on motility plates with the exception of TH10418 (*tetRA* at the 3'-end of *fliR*). This result might be explained with the presumption, that insertion of *tetRA*-cassettes in *fliO*, *fliP*, *fliQ* and *fliR* respectively, prevent correct translation of the polycistronic mRNA of *fliLMNOPQR*. Since *fliR* is the last gene in this operon, the insertion of the *tetRA*-cassette at the end of *fliR* has presumably no effect on the upstream genes.

In the presence of tetracycline, the genes of the *tetRA* cassette are induced. The *tetRA* genes are transcribed in opposite direction, whereas *tetR* reads out of the 5'-end and *tetA* reads out of the 3'-end. It is likely, that the transcription of the *tetRA* genes results in polar effects on the transcription of the up- and downstream genes and consequently, most of the *tetRA*-insertions at the 5'-start or 3'-end are non-motile. Surprisingly, the *tetRA*-insertions at the 3'-end of *fliO* (TH10412) and *fliR* (TH10418) are slightly motile, as shown in Figure 4.4. In the case of TH10418 one can argue that expression of the *tetRA* genes can only interfere with transcription of *fliR* and since the *tetRA*-insertion is located at the 3'-end, some functional FliR protein might be made. If this is the case and if only a few copies of functional FliR protein are necessary, this might be the explanation for the observed slightly motile phenotype. In the case of TH10412, the insertion of the *tetRA*-cassette at the 3'-end of *fliO* most likely interferes with *fliO* transcription, but might allow correct expression of the downstream genes *fliP*, *fliQ* and *fliR*. In the presence of tetracycline, the

tetRA genes are highly induced and since *tetA* reads out of the 3'-end, the expression of *tetA* might result in an over-expression of the downstream genes *fliP, fliQ* and *fliR* and thus leading to the observed slightly motile phenotype, if expression of *fliO* is not essential and can be complemented by over-expression of *fliP, fliQ* and *fliR*.

Furthermore, we showed that *fliO*, *fliP*, *fliQ* and *fliR* respectively are essential for motility of *S. typhimurium*, which confirms the results of Minamino and Macnab (56). The clean-deletion strains constructed in this study showed no motility, but could be complemented by phage complementation, as well as by introduction of plasmids expressing a wildtype version of the respective deleted gene (Koushik Paul, unpublished data). Interestingly, over-expression of *fliP* in the Δ*fliO* background was able to complement the loss of *fliO*, which leads to a motile phenotype (Koushik Paul, unpublished data). This result is consistent with the observed motile phenotype of the *tetRA* insertion strain at the 3'-end of *fliO* (TH10412) in the presence of tetracycline as described above.

In addition, this work shows that clean deletions of Δ*fliO*, Δ*fliP*, Δ*fliQ* and Δ*fliR* were non-polar by complementing the deletion strains using phage P22 grown on *fliO*$^-$, *fliP*$^-$, *fliQ*$^-$ and *fliR*$^-$ strains respectively. This is an important finding, since it allows the use of the Δ*fliO*, Δ*fliP*, Δ*fliQ* and Δ*fliR* clean deletion strains for complementation studies, like the verification of the functional expression of plasmid-based *fliO*, *fliP*, *fliQ* and *fliR* constructs.

5 DETERMINATION OF FliOPQR TOPOLOGY

5.1 Introduction

The topology of FliO, FliP, FliQ and FliR was first predicted by Ohnishi *et al.* (61) as displayed in Figure 5.1.

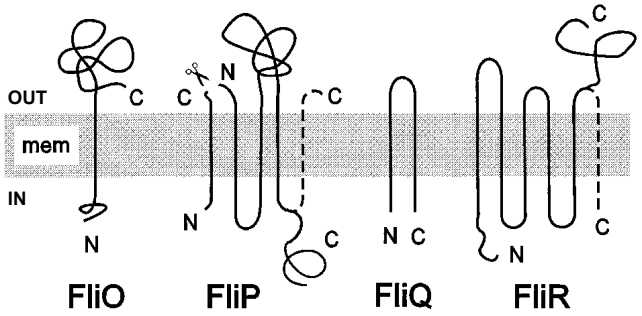

FIGURE 5.1: Schematic of the topology of FliO, FliP, FliQ and FliR respectively as predicted by Ohnishi *et al.* (61). Dashed lines illustrate different possibilities for the transmembrane helices. The figure is adapted from Ohnishi *et al.* (61), Figure 5.

The authors predicted that FliO has a small N-terminal cytoplasmic domain, a single transmembrane (TM) spanning helix and a large C-terminal periplasmic domain. FliP is predicted to have either 4 or 5 TM spanning helices, with a large periplasmic loop between TM 3 and 4, and the C-terminus facing to either the cytoplasm or the periplasm, depending on the number of TM helices. Ohnishi *et al.* (61) also showed that FliP harbors a N-terminal signal peptide and, after cleavage of the signal peptide, the N-terminus of the mature FliP is predicted to be located in the

periplasm. FliQ is predicted to have two TM helices with the N- and the C-terminus located in the cytoplasm. The topology of FliR is predicted to have either 5 or 6 TM spanning helices, a cytoplasmic N-terminus and the C-terminus located in either the cytoplasm or the periplasm, depending on the number of TM helices.

However, no experimental data on the topology of FliOPQR was available until now. In this chapter, new topology predictions are discussed, which were obtained by using the program HMMTOP (Tusnady and Simon (79, 80)) as described in Materials and Methods. Furthermore, LacZ and PhoA activity of plasmid-based FliOPQR C-terminal β-galactosidase (LacZ) and alkaline phosphatase (PhoA) fusion constructs is discussed.

5.2 Results

5.2.1 FliOPQR topology prediction using HMMTOP v. 2.0

The protein sequence of *S. typhimurium* FliO, FliP, FliQ and FliR respectively, was used for a homology search, followed by subsequent alignment of selected sequences using ClustalW (Chenna *et al.* (15)). The alignment data was used for prediction of transmembrane spanning helices and topology using the HMMTOP v. 2.0 server (Tusnady and Simon (79, 80)) as described in Materials and Methods. Figure 5.2 displays a so-called fingerprint alignment of *S. typhimurium* FliO and FliP with selected homologous sequences, and Figure 5.3 displays the fingerprint alignment of *S. typhimurium* FliQ and FliR. The method of visualisation of an alignment as a fingerprint was first described by Frohlich (26) and implemented by Beitz (7) in his alignment shading software TEXshade for LATEX2e. In a fingerprint alignment, the single residues are presented as vertical lines, whereas the similarity of the single residues in the alignment is converted to shades of gray. The darker the vertical lines are, the higher is the similarity of the aligned residues.

As displayed in Figure 5.2 panel A, FliO is highly conserved in the region of the

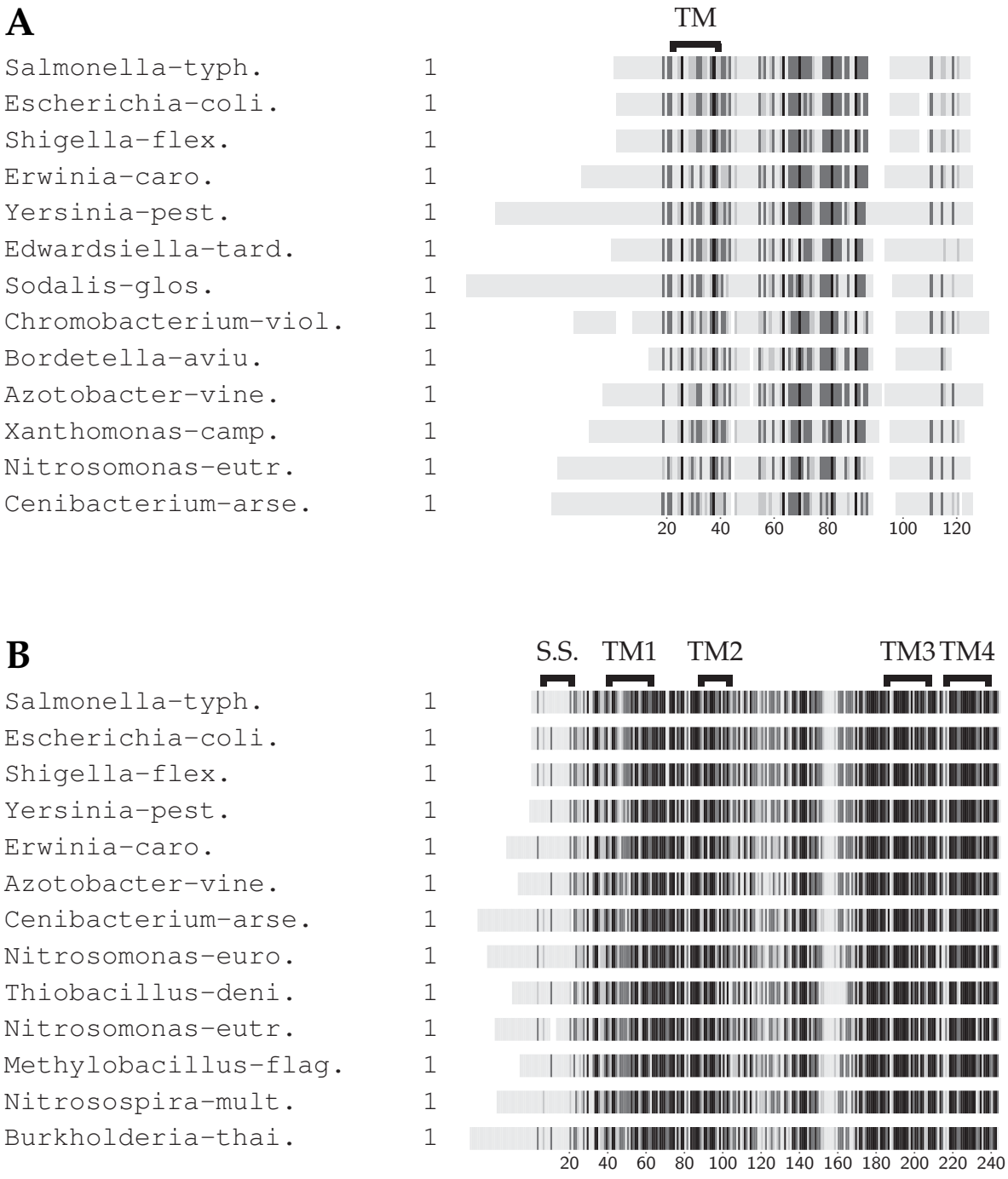

FIGURE 5.2: Fingerprint alignment of FliO and FliP with selected sequences from a homology search. The alignment of FliO is displayed in the upper panel A, and the alignment of FliP is displayed in the lower panel B. The transmembrane (TM) spanning helices were determined using the topology prediction program HMMTOP (Tusnady and Simon (79, 80)) and are shown at the top of the alignment. The similarity of the residues is presented in shades of grey, with white corresponding to lack of identity and black corresponding to complete identity. TM = transmembrane helix; S.S. = signal sequence.

predicted transmembrane helix and also in the region of residues 55 to 95 of the C-terminal, cytoplasmic domain. It is quite striking that most parts of FliO appear to be only weakly conserved, with the remarkable exception of the conserved TM helix and the conserved region in the C-terminal domain. The program HMMTOP predicted for FliO a N-terminal periplasmic and a C-terminal cytoplasmic domain, contrary to the previous prediction of Ohnishi *et al.* (61). Our prediction is also supported by the fact that highly conserved positively charged lysine and arginine residues are located directly after the predicted TM helix (Figure 6.1), indicating a cytoplasmic location of the C-terminus because of the positively charged periplasm.

The fingerprint alignment of FliP is displayed in Figure 5.2 panel B. FliP is predicted to have 4 TM helices with both the N-terminus, after cleavage of the N-terminal signal peptide, and the C-terminius located in the periplasm. It is intriguing that most parts of FliP seem to be highly conserved, with the exception of the N-terminal signal peptide and parts of the large periplasmic loop between TM2 and TM3. The TM helices and the end of the large periplasmic loop right before TM3, are the most conserved parts of the protein, indicating functionally important regions.

Figure 5.3 displays the fingerprint alignments of FliQ and FliR respectively. FliQ is predicted to have two TM helices with both the N-terminus and the C-terminus of the protein located in the cytoplasm, confirming the previous prediction of Ohnishi *et al.* (61). The fingerprint alignment shows a highly conserved periplasmic loop between the two TM domains (Figure 5.3 panel A), but also parts of the TM helix 2 and the N-terminus of FliQ appear to be conserved.

The topology prediction of FliR is rather uncertain. Therefore, our prediction of 8 TM spanning helices is distinct from the previous FliR topology prediction of FliR by Ohnishi *et al.* (61), who predicted 5 or 6 TM helices. In our prediction, both the N-terminus and the C-terminus are located in the cytoplasm. Similarly to FliO, most parts of FliR are not conserved. As shown in Figure 5.3 panel B, only the residues around TM3 and TM4 (residues 80 - 120) as well as around TM7 and TM8 (residues 180 - 220) are conserved. The loop between TM3 and TM4 as well as the loop between TM7 and TM8, is predicted to be located in the periplasm, suggesting a possible important structural and / or functional role of these parts of the protein.

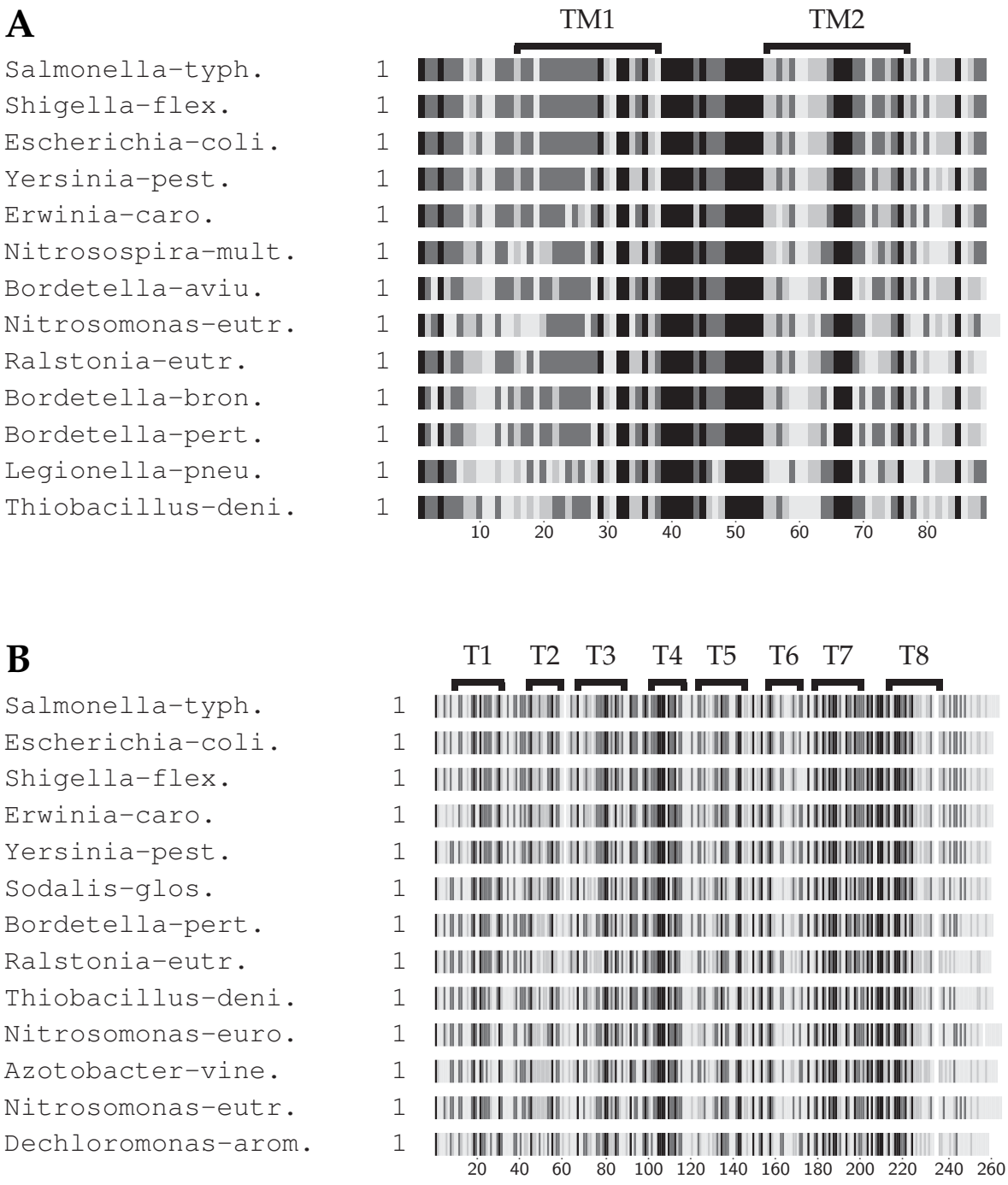

FIGURE 5.3: Fingerprint alignment of FliQ and FliR with selected sequences from a homology search. The alignment of FliQ is displayed in the upper panel A, and the alignment of FliR is displayed in the lower panel B. The transmembrane (TM) spanning helices were determined using the topology prediction program HMMTOP (Tusnady and Simon (79, 80)) and are shown at the top of the alignment. The similarity of the residues is presented in shades of grey, with white corresponding to lack of identity and black corresponding to complete identity. TM (T) = transmembrane helix.

5.2.2 Activity of FliO, FliP, FliQ and FliR, C-terminal β-galactosidase (LacZ) and alkaline phosphatase (PhoA) fusions

The isolation of β-galactosidase (LacZ) and alkaline phosphatase (PhoA) fusions to FliO, FliP, FliQ and FliR respectively, using *in vivo* transposon mutagenesis of Tn*lacZ*/IN and Tn*phoA*/IN (Manoil and Bailey (49)), was not successful. Therefore, plasmid-based C-terminal LacZ and PhoA fusions to FliOPQR were constructed *in vitro* as described in Materials and Methods.

TABLE 5.1: List of β-galactosidase (LacZ) and alkaline phosphatase (PhoA) activity of FliOPQR fusion constructs. Plasmids pEM8 - 11 were electroporated in TH10548 (Δ*fliO6708*), TH10549 (Δ*fliP6709*), TH10550 (Δ*fliQ6710*) and TH10551 (Δ*fliR6711*) respectively and motility was assayed on motility plates in the presence and absence of 100 μM IPTG. Plasmids pEM12 - 15 were transformed in TH3357 (*E. coli* CC191 Δ*lac* Δ*phoA*) and LacZ activity was assayed on plates containing 40 μg/ml X-Gal and 100 μM IPTG. Plasmid pEM18 was transformed in CC191 and PhoA activity was assayed on plates containing 40 μg/ml X-Pho and 100 μM IPTG.

PLASMID	**DESCRIPTION**	**MOTILITY (+/- IPTG)**	**LacZ ACTIVITY (+/- IPTG)**	**PhoA ACTIVITY (+/- IPTG)**
pEM8	*fliO* w/o stop, P_{trc}	+/+	N/A	N/A
pEM9	*fliP* w/o stop, P_{trc}	-/+	N/A	N/A
pEM10	*fliQ* w/o stop, P_{trc}	-/-	N/A	N/A
pEM11	*fliR* w/o stop, P_{trc}	+/+	N/A	N/A
pEM12	*fliO-lacZ* under P_{trc}	N/A	+/+	N/A
pEM13	*fliP-lacZ* under P_{trc}	N/A	-/-	N/A
pEM14	*fliQ-lacZ* under P_{trc}	N/A	+/+	N/A
pEM15	*fliR-lacZ* under P_{trc}	N/A	+/+	N/A
pEM16	*fliO-phoA* under P_{trc}	N/A	N/A	N/A
pEM17	*fliP-phoA* under P_{trc}	N/A	N/A	N/A
pEM18	*fliR-phoA* under P_{trc}	N/A	N/A	-/-

Table 5.1 displays the constructed plasmids as well as the motility, LacZ activity and PhoA activity of the constructs as far as tested. It has to be noted that a 5'-*Nco*I restriction site has been used for cloning of *fliO*, *fliP*, *fliQ* and *fliR* (the genes lacking the respective stop codon) into pTrc99A. The *Nco*I restriction site introduced an additional, out-of-frame 5'-ATG, which may affect the correct expression of the cloned genes. As displayed in Table 5.1, pEM8 (*fliO* without stop) and pEM11(*fliR* without stop) were able to complement *fliO* and *fliR* null strains respectively, and showed motility comparable to the wildtype. This result indicates a normal expression of the cloned genes despite of the additional 5'-ATG. In the case of pEM9 (*fliP* without stop), motility was only observed in the presence of IPTG, and in the case of pEM10 (*fliQ* without stop) no motility was observed.

The LacZ and PhoA activity was assayed in *E. coli* CC191 (Δ*lac* Δ*phoA*). The β-galactosidase fusions to FliO, FliQ and FliR showed LacZ activity, whereas the PhoA fusion to FliR lacked PhoA activity. These preliminary results support the topology predictions that were obtained by the program HMMTOP as described above.

5.3 Discussion

In this chapter, new insights in the topology of the putative flagellar type III secretion apparatus components FliOPQR are discussed. The previous topology prediction of Ohnishi *et al.* (61) has been compared to a new topology prediction, obtained by using the HMMTOP server (Tusnady and Simon (79, 80)). Furthermore, C-terminal LacZ and PhoA fusions to FliOPQR were constructed and analyzed in order to confirm the topology predictions.

However, it has to be mentioned that the choice of restriction sites for cloning of *fliO*, *fliP*, *fliQ* and *fliR* respectively into pTrc99A was sub-optimal and due to the fact that the FliP and FliQ construct did not properly complement the respective null strain, correct expression of these constructs could not be confirmed. One might assume that FliQ is indeed expressed correctly, since the FliQ-LacZ fusion construct

showed β-galactosidase activity, and for functional LacZ expression the in-frame fusion construct has to be expressed properly. In addition, it has been observed before that N-terminal or C-terminal fusions to FliQ renders the fusion protein non-functional in terms of motility. Neither a C-terminal YFP fusion construct as shown later in this work, nor N- or C-terminal His_6-tag constructs (Ohnishi *et al.* (61) and K. Paul, personal communication) were able to complement *fliQ*$^-$ strains. Based on these observations it is not surprising that pEM10 (*fliQ* without stop) could not complement the *fliQ* null strain.

In the case of FliO, we predicted one TM spanning helix and a C-terminal cytoplasmic domain, in contrast to the previous prediction of Ohnishi *et al.* (61). This prediction was confirmed by the construction of a C-terminal LacZ fusion, which showed β-galactosidase activity on LB plates containing X-Gal (5-bromo-4-chloro-3-indolyl-13-D-galactopyranoside). In this respect, it has to be noted that a C-terminal YFP fusion to FliO was also constructed in this work. The strain expressing FliO-YFP fusion protein showed fluorescence while complementing a *fliO* null strain, indicating that the fusion protein is both active (in terms of fluorescence) and functional (in terms of motility). As discussed later in this work, GFP (and the derivative YFP) is only folded properly in the cytoplasm, thus indicating a cytoplasmic location of the C-terminus of FliO.

As displayed in Figure 5.2 panel A, only two parts of FliO are highly conserved. It is quite striking that only the transmembrane spanning helix and the region around residues 55 - 95 in the C-terminal domain appear to be highly conserved. The alignment data indicates that for FliO function, the insertion in the membrane as well as the conserved region of the cytoplasmic domain, is important. Additionally, K. Paul showed that FliO binds specifically to the cytoplasmic protein FliN, but several FliO mutations located in the putative cytoplasmic domain (V72G, L91R, ΔL91-L94) disrupt the binding (K. Paul, unpublished data). Based on these findings, we conclude that the functionally essential C-terminal domain of FliO is indeed located in the cytoplasm, where FliO interacts with FliN.

Our topology prediction data of FliP as well as FliQ, is consistent with the previ-

ous prediction of Ohnishi *et al.* (61). The LacZ fusion to the C-terminus of FliP did not show any β-galactosidase activity. However, correct expression of the cloned FliO-LacZ fusion protein could not be confirmed for reasons discussed above. As displayed in Figure 5.2 panel B, FliP is highly conserved in most parts with the exception of the N-terminal signal peptide sequence and the periplasmic loop between TM helix 2 and TM helix 3. The fact that the transmembrane spanning helices of FliP are highly conserved, implies an important functional role, for example the function as a proton-conducting channel as discussed at the end of this work.

FliQ is predicted to have two TM spanning helices, with both the N-terminus and the C-terminus located in the cytoplasm. The functional C-terminal LacZ fusion confirms this prediction. Figure 5.3 panel A shows an alignment of FliQ and it is striking that the periplasmic loop between TM helix 1 and TM helix 2 is highly conserved, indicating a putative functionally important region, whereby FliQ could interact with periplasmic proteins.

In the case of FliR, we predicted 8 TM spanning helices as opposed to 5 - 6 TM helices by the previous prediction of Ohnishi *et al.* (61). As displayed in Figure 5.3 panel B, most parts of FliR are not conserved. Interestingly, the loop between TM helix 3 and 4, and the loop between TM helix 7 and 8 display conserved residues. According to our prediction, these two loops are predicted to be located in the periplasm and are therefore putative functionally important interaction sites. By using LacZ and PhoA fusions to the very C-terminus of FliR, we could show that the C-terminus is most likely located in the cytoplasm, confirming the topology prediction data. Based on our results, we conclude that the topology prediction obtained by the program HMMTOP is probably correct, although more confirming experiments have to be carried out. β-galactosidase and alkaline phosphatase fusions to the very C-terminus of membrane proteins provide a useful tool for experimentally confirming predicted topologies. The knowledge of the location of conserved domains is important for determining targets for subsequent functional studies and mutagenesis.

6 SUPPRESSOR MUTANTS OF *fliO*

6.1 Introduction

Basically nothing is known about the function and localization of the proteins FliO, FliP, FliQ and FliR respectively. However, insertion of a tetracycline resistance cassette or clean deletion of any of the four genes resulted in a non-motile phenotype, thus confirming the results of Minamino and Macnab (56), who showed that FliOPQR are essential for the export of flagellar secretion substrates. In order to further characterize FliO, we sequenced non-motile *fliO* and *fliP* mutants and isolated motile revertants of two *fliO* point mutations, *fliO1087* (L91R) and *fliO1089* (V72G). The approximate chromosomal location of the suppressor mutations of *fliO1087* and *fliO1089* were mapped and in addition, the non-motile mutations of *fliO* and *fliP*, which were revealed by sequencing analysis, are discussed in this chapter.

6.2 Results

6.2.1 Sequencing analysis of non-motile *fliO* and *fliP* mutants

Non-motile *fliO* and *fliP* mutants TH1756, TH1757, TH10602 - TH10613 (kind gift of S. Yamaguchi) were analyzed by sequencing analysis at the University of Utah HSC Core DNA Sequencing Facility. Genomic DNA was prepared by repeated freeze-boil cycles of cultures grown to mid-log phase and used as a template for

PCR amplification of *fliO* (primers #458 and #2021) and *fliP* (primers #2018 and #2023) respectively. The PCR product was used as the template for sequencing analysis with the following primers. Primer #458 for 5′ to 3′ sequencing of *fliO*, primer #2018 for 5′ to 3′ sequencing of *fliP* and primer #2023 for 3′ to 5′ sequencing of *fliP*. A summary of the revealed mutations of *fliO* and *fliP* respectively is shown in Table 6.1.

TABLE 6.1: List of non-motile *fliO* and *fliP* mutants (S. Yamaguchi) and summary of the mutations revealed by sequencing analysis.

STRAIN	**GENOTYPE**	**DESCRIPTION OF THE MUTATION**
TH1756	*fliO2008*	8 bp-deletion after nt239; out-of-frame after aa80
TH10602	*fliO1077*	single-bp insertion after nt254; out-frame after aa84
TH10603	*fliO1084*	11 bp-deletion after nt252; out-of-frame after aa84
TH10604	*fliO1086*	base exchange C61T; new stop after aa20
TH10605	*fliO1087*	base exchange T272G; **point mutation L91R**
TH10606	*fliO1088*	13 bp-deletion after nt211; out-of-frame after aa70
TH10607	*fliO1089*	base exchange T215G; **point mutation V72G**
TH10608	*fliO1431*	12 bp-deletion after nt271; deletion ΔL91-L94
TH10609	*fliO1485*	12 bp-deletion after nt271; deletion ΔL91-L94
TH1757	*fliP2041*	single-bp deletion at nt668; out-of-frame after aa222
TH10610	*fliP1191*	75 bp-deletion after nt536; **deletion ΔK180-L204**
TH10611	*fliP1193*	single-bp deletion at nt711; out-of-frame after aa237
TH10612	*fliP1544*	414 bp-deletion after nt7; deletion ΔR2-R140
TH10613	*fliP1628*	57 bp-deletion after nt488; **deletion ΔA164-A182**

The sequencing analysis revealed two point mutants of *fliO* with single amino acid exchange as displayed in Table 6.1. It seems striking that all sequenced non-motile *fliO* mutations are located after amino acid 70 in the C-terminal, cytoplasmic domain of FliO. In addition, a multiple sequence alignment of FliO is shown in Figure 6.1. As displayed, all non-motile mutations of FliO are located in a highly

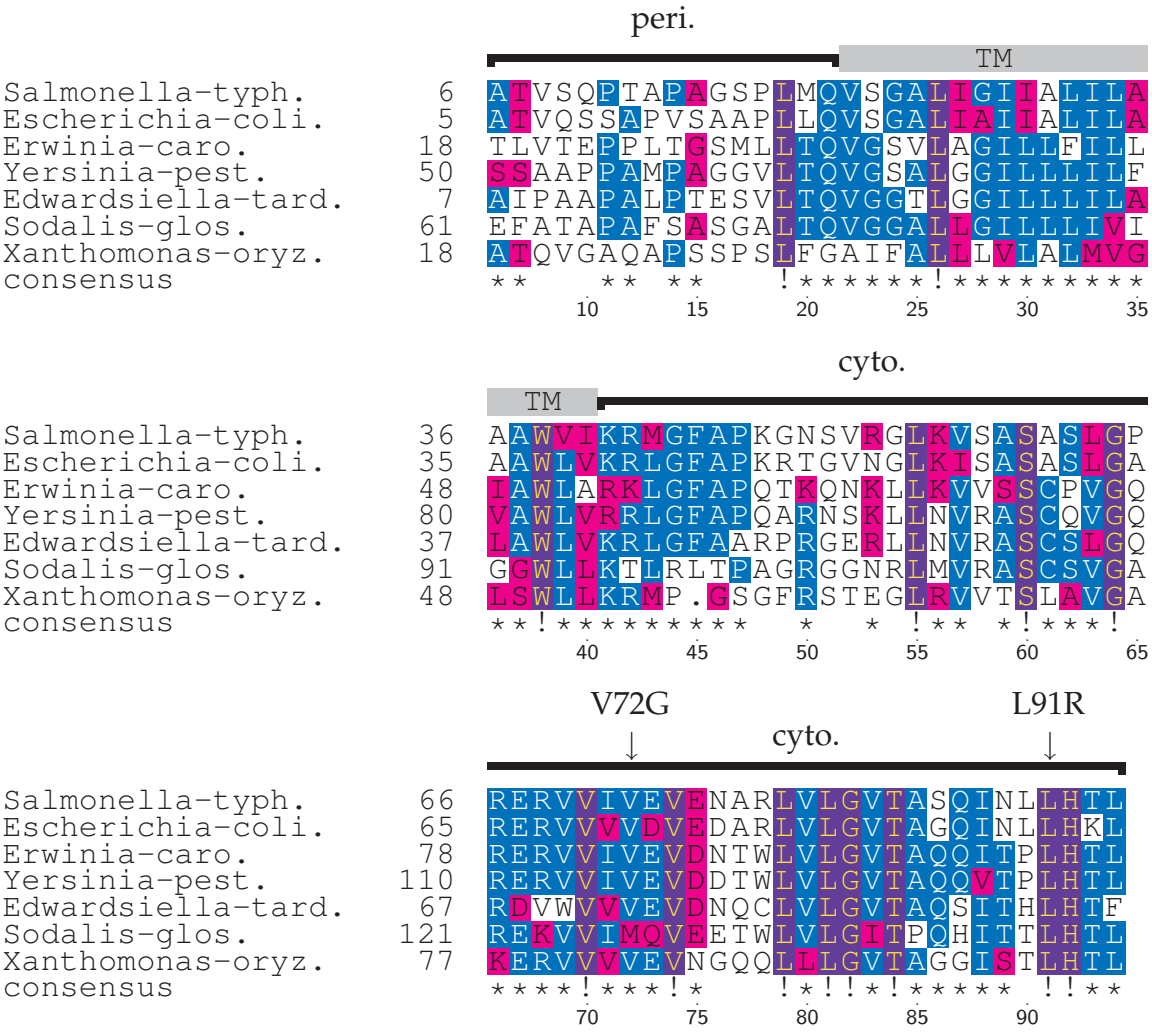

FIGURE 6.1: Alignment of FliO (residues 6 - 94) with selected sequences from a homology search. The transmembrane (TM) spanning helix of FliO was determined using HMMTOP (Tusnady and Simon (79, 80)) and is shown at the top of the alignment. The location of the point mutations V72G (*fliO1089*) and L91R (*fliO1087*) respectively, is indicated with an arrow at the top of the alignment. TM = transmembrane helix; peri. = periplasmic domain; cyto. = cytoplasmic domain. Residues are shaded as follows: conserved residues; similar residues; all match residues

conserved part of the cytoplasmic domain, spanning from residue 55 to residue 95. Likewise, the residues of the point mutations, V72G and L91R, are highly conserved as well.

The sequence analysis of *fliP* revealed two large in-frame deletions (26 and 19 residues respectively). However, no point mutation of *fliP* has been discovered. Interestingly, the deletion of 26 residues of TH10610 (ΔK180 - L204) removes almost

the complete third transmembrane domain of FliP and the deletion of 19 residues of TH10613 (ΔA164 - A182) removes part of the periplasmic loop right before the third transmembrane domain.

6.2.2 Mapping of *fliO1087* and *fliO1089* suppressor mutants

For mapping of the suppressor mutants of *fliO1087* (L91R) and *fliO1089* (V72G), *motA5461::*Mu*d*J was transduced in the respective motile revertant strains as described in Materials and Methods. The resulting strains TH11531, TH11532, TH11534 - TH11543 were crossed with phage P22 grown on TH10738 (*motA5461::*Mu*d*J *fliO1087 zec-8469::*Tn*10*Tc) or TH10739 (*motA5461::*Mu*d*J *fliO1089 zec-8469::*Tn*10*Tc) and transductants were selected for tetracycline resistance (Tc^R near *fliR*). Afterwards, 400 to 600 transductants were screened for Lac^- phenotype on MacConkey-lactose plates. The resulting co-transduction frequencies, based on the linkage between the suppressor mutations of *fliO1087* and *fliO1089* and the Tc^R near *fliR*, are displayed in Table 6.2.

In previous experiments, the distance of the Tc^R near *fliR* (*zec-8469::*Tn*10*Tc) to *fliO1087* and *fliO1089* respectively was determined to be 2.59 kB and 1.95 kB respectively. Using this linkage data, the approximate location of the Tc^R near *fliR* was estimated to be about 260 Bp downstream of the 3'-end of *fliR*. Subsequently, the approximate location of the suppressor mutation was calculated, based on the estimated location of the Tc^R near *fliR* and using the co-transduction data, which was obtained by crossing the motile revertant strains with phage grown on TH10738 and TH10739 respectively. The resulting putative location of the suppressor mutation is displayed in Table 6.2. As shown in Table 6.2, the *fliO1087* (L91R) suppressor mutations map around *fliK - fliL* and the *fliO1089* (V72G) suppressor mutations map around *fliI - fliK*.

TABLE 6.2: Co-transduction frequencies of motile revertant strains TH11531, TH11532 and TH11534 - TH11543 linked to *zec-8469::*Tn*10*Tc (Tc^R near *fliR*). Transductants were screened for lac^- (mot^-) phenoype on MacConkey-lactose plates as described in Materials and Methods. Displayed are the co-transduction frequency (percentage of lac^- (mot^-) transductants) and the resulting distance between the Tc^R near *fliR* and the suppressor mutation. Based on the known linkage of *zec-8469::*Tn*10*Tc to *fliO1087* and *fliO1089*, the putative location of the suppressor mutation was estimated.

MOTILE REVERTANT STRAIN	**CO-TRANSD. FREQUENCY**	**CO-TRANSD. DISTANCE**	**LOCATION OF MUTATON**
TH11531 (*fliO1087* (L91R))	67.9 %	5.18 kB	middle of *fliK*
TH11532 (*fliO1087* (L91R))	72.4 %	4.37 kB	$P_{fliLMNOPQR}$
TH11534 (*fliO1087* (L91R))	74.4 %	4.03 kB	middle of *fliL*
TH11535 (*fliO1087* (L91R))	70.7 %	4.68 kB	end of *fliK*
TH11536 (*fliO1087* (L91R))	74.3 %	4.04 kB	middle of *fliL*
TH11537 (*fliO1089* (V72G))	69.1 %	4.96 kB	middle of *fliK*
TH11538 (*fliO1089* (V72G))	64.1 %	5.89 kB	end of *fliJ*
TH11539 (*fliO1089* (V72G))	69.0 %	4.98 kB	middle of *fliK*
TH11540 (*fliO1089* (V72G))	68.0 %	5.16 kB	middle of *fliK*
TH11541 (*fliO1089* (V72G))	65.1 %	5.70 kB	end of *fliJ*
TH11542 (*fliO1089* (V72G))	64.7 %	5.78 kB	end of *fliJ*
TH11543 (*fliO1089* (V72G))	58.8 %	6.93 kB	middle of *fliI*

6.3 Discussion

In this work, previously uncharacterized non-motile *fliO* and *fliP* mutants, which were originally isolated by S. Yamaguchi, were examined by sequencing analysis. Out of 9 examined *fliO* mutants, 2 point mutations with single amino acid exchange, *fliO1087* (L91R) and *fliO1089* (V72G), and two identical in-frame deletions, TH10608 and TH10609 (ΔL91-L94), were revealed. All other sequenced mutations of *fliO* are also located in the C-terminal, cytoplasmic domain of FliO. As displayed in Figure 5.2 and Figure 6.1, residues 55 - 95 of the C-terminal domain of FliO appear to be

highly conserved, indicating a functionally important region.

In order to further characterize the point mutations of *fliO*, we isolated 6 motile revertants of *fliO1087* (L91R) and 7 motile revertants of *fliO1089* (V72G). The mapping of the suppressor mutation using co-transduction of Tc^R near *fliE* and near *fliR* respectively, and screening for motility as described in Materials and Methods, showed linkage of all suppressor mutations to the Tc^R near *fliE* as well as to the Tc^R near *fliR*. Based on this mapping data, the 3'-end of *fliM* and the complete *fliN* gene of six motile revertants were analyzed by sequencing analysis. However, no mutation has been found in the sequenced genes (data not shown). This result is surprising considering the fact that the mutated FliO proteins (L91R and V72G) did not bind to FliN, in contrast to the strong binding of wildtype FliO to FliN (K. Paul, unpublished data).

For more precise mapping of the suppressor mutation, *motA5461::*Mu*d*J was transduced into the motile revertant strains and, using co-transduction of Tc^R near *fliR*, the location of the suppressor mutation was analyzed by screening for lac^- (mot^-) phenotypes. The *fliO1087* (L91R) suppressor mutations map around *fliK* - *fliL* and the *fliO1089* (V72G) suppressor mutations map around *fliI* - *fliK* (displayed in Table 6.2). Based on the observation that over-expression of *fliP* can complement a Δ*fliO* mutation (K. Paul, unpublished data), we suggest that the suppressor mutation is located in the *fliLMNOPQR* promotor region, resulting in a higher expression level of *fliP* and therefore complementing the non-functional *fliO* mutation.

Out of 5 sequenced *fliP* mutants, no point mutation with single amino acid exchange was found. However, one in-frame deletion of the third transmembrane (TM) domain (TH10610 (ΔK180 - L204)) and one in-frame deletion in one part of the periplasmic loop right before the third transmembrane domain (TH10613 (ΔA164 - A182)) were revealed. As shown in Figure 5.2, most parts of FliP are highly conserved, especially the regions around TM1 - TM2 and TM 3 - TM4. It is quite striking that the deletion of the highly conserved TM3 and the partially deletion of the periplasmic loop before TM3 resulted in a non-motile phenotype, indicating an essential role of this part of FliP.

7 CONSTRUCTION AND localizATION OF FliO-YFP

7.1 Introduction

It has been previously proposed that the membrane components of the flagellar type III secretion apparatus (consisting of the membrane proteins FlhA, FlhB, FliO, FliP, FliQ and FliR) are located within the central pore of the MS-ring in the flagellar basal body (Minamino and Macnab (56), Ohnishi *et al.* (61)). Although Fan *et al.* (23) showed that FliP and FliR are probably located in the flagellar basal body, the cellular localization of FliO and FliQ remains elusive. Sourjik and Berg (74) used YFP fusions to the switch complex protein FliM to visualize localization of components of the flagellar basal body in *Escherichia coli*. The FliM-YFP fusion protein appeared as discrete spots on the side of the cells, which were shown to co-localize with flagellar basal bodies. Similarly to the experiments of Sourjik and Berg (74), we constructed a functional FliO-YFP fusion protein and examined the cellular localization of the fusion protein using fluorescent microscopy. Since it has been shown before that FliM is located within the flagellar basal body structure, we furthermore constructed the motile *S. typhimurium* strain TH10836, expressing functional FliM-CFP and FliO-YFP, in order to show co-localization of FliM-CFP and FliO-YFP.

The cellular localization of FliO-YFP, the localization of FliO-YFP in a Δ*fliF* background, the detection of FliO-YFP and FliQ-YFP fusion proteins by Western Blot analysis and the construction of TH10836 expressing FliM-CFP and FliO-YFP are discussed in this chapter.

7.2 Results

7.2.1 Cellular localization of chromosomally expressed and over-expressed *fliO-YFP*

In this study, we constructed C-terminal YFP fusions to FliO, FliP, FliQ and FliR respectively, using λ-RED mediated recombination as described in Materials and Methods. The FliOPQR-YFP fusion constructs inserted at the normal chromosomal location for the respective genes. A summary of the constructed strains and a brief description of the phenotype is given in Table 7.1.

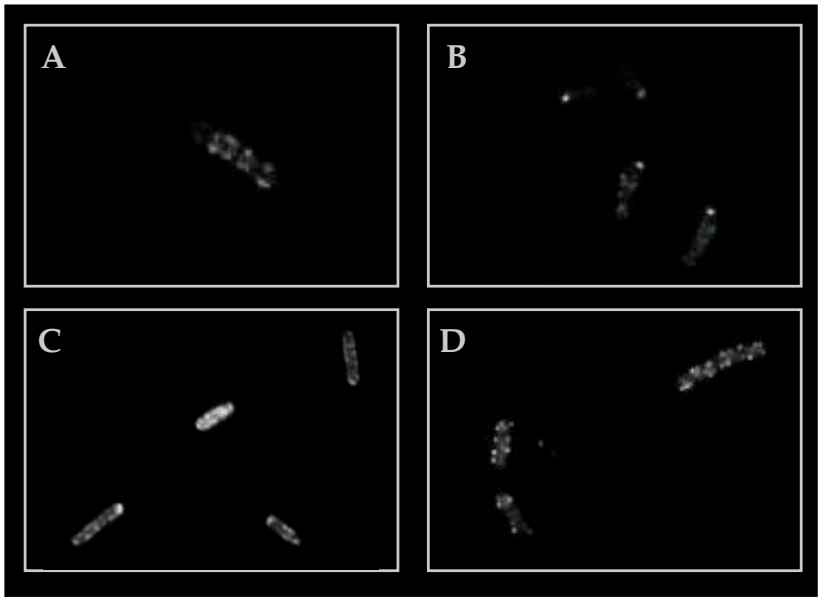

FIGURE 7.1: Cellular localization of chromosomally expressed FliO-YFP, FliM-CFP and over-expressed FliO-YFP. Panel A: discrete spots of fluorescence of chromosomally expressed FliO-YFP in TH10595; panel B: chromosomally expressed FliO-YFP in TH10595; panel C: fluorescence all over the membrane of over-expressed FliO-YFP in TH10766 (Δ*fliO6708* / pEM7 *(FliO-GAGAGA-YFP)*), expression of FliO-YFP induced with 10 μM Na-salicylate; panel D: discrete spots of fluorescence of chromosomally expressed FliM-CFP in TH7503.

C-terminal YFP fusions to FliO, FliP, FliQ as well as FliR were constructed, however only TH10595 expressing FliO-YFP fusion protein showed fluorescence. The FliO-YFP construct is functional, since motility of TH10595 is comparable to

wildtype *S. typhimurium* LT2 (data not shown). As displayed in Figure 7.1 panel A and panel B, the fluorescence of FliO-YFP appeared to be localized in discrete spots, although in same cases only one spot of fluorescence was visible (Figure 7.1 panel B). In cases where FliO-YFP was over-expressed of a pKG116-derived vector, the fluorescence appeared to be all over the membrane, but still in discrete spots as shown in Figure 7.1 panel C. For comparison, the discrete spots of fluorescence observed with a FliM-CFP fusion construct are displayed in Figure 7.1 panel D. The fluorescence of FliM-CFP has been previously shown to co-localize with the flagellar basal body (Aldridge *et al.* (4), Sourjik and Berg (74)).

TABLE 7.1: Summary of FliOPQR C-terminal YFP fusion strains constructed in this study. Strain number, relevant genotype, observed fluorescence and motility are summarized.

STRAIN	**GENOTYPE**	**FLUORESCENCE**	**MOTILITY**
TH10595	*fliO6721* (FliO-$(GA)_3$-YFP)	+	motile
TH10671	*fliP6735* (FliP-$(GA)_3$-YFP)	-	non-motile
TH10552	*fliQ6712* (FliQ-$(GA)_3$-YFP)	-	non-motile
TH10594	*fliR6720* (FliR-$(GA)_3$-YFP)	-	motile
TH10766	Δ*fliO6708* / pEM7 (FliO-YFP)	+	motile
TH10670	Δ*fliF5629::FKF fliO6721* (FliO-YFP)	+	non-motile
TH10668	Δ*fliF5629::FKF fliQ6712* (FliQ-YFP)	-	non-motile
TH10669	Δ*fliF5629::FKF fliR6720* (FliR-YFP)	-	non-motile

Based on the observation of Aldridge *et al.* (4), who showed that the discrete fluorescence spots of FliM-CFP and FliM-YFP disappear in a Δ*fliF* background, a *fliF::FKF* cassette was transduced in TH10595, TH10552 and TH10594. The fluorescence of FliM-CFP in the Δ*fliF* background disappears because FliM assembles onto the MS-ring structure, which is formed by FliF. However, the deletion of *fliF* had no effect on the discrete fluorescence spots of FliO-YFP (data not shown), indicating that FliO is not directly associated with the flagellar basal body.

7.2.2 Detection of FliO-YFP and FliQ-YFP fusion proteins by Western Blot analysis

Since only the C-terminal fusion of YFP to FliO showed fluorescence, the question remained whether the YFP fusions to FliP, FliQ and FliR were degraded immediately after translation. To test this possibility, the YFP fusion proteins were detected by Western Blot analysis using anti-GFP antibodies (kind gift of M. Babst). FliO-YFP and FliQ-YFP fusion protein was detected as displayed in Figure 7.2 lane 4 (plasmid-expressed FliO-YFP without induction), lane 5 (plasmid-expressed FliO-YFP with 10 μM Na-salicylate induction), lane 6 (chromosomally expressed FliO-YFP) and lane 8 (chromosomally expressed FliQ-YFP).

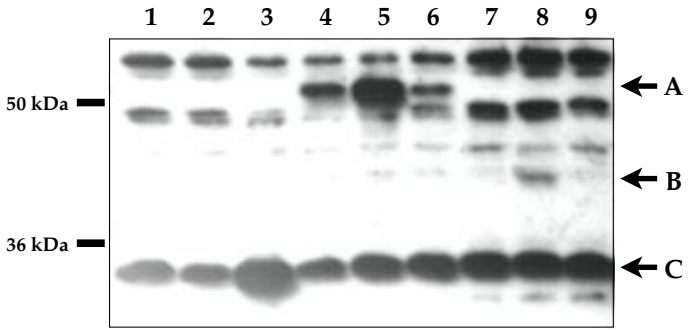

FIGURE 7.2: Detection of FliO-YFP and FliQ-YFP fusion proteins by Western Blot analysis using primary anti-GFP polyclonal antibodies (rabbit; Invitrogen) and secondary horseraddish-peroxidase conjugated polyclonal anti-rabbit antibodies (goat; Biorad). Lane 1, *S. typhimurium* LT2 control; lane 2, TH8537 (Δ*araBAD949::yfp*); lane 3, TH8537 induced with 0.2 % L-arabinose; lane 4, TH10766 (Δ*fliO6708* / pEM7 (FliO-GAGAGA-YFP)); lane 5, TH10766 induced with 10 μM Na-salicylate; lane 6, TH10595 (*fliO6721-yfp* (FliO-GAGAGA-YFP)); lane 7, TH10671 (*fliP6735-yfp* (FliP-GAGAGA-YFP)); lane 8, TH10552 (*fliQ6712-yfp* (FliQ-GAGAGA-YFP)); lane 9, TH10594 (*fliR6720-yfp* (FliR-GAGAGA-YFP)). Arrow labeled with A: putative FliO-YFP fusion protein; Arrow labeled with B: putative FliQ-YFP fusion protein; Arrow labeled with C: putative YFP protein, only visible in lane 3 because of unspecific background as explained in the text.

Although the calculated molecular mass of FliO-YFP fusion protein is about 40 kD, the detected FliO-YFP fusion protein appears to run at about 55 kDa. FliQ-YFP fusion protein shows a similar behavior, with a calculated molecular mass of the fusion protein of about 37 kDa and a detected band running at estimated 40 -

42 kDa. Because of unspecific background, unfused YFP protein was only detected in cases when YFP was over-expressed (Figure 7.2 lane 3). However, in subsequent experiments using higher salt conditions for the Western transfer, no unfused or degraded YFP protein was detected in cases of FliO-YFP, FliP-YFP, FliQ-YFP and FliR-YFP (data not shown).

7.2.3 Construction of TH10836 (*fliM-CFP* and *fliO-YFP*)

For the construction of TH10836 (*fliM5980* (FliM-GAGAGA-CFP) *fliO6721* (FliO-GAGAGA-YFP) *zea3525::*Tn*10*dCm) P22-mediated transduction was used. A summery of the respective crossings in the construction procedure is given in the following list:

1. ΦTH3073 (*fliM5292::*Mu*d*K) [Phage P22 grown on TH3073] X TH10419 (Δ*fliO6658::tetRA (*Δ*aa6-121)*)
   ⇒ select Kan^R + Tet^R = **TH10737** (*fliM5292::*Mu*d*K Δ*fliO6658::tetRA*)

2. ΦTH1042 (*zea-3525::*Tn*10*dCm near *fliR*) X TH10419
   ⇒ select Cm^R + Tet^R = **TH10736** (*zea-3525::*Tn*10*dCm Δ*fliO6658::tetRA*)

3. ΦTH10736 X TH10595 (*fliO6721-yfp* (FliO-GAGAGA-YFP))
   ⇒ select Cm^R + Tet^S = **TH10759** (*zea-3525::*Tn*10*dCm *fliO6721* (FliO-GAGAGA-YFP))

4. ΦTH10759 X TH10737
   ⇒ select Cm^R + Kan^R + Tet^S = **TH10822** (*fliM5292::*Mu*d*K *fliO6721* (FliO-GAGAGA-YFP) *zea3525*::Tn*10*dCm)

5. ΦTH10737 X TH7503 (*fliM5980* (FliM-GAGAGA-CFP))
   ⇒ select Tet^R + Kan^S = **TH10760** (*fliM5980* (FliM-GAGAGA-CFP) Δ*fliO6658::tetRA*)

6. ΦTH10822 X TH10760
   ⇒ select Cm^R + Kan^S + Tet^S = **TH10836** (*fliM5980* (FliM-GAGAGA-CFP) *fliO6721* (FliO-GAGAGA-YFP) *zea3525::*Tn*10*dCm)

TH10836 (*fliM5980* (FliM-GAGAGA-CFP) *fliO6721* (FliO-GAGAGA-YFP) *zea3525::*Tn*10*dCm) showed motility comparable to wildtype *S. typhimurium* LT2 on motility plates, indicating that both FliM-CFP and FliO-YFP fusion proteins are functional and do not affect expression of up- or downstream genes.

7.2.4 Cellular localization of FliM-CFP and FliO-YFP in TH10836

The *S. typhimurium* strain TH10836, chromosomally expressing a C-terminal fusion of CFP to FliM (FliM-CFP) and a C-terminal fusion of YFP to FliO (FliO-YFP), was used for fluorescence microscopy analysis.

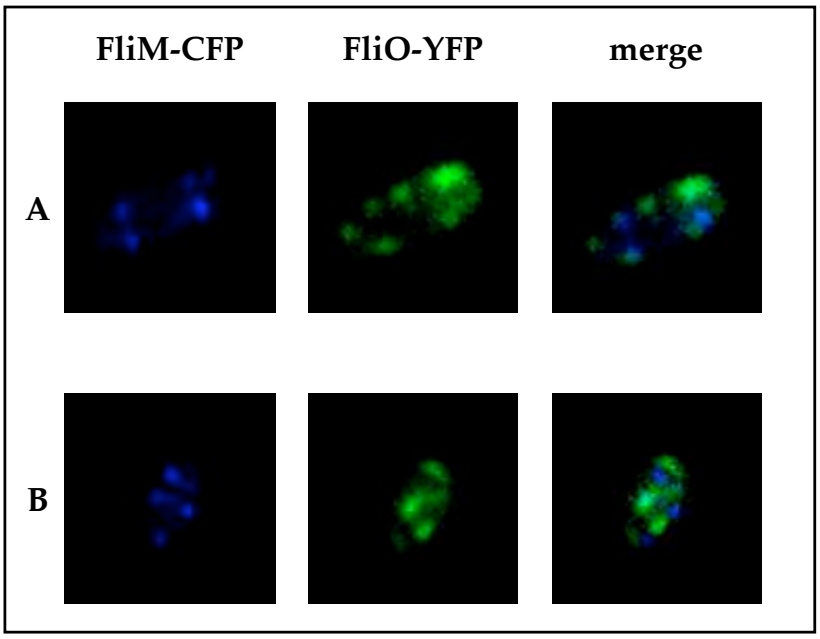

FIGURE 7.3: Cellular localization of chromosomally expressed FliM-CFP and FliO-YFP in TH10836. Displayed are two different cells, labeled as A and B respectively. The visualization of FliM-CFP and FliO-YFP shows that FliO and FliM appear as discrete spots in the cell membrane, but are not co-localized. Left column: FliM-CFP (blue); middle column: FliO-YFP (green); right column: images of FliM-CFP and FliO-YFP are merged.

As displayed in Figure 7.1, FliO-YFP or FliM-CFP fusions alone show fluorescence in discrete spots, which appear at both sides of the cells. Since it has been shown before that FliM-YFP and FliM-CFP fusion proteins are localized within the flagellar basal body structure (Aldridge *et al.* (4), Sourjik and Berg (74)), and FliO is predicted to be localized within the MS-ring structure (Minamino and Macnab

(56), Ohnishi *et al.* (61)), the question remained whether FliO and FliM fusion proteins are indeed co-localized. As described above, we constructed the *S. typhimurium* strain TH10836 for determination of co-localization of FliM and FliO. As displayed in Figure 7.3, FliM-CFP and FliO-YFP fusion proteins appear as discrete spots at the sides of the cells. Visualization of FliM-CFP and FliO-YFP at the same time revealed no co-localization of FliM and FliO respectively as shown in Figure 7.3 (Merged image, right column). This result indicates that FliO is not localized within the flagellar basal body structure, additionally confirming the observation that deletion of *fliF* does not result in disappearance of FliO-YFP discrete fluorescence spots as discussed above.

7.3 Discussion

Little is known about the cellular localization of the putative type III secretion apparatus components FliO, FliP, FliQ and FliR respectively. We constructed chromosomally expressed YFP fusions to the C-terminus of FliO, FliP, FliQ and FliR respectively. However, out of the four constructs only the FliO-YFP fusion construct showed fluoresence. Additionally, strain TH10595 expressing FliO-YFP showed normal motility, indicating that the FliO-YFP fusion protein is functional. FliP-YFP, FliQ-YFP are non-motile and showed no fluorescence, whereas FliR-YFP is motile but no fluorescence was observed. It has been previously shown by Feilmeier *et al.* (24) and Thomas *et al.* (77) that GFP is improperly folded when localized outside the cytoplasm, therefore GFP (and the derivative YFP) can be used as a reporter protein for the cytoplasmic localization of fusion proteins. Since the C-terminal YFP fusion to FliO is functional (motile) and fluoresence could be observed, FliO as well as YFP have to be folded properly. We therefore conclude that the C-terminus of FliO is located in the cytoplasm, confirming topology predictions obtained by using the HMMTOP v.2.0 server (Tusnady and Simon (79, 80)) as discussed in the chapter "Determination of FliOPQR topology".

This work also shows that FliO is probably not localized within flagellar basal body structures using visualization of a C-terminal YFP fusion to FliO. It has been proposed by Minamino and Macnab (56) and Ohnishi *et al.* (61) that FliO is localized within the central pore of the MS-ring of the flagellar basal body. The constructed FliO-YFP fusion protein is expressed from its normal chromosomal location and we observed appearance of fluorescence in discrete spots at the sides of the cell as displayed in Figure 7.1. The same punctuate appearance of fluoresence can be observed with YFP and CFP fusions to FliM (Aldridge *et al.* (4), Sourjik and Berg (74)), where it has been shown that the observed FliM fluorescence co-localizes with flagellar basal body structures. However, the discrete spots of fluorescence of FliO-YFP still appear in a Δ*fliF* strain, whereas the deletion of *fliF* (encoding for the MS-ring) resulted in a disappearance of FliM-CFP and FliM-YFP fluorescence (Aldridge *et al.* (4)), because FliM assembles onto the MS-ring, which is constructed of FliF. This results indicates that FliO is probably not associated with the MS-ring.

Another explanation for the still visible, discrete spots of FliO-YFP fluoresence in the Δ*fliF* strain and for the punctuate fluorescence of FliO-YFP in general, would be degradation of FliO-YFP fusion protein and accumulation in insoluble aggregates (inclusion bodies). However, no unfused or degraded YFP protein was detected by Western Blot analysis of FliOPQR-YFP fusion protein using anti-GFP antibodies. As displayed in Figure 7.2, only FliO-YFP and FliQ-YFP fusion proteins were detected. FliP-YFP and FliR-YFP fusion proteins were not detected, presumably due to low expression levels of FliP and FliR. The detected FliO-YFP and FliQ-YFP constructs appear to run at a higher molecular mass, compared to the calculated molecular mass of the fusion protein, most likely due to big hydrophobic patches of the membrane proteins FliO and FliQ respectively. However, since no potent anti-FliO or anti-FliQ antibodies were available, we could not ultimately confirm the identity of the detected YFP fusion proteins.

For further examination of the cellular localization of FliO, we constructed the *S. typhimurium* strain TH10836, expressing a C-terminal fusion of CFP to FliM (FliM-CFP) and a C-terminal fusion of YFP to FliO (FliO-YFP) from its normal chromosomal location. As displayed in Figure 7.3, discrete spots of fluorescence appeared for

FliO-YFP as well as FliM-CFP, however no co-localization was observed. Since FliM was shown to be localized within the flagellar basal body, this results indicates that FliO is not associated with FliM and therefore not associated with flagellar basal body structures. The co-localization data of FliM-CFP and FliO-YFP confirms the previous observation that discrete spots of FliO-YFP fluorescence are still visible in the Δ*fliF* background.

Based on this results, we conclude that the majority of FliO protein is not associated with the MS-ring and not localized within flagellar basal body structures, contrary to the suggestion of Minamino and Macnab (56) and Ohnishi *et al.* (61).

8 FLAGELLAR TYPE III SECRETION IS DEPENDENT ON THE PMF

8.1 Introduction

The flagellar-specific type III secretion (T3S) apparatus is believed to consist of six integral membrane components (FlhA, FlhB, FliO, FliP, FliQ, FliR) and three soluble components (FliH, FliI, FliJ) (Minamino and Macnab (56)). Most subunits of the flagellum are secreted via the flagellar T3S apparatus (Minamino and Macnab (56)) and Fan and Macnab (22) showed that the secretion is dependent on ATP hydrolysis by the ATPase FliI.

However, Wilharm *et al.* (86) recently showed that *Yersinia enterocolitica* type III secretion is dependent on the proton motive force (PMF). In addition, Galperin *et al.* (27) published in 1982 that the PMF is required for flagellar growth in *Escherichia coli*. Wilharm *et al.* (86) demonstrated that the secretion of the pathogenic proteins called Yops (*Yersinia* outer proteins) by the plasmid-encoded T3S system of *Y. enterocolitica*, can be inhibited by the ionophore carbonyl cyanide m-chlorophenylhydrazone (CCCP). The authors suggested that the export of all T3S systems is driven by the proton motive force in addition to the requirement of ATP hydrolysis for unfolding of secretion substrates.

We were therefore encouraged to examine this hypothesis for the flagellar type III

secretion of *Salmonella enterica* serovar Typhimurium (*S. typhimurium*) and we chose for our analysis the anti-σ^{28} factor FlgM as a known flagellar export protein. In this chapter, we show that flagellar T3S of FlgM is indeed dependent on the proton motive force and moreover, that the proton gradient ΔpH and/or the intracellular proton concentrations are necessary for the export of flagellar secretion substrates.

8.2 Results

8.2.1 Secretion of FlgM is dependent on the proton motive force

It has been previously shown that secretion of the pathogenic Yop proteins of *Yersinia enterocolitica* can be inhibited by treatment with the uncoupler carbonyl cyanide m-chlorophenylhydrazone (CCCP) (Wilharm *et al.* (86)).

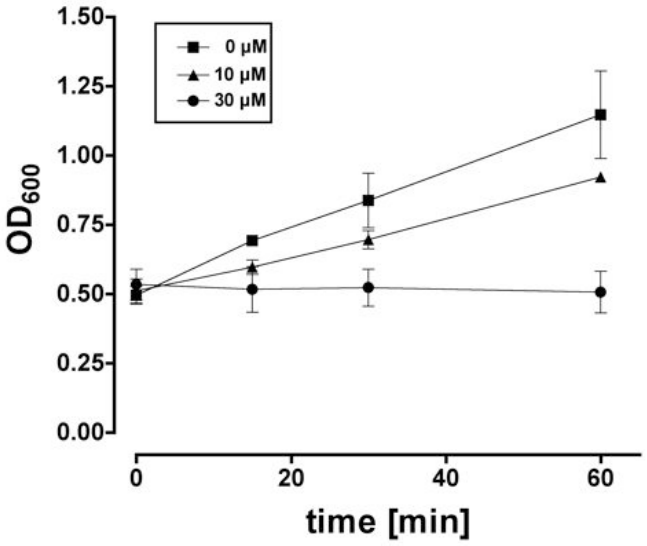

FIGURE 8.1: Growth of *S. typhimurium* LT2 under 0, 10 and 30 μM CCCP treatment. For each CCCP concentration, three independent cultures of LT2 were grown in parallel to an OD_{600} of 0.5. CCCP (10 and 30 μM) or DMSO (0.5 %, untreated control) respectively, was added and the cells grown for an additional 60 minutes at 37 °C. Data are the mean ± SD; 3 independent cultures per data point. (■) 0 μM CCCP; (▲) 10 μM CCCP; (●) 30 μM CCCP.

The ionophore CCCP can diffuse through the cytoplasmic membrane in protonated or non-protonated form respectively (Patton *et al.* (62)). Due to the ΔpH component of the PMF, the protonated form of CCCP diffuses across the cytoplasmic membrane and releases a proton inside the cell. The non-protonated form diffuses back into the periplasm because of the membrane potential ΔΨ, until both components of the proton motive force are completely abolished.

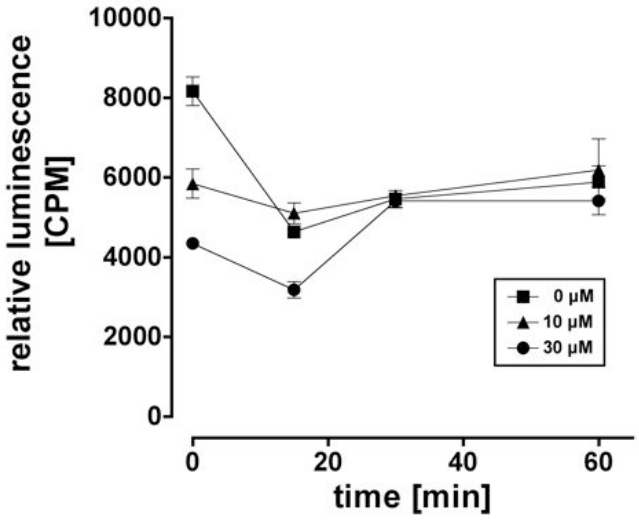

FIGURE 8.2: Effect of CCCP treatment on cytoplasmic ATP levels of *S. typhimurium* LT2. Measurements of cytoplasmic ATP levels were performed in parallel with three independent cultures (two in case of 30 μM CCCP) for each CCCP concentration. The wildtype strain LT2 was grown to an OD_{600} of 0.5. CCCP (10 and 30 μM respectively) or DMSO (0.5 %, untreated control) respectively was added and the cells were grown for an additional 60 minutes at 37 °C. Samples were taken at time points 0, 15, 30 and 60 minutes after addition of CCCP and cytoplasmic ATP was detected using the firefly luziferase assay as described in Materials and Methods. Data are the mean ± SD; 3 independent cultures per data point (2 in case of 30 μM CCCP). (■) 0 μM CCCP; (▲) 10 μM CCCP; (●) 30 μM CCCP.

Overnight cultures of *S. typhimurium* strain LT2 were grown in medium lacking CCCP, washed twice in medium containing appropriate dilutions of CCCP (0, 1, 5, 10, 20, 30 μM) and incubated at 37 °C before analyzing secreted FlgM levels by quantitative immunoblotting as described in Materials and Methods. Concentrations of 10 μM CCCP were sufficient to completely abolish FlgM secretion (data not shown). We found that treatment with 30 μM CCCP resulted in a complete growth

arrest, whereas treatment with 10 μM CCCP resulted in about 20 % slower growth compared to the untreated control (Figure 8.1). At the same time we examined cytoplasmic ATP levels under CCCP inhibition using the Firefly luziferase assay. It has been demonstrated that the ATPase FliI is necessary for flagellar assembly in *S. typhimurium* (Fan and Macnab (22)) and therefore the lack of cytoplasmic ATP could be the reason for the inhibition of FlgM secretion. As shown in Figure 8.2, the cytoplasmic ATP level did not decrease significantly over 60 minutes under 10 and 30 μM CCCP treatment. Our result is consistent with previous reports of the effect of CCCP on intracellular ATP levels (Letellier *et al.* (40), Patton *et al.* (62), Wilharm *et al.* (86)).

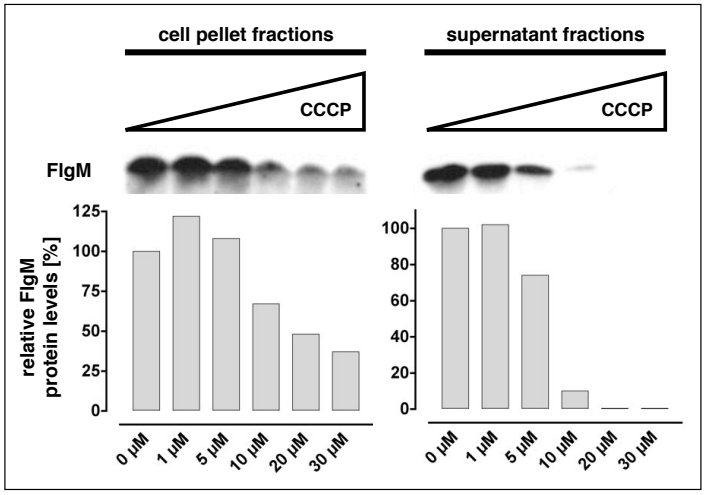

FIGURE 8.3: FlgM secretion in strain TH3730 (Tc-induced flagellar gene expression). TH3730 cells were grown to OD_{600} of 0.5, 15 μg/ml tetracycline was added for induction of the *flhDC* operon and grown for an additional 60 minutes. CCCP was added in concentrations of 0, 1, 5, 10, 20 and 30 μM respectively. 0.5 % DMSO was added to the untreated control. After 30 minutes growth, FlgM secretion was analyzed as described in Materials and Methods and samples of cell pellets and supernatant were immunoblotted using anti-FlgM antibodies.

Overnight cultures of *S. typhimurium* strain TH3730 (Tc-induced flagellar gene expression) were grown to OD_{600} of 0.5 and expression of FlhDC was induced by addition of 15 μg/ml tetracycline, followed by an additional incubation for 1 hour at 37 °C. Afterwards, the cultures were treated with CCCP as described above and FlgM levels in the intra- and extracellular fractions were analyzed. As shown in

Figure 8.3, FlgM secretion was inhibited by 10 μM CCCP and completely abolished by treatment with 20 μM CCCP. Cytoplasmic levels of FlgM decreased about 50 % because of autoregulatory effects of FlgM. If FlgM secretion was PMF dependent, then the abolishment of the PMF would result in cytoplasmic accumulation of FlgM and inhibition of σ^{28}-dependent transcription. This would prevent expression of FlgM from its Class 3 promotor and account for the reduced FlgM levels.

In order to show that the decrease of cytoplasmic FlgM was a result of FlgM auto-inhibition of the σ^{28}-dependent Class 3 *flgM* promotor, we constructed the strain TH10874 (Δ*flgM5628*::FRT Δ*araBAD923*::*flgM*-FRT-Km-FRT $P_{araB934}$) with FlgM under control of a mutated P_{araB} promotor that expresses FlgM at wildtype levels (Aldridge *et al.* (5)). Under these conditions, when *flgM* gene transcription is independent of auto-inhibition, FlgM secretion was abolished by 10 μM CCCP, whereas cytoplasmic FlgM levels remained constant (Figure 8.4).

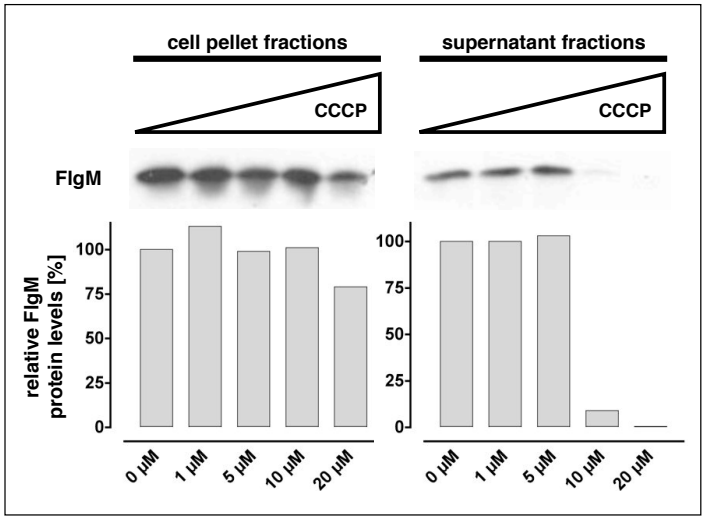

FIGURE 8.4: FlgM secretion in strain TH10874 (P_{ara}-*flgM*$^{+}$). TH10874 cells were grown in LB supplemented with 0.2 % L-arabinose to OD_{600} of 0.8. CCCP was added in concentrations of 0, 1, 5, 10 and 20 μM respectively. 0.5 % DMSO was added to the untreated control. After 30 minutes growth, FlgM secretion was analyzed as described in Materials and Methods and samples of cell pellets and supernatant were immunoblotted using anti-FlgM antibody.

From these experiments we conclude that flagellar type III secretion is also dependent on the proton motive force, in addition to the requirement of ATP as described

previously by Fan and Macnab (22).

8.2.2 Inhibited FlgM secretion can be restored after CCCP treatment

As shown above, FlgM secretion is completely inhibited in cases when the proton motive force is abolished by the uncoupler CCCP. We were interested to see if FlgM secretion could be restored after CCCP treatment by growing the cells in medium lacking CCCP, in order to show the importance of the PMF for flagellar type III secretion.

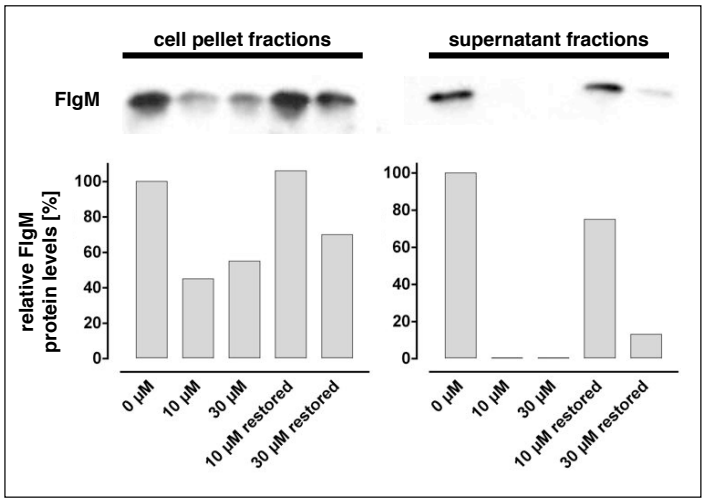

FIGURE 8.5: Restoration of FlgM secretion in strain TH3730. TH3730 cells were grown to OD_{600} of 0.5, 15 μg/ml tetracycline was added for induction of *flhDC* transcription and grown for an additional 60 minutes. CCCP was added in concentrations of 0, 10, and 30 μM respectively. 0.5 % DMSO was added to the untreated control. After 30 minutes growth under CCCP inhibition, samples were taken and CCCP treated cells were washed two times with LB medium lacking CCCP and grown for an additional 30 minutes in LB medium lacking CCCP. FlgM secretion was analyzed as described in Materials and Methods and samples of cell pellets and supernatant were immunoblotted using anti-FlgM antibody.

S. typhimurium strains LT2 and TH3730 were treated as described above and secretion of FlgM was inhibited by addition of 10 and 30 μM CCCP respectively. After 30 minutes of CCCP treatment samples were taken and analyzed for secreted FlgM. FlgM secretion was inhibited completely by abolishment of the proton motive force as shown in Figure 8.5 (data shown for TH3730 FlgM secretion). Afterwards, the

CCCP treated cells were washed two times with medium lacking CCCP, incubated for an additional 30 minutes at 37 °C and secreted FlgM was analyzed again. As shown for TH3730 in Figure 8.5, FlgM secretion was restored to levels of 75 % (10 μM CCCP) and 13 % (30 μM CCCP) respectively as compared to secreted FlgM levels of the untreated control.

8.2.3 Effect of cytoplasmic pH on FlgM secretion

We have described above that the proton motive force is essential for flagellar type III secretion. By using the uncoupler CCCP, both the proton gradient ΔpH and the membrane potential ΔΨ have been abolished.

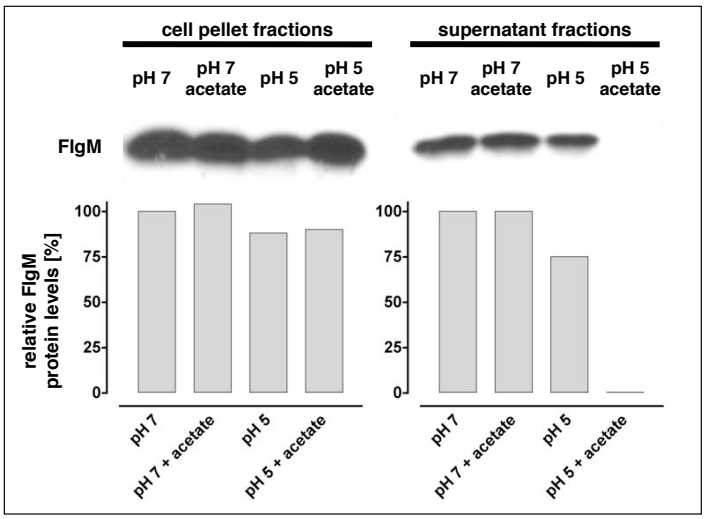

FIGURE 8.6: FlgM secretion in strain TH10874 (P_{ara}-*flgM*$^{+}$) under 34 mM potassium acetate treatment. TH10874 cells were grown in LB supplemented with 0.2 % L-arabinose to OD_{600} of 0.9. The cells were washed twice and resuspended in LB supplemented with 0.2 % arabinose at pH 7 and pH 5 respectively in the presence or absence of 34 mM potassium acetate. After 30 minutes growth, FlgM secretion was analyzed as described in Materials and Methods and samples of cell pellets and supernatant were immunoblotted using anti-FlgM antibody.

To further clarify which component of the PMF is predominantly used for energizing the secretion of substrates, we examined FlgM secretion by treating the cells with potassium acetate. Weak acids such as acetate cross the cytoplasmic membrane in neutral form and release a proton in the cytoplasm, thereby lowering the

cytoplasmic pH, which results in a decrease of the proton gradient ΔpH. It has been previously shown that the collapse of the proton gradient ΔpH by addition of potassium acetate at pH 5, decreases the swimming speed of *E. coli* significantly without major change of the total proton motive force (Minamino *et al.* (55)).

Overnight cultures of TH10874 were grown to OD_{600} of 0.9 in LB medium supplemented with 0.2 % L-arabinose. Afterwards, the cells were washed twice and resuspendend in LB supplemented with 0.2 % L-arabinose at pH 7 and pH 5 respectively, in the presence or absence of 34 mM potassium acetate. The cells were grown an additional 30 minutes and FlgM was detected as described above. As shown in Figure 8.6, we found that FlgM secretion was completely abolished at pH 5 in the presence of 34 mM potassium acetate. This result indicates a dominant role of the proton gradient ΔpH and/or the intracellular proton concentration for the export of flagellar type III secretion substrates.

8.3 Discussion

In this work we show that the export of the flagellar type III secretion substrate FlgM of *S. typhimurium* is dependent on the proton motive force. It has been previously described that the flagellar type III secretion ATPase FliI is necessary for assembly of the flagellum (Fan and Macnab (22)) and although the export of flagellar secretion substrates is ATP-dependent, there are several indications that the hydrolysis of ATP cannot be the only energizing factor of flagellar type III secretion. An important aspect is the necessary speed of flagellar subunits translocation, since the flagellum is usually build within one generation. A simple calculation may clarify the argumentation. One single filament can consist of as many as 20,000 FliC subunits (Macnab (43)) and therefore almost 10 million residues have to be secreted within one generation, which lasts about 20 to 30 minutes. This translates in 5,500 to 8,250 translocated residues per second for the assembly of one flagellum. In the case of the Sec system of *Escherichia coli* (consisting of the integral membrane pro-

tein complex SecYEG and the peripherally bound ATPase SecA) secretory proteins are stepwise translocated over the inner membrane in an ATP-dependent manner. It has been previously shown that around 40 to 50 residues are translocated per cycle (van der Wolk *et al.* (82)) and Tomkiewicz *et al.* (78) calculated the translocation speed of the Sec system to be about 270 residues per minute *in vitro* in the case of proOmpA, which may be even lower *in vivo*. Contrary, the flagellar type III secretion apparatus has to translocate subunits of the flagellum about 1000 times faster, if compared to the ATP-dependent Sec system, which we believe is not possible by hydrolysis of ATP alone. Moreover, the secreted proteins are translocated over the cytoplasmic membrane, through the hook-basal-body and the filament, via a narrow channel of about 2.0 nm in diameter (Yonekura *et al.* (87)). Therefore, it is likely that most substrates have to be secreted in an unfolded state. The work of Lupas and Martin (42) suggests that T3S ATPases belong to a group of unfoldases, thus indicating that the function of FliI may be the unfolding of flagellar secretion substrates prior to the actual export process.

A similar hypothesis has been previously described by Wilharm *et al.* (86), who propose that the *Y. enterocolitica* T3S ATPase YscN unfolds the pathogenic proteins Yops prior to the export process and possibly pushes the unfolded polypeptids into the export channel. The PMF-dependency of *Y. enterocolitica* Yops secretion has been demonstrated by abolishing the proton motive force using the ionophore carbonyl cyanide m-chlorophenylhydrazone (CCCP) (Wilharm *et al.* (86)). Since the flagellar type III secretion apparatus is believed to be the common ancestor of all T3S systems, it seemed quite intriguing that the export of flagellar type III secretion substrates in *S. typhimurium* is also dependent on the proton motive force.

In this work we show the PMF-dependency of flagellar type III secretion using the known T3S substrate FlgM (anti-σ^{28}) for our analysis. Secretion of FlgM could be completely inhibited by addition of 10 μM CCCP in *S. typhimurium* strains LT2, TH3730 and TH10874 as described above. In the case of LT2 and TH3730, cytoplasmic FlgM levels decreased as well due to an autoregulatory effect of FlgM. By inhibiting the export of flagellar type III secretion substrates using CCCP, FlgM cannot be secreted anymore and binds to the flagellar-specific sigma factor σ^{28}, thus

preventing the transcription of class 3 genes (Hughes *et al.* (34)). Since 80 % of the *flgM* gene transcription occurs from a σ^{28}-dependent class 3 promotor (Gillen and Hughes (29), Karlinsey *et al.* (36)), cytoplasmic FlgM protein levels decrease significantly under inhibition of FlgM secretion. Therefore, we had to demonstrate that the decreased cytoplasmic FlgM protein levels were not the reason for the inhibition of FlgM secretion. Expression of wildtype FlgM protein levels from a σ^{28}-independent P_{araB} promotor (Aldridge *et al.* (5)) using strain TH10874, showed constant cytoplasmic FlgM protein levels while inhibiting FlgM secretion under CCCP abolishment of the proton motive force.

Since the previous study of Fan and Macnab (22) showed that flagellar type III secretion is dependent on ATP, one could argue that the lack of cellular ATP under CCCP abolishment of the proton motive force could be the reason for the inhibited FlgM secretion. We examined cytoplasmic ATP levels under CCCP treatment and found no significant decrease of cytoplasmic ATP levels under 10 and 30 μM CCCP inhibition over 60 minutes (Figure 8.2). The initial decrease in the measured relative luminescence can be explained with a regulatory response of the cell to the abolishment of the PMF by the uncoupler CCCP. As soon as the proton gradient collapses, the cell will try to rebuild the ΔpH by pumping protons across the inner membrane under ATP hydrolysis using the F_0F_1 ATPase. Since the proton gradient cannot be restored under CCCP treatment, we presume that the cell will abandon, due to possible regulatory response, the proton pumping under ATP hydrolysis in favor of ATP synthesis by substrate-level phosphorylation in order to maintain cellular functions. This is a possible explanation for the increasing ATP levels after 15 minutes. However, this does not explain the decrease in the measured relative luminescence in the case of the untreated control. One might speculate that the experimental procedure caused stress for the treated cells, resulting in the initially decreased ATP levels, or that the some time is necessary for the cell to switch from aerobic to fermentative growth. In any case, the construction of a mutant where the ATP synthesis is uncoupled from the PMF will be required to address this question appropriately. An uncoupler strain with a *tetRA* deletion of the gene *atpA*, encoding for the α subunit of the ATP synthase, has already been constructed and will be

used for further experiments (F. F. V. Chevance, personal communication).

This work furthermore showed that secretion of FlgM can be restored after CCCP inhibition by growing the cells in medium lacking CCCP. Complete abolishment of the proton motive force by the uncoupler CCCP resulted in inhibition of FlgM secretion, but the PMF rebuilds rapidly by washing and growing the cells in medium lacking CCCP. We showed that FlgM secretion after 30 minutes growth in medium lacking CCCP could be restored up to 80 % of the secretion level of the untreated control, thus demonstrating the importance of the PMF on flagellar type III secretion.

In order to address which component of the proton motive force is the main energizing factor of flagellar type III secretion, we examined FlgM secretion under potassium acetate treatment. Weak acids like acetate cross the membrane in protonated form and acidify the cytoplasm. This results in a decrease in the ΔpH component of the PMF, without affecting the membrane potential $\Delta\Psi$. Addition of 34 mM potassium acetate at pH 5 inhibits motility of *E. coli* (Minamino *et al.* (55)). We found that FlgM secretion could be completely abolished by treatment with acetate at pH5, thus indicating an dominant role of the proton gradient ΔpH and/or the intracellular proton concentration on the export of flagellar type III secretion substrates. This result is supported by the fact that the theoretical pI of several examined flagellar secretion substrates of *S. typhimurium* ranges from 4.68 to 9.1, thus a electrophoretic model cannot account for energization of flagellar type III secretion.

How can the proton gradient ΔpH energize the export of flagellar proteins? One might speculate that the export process uses the conduction of protons from the periplasm to the cytoplasm for conformational changes of the export apparatus. However, our results do not clearly show that it is the proton gradient ΔpH which drives the export process. Another explanation for the inhibited secretion would be protonation of residues of the export apparatus due to high cytoplasmic proton concentration under acetate treatment at pH 5, therefore preventing secretion.

The flagellar type III secretion apparatus consists of 9 proteins, six integral membrane proteins (FlhA, FlhB, FliO, FliP, FliQ, FliR) and three cytoplasmic proteins

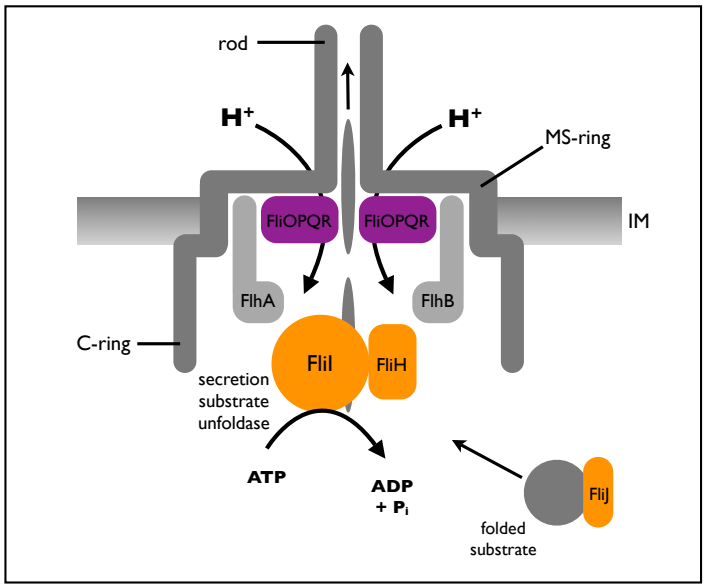

FIGURE 8.7: Hypothetical model of the flagellar type III (T3S) secretion apparatus. The flagellar T3S apparatus consists of 9 proteins, six integral membrane proteins (FlhA, FlhB, FliO, FliP, FliQ, FliR) and three cytoplasmic proteins (FliH, FliI, FliJ)(Minamino and Macnab (56)). In this work we show that flagellar T3S is dependent on the proton motive force, in addition to the requirement of ATP. In the displayed model, we propose that the flagellar-specific ATPase FliI unfolds secretion substrates in an ATP-dependent manner (Fan and Macnab (22)) prior to the actual export process. The translocation of flagellar substrates is energized by the use of the proton motive force. We propose that the integral membrane proteins FliO, FliP, FliQ and FliR form the proton-conducting channel, which uses the PMF as the driving force for the secretion of flagellar substrates. ATP = adenosine 5′-triphosphate; ADP = adenosine 5′-diphosphate; P_i = inorganic phosphate; IM = inner membrane.

(FliH, FliI, FliJ) (Minamino and Macnab (56)). FliH is a regulator of the flagellar-specific ATPase FliI and FliJ is a general chaperone. FlhA and FlhB interact with their large cytoplasmic domains with FliH, FliI and FliJ (Minamino and MacNab (57)) and FlhB regulates the export specificity of the flagellar secretion apparatus. FlhA probably interacts with FliO, FliP and FliQ (McMurry *et al.* (53)), but the function of FliO, FliP, FliQ and FliR remains elusive.

In this work we demonstrated that flagellar type III secretion is dependent on the proton motive force. Based on our results, we propose that FliOPQR form the proton-conducting channel which uses the PMF as the driving force for the export of flagellar secretion substrates after unfolding by the ATPase FliI (Figure 8.7).

REFERENCES

[1] **Adler, J. and Templeton, B.** (1967); The effect of environmental conditions on the motility of *Escherichia coli*.; *J Gen Microbiol*; **46** (2): 175–184.

[2] **Aizawa, S. I.** (1996); Flagellar assembly in *Salmonella typhimurium*.; *Mol. Microbiol.*; **19** (1): 1–5.

[3] **Aldridge, P. and Hughes, K.** (2002); Regulation of flagellar assembly.; *Curr. Opin. Microbiol.*; **5** (2): 160–165.

[4] **Aldridge, P., Karlinsey, J. E., Becker, E., Chevance, F. F. V. and Hughes, K. T.** (2006); Flk prevents premature secretion of the anti-sigma factor FlgM into the periplasm.; *Mol. Microbiol.*; **60** (3): 630–643.

[5] **Aldridge, P. D., Karlinsey, J. E., Aldridge, C., Birchall, C., Thompson, D., Yagasaki, J. and Hughes, K. T.** (2006); The flagellar-specific transcription factor, σ^{28}, is the Type III secretion chaperone for the flagellar-specific anti-σ^{28} factor FlgM.; *Genes Dev.*; **20** (16): 2315–2326.

[6] **Amann, E., Ochs, B. and Abel, K. J.** (1988); Tightly regulated *tac* promoter vectors useful for the expression of unfused and fused proteins in *Escherichia coli*.; *Gene*; **69** (2): 301–315.

[7] **Beitz, E.** (2000); TEXshade: shading and labeling of multiple sequence alignments using LATEX2e.; *Bioinformatics*; **16** (1367-4803): 135–139.

[8] **Beitz, E.** (2006); Subfamily logos: visualization of sequence deviations at alignment positions with high information content.; *BMC Bioinformatics*; **7** (1471-2105): 313.

[9] **Benson, N. R. and Goldman, B. S.** (1992); Rapid mapping in *Salmonella typhimurium* with Mu*d*-P22 prophages.; *J Bacteriol*; **174** (5): 1673–1681.

[10] **Berg, H.** (2003); The rotary motor of bacterial flagella.; *Annu. Rev. Biochem.*; **72**: 19–54.

[11] **Berg, H. C. and Anderson, R. A.** (1973); Bacteria swim by rotating their flagellar filaments.; *Nature*; **245** (5425): 380–382.

[12] **Bochner, B. R., Huang, H. C., Schieven, G. L. and Ames, B. N.** (1980); Positive selection for loss of tetracycline resistance.; *J. Bacteriol.*; **143** (2): 926–933.

[13] **Bonifield, H. and Hughes, K.** (2003); Flagellar phase variation in *Salmonella enterica* is mediated by a posttranscriptional control mechanism.; *J. Bacteriol.*; **185** (12): 3567–3574.

[14] **Chan, R. K., Botstein, D., Watanabe, T. and Ogata, Y.** (1972); Specialized transduction of tetracycline resistance by phage P22 in *Salmonella typhimurium*. II. Properties of a high-frequency-transducing lysate.; *Virology*; **50** (3): 883–898.

[15] **Chenna, R., Sugawara, H., Koike, T., Lopez, R., Gibson, T. J., Higgins, D. G. and Thompson, J. D.** (2003); Multiple sequence alignment with the Clustal series of programs.; *Nucleic Acids Res*; **31** (13): 3497–3500.

[16] **Chilcott, G. and Hughes, K.** (2000); Coupling of flagellar gene expression to flagellar assembly in *Salmonella enterica* serovar Typhimurium and *Escherichia coli*.; *Microbiol. Mol. Biol. Rev.*; **64** (4): 694–708.

[17] **Chung, C. T., Niemela, S. L. and Miller, R. H.** (1989); One-step preparation of competent *Escherichia coli*: transformation and storage of bacterial cells in the same solution.; *Proc Natl Acad Sci U S A*; **86** (7): 2172–2175.

[18] **Datsenko, K. A. and Wanner, B. L.** (2000); One-step inactivation of chromosomal genes in *Escherichia coli* K-12 using PCR products.; *Proc. Natl. Acad. Sci.*; **97** (12): 6640–6645.

[19] **Davis, R. W., Botstein, D. and Roth, J. R.**; Advanced bacterial genetics (Cold Spring Harbor Laboratory, Cold Spring Harbor, New York, 1980).

[20] **DePamphilis, M. L. and Adler, J.** (1971); Fine structure and isolation of the hook-basal body complex of flagella from *Escherichia coli* and *Bacillus subtilis*.; *J. Bacteriol.*; **105** (1): 384–395.

[21] **DePamphilis, M. L. and Adler, J.** (1971); Purification of intact flagella from *Escherichia coli* and *Bacillus subtilis*.; *J. Bacteriol.*; **105** (1): 376–383.

[22] **Fan, F. and Macnab, R. M.** (1996); Enzymatic characterization of FliI. An ATPase involved in flagellar assembly in *Salmonella typhimurium*.; *J. Biol. Chem.*; **271** (50): 31,981–31,988.

[23] **Fan, F., Ohnishi, K., Francis, N. R. and Macnab, R. M.** (1997); The FliP and FliR proteins of *Salmonella typhimurium*, putative components of the type III flagellar export apparatus, are located in the flagellar basal body.; *Mol. Microbiol.*; **26** (5): 1035–1046.

[24] **Feilmeier, B. J., Iseminger, G., Schroeder, D., Webber, H. and Phillips, G. J.** (2000); Green fluorescent protein functions as a reporter for protein localization in *Escherichia coli*.; *J. Bacteriol.*; **182** (14): 4068–4076.

[25] **Ferris, H. U. and Minamino, T.** (2006); Flipping the switch: bringing order to flagellar assembly.; *Trends Microbiol.*; **14** (12): 519–526.

[26] **Frohlich, K. U.** (1994); Sequence Similarity Presenter: a tool for the graphic display of similarities of long sequences for use in presentations.; *Comput. Appl. Biosci.*; **10** (2): 179–183.

[27] **Galperin, M. Y., Dibrov, P. A. and Glagolev, A. N.** (1982); $\Delta\mu$H+ is required for flagellar growth in *Escherichia coli*.; *FEBS Lett.*; **143** (2): 319–322.

[28] **Gasteiger, E., Gattiker, A., Hoogland, C., Ivanyi, I., Appel, R. D. and Bairoch, A.** (2003); ExPASy: The proteomics server for in-depth protein knowledge and analysis.; *Nucleic Acids Res*; **31** (13): 3784–3788.

[29] **Gillen, K. L. and Hughes, K. T.** (1993); Transcription from two promoters and autoregulation contribute to the control of expression of the *Salmonella typhimurium* flagellar regulatory gene *flgM*.; *J. Bacteriol.*; **175** (21): 7006–7015.

[30] **Hirano, T., Yamaguchi, S., Oosawa, K. and Aizawa, S.** (1994); Roles of FliK and FlhB in determination of flagellar hook length in *Salmonella typhimurium*.; *J. Bacteriol.*; **176** (17): 5439–5449.

[31] **Homma, M., DeRosier, D. J. and Macnab, R. M.** (1990); Flagellar hook and hook-associated proteins of *Salmonella typhimurium* and their relationship to other axial components of the flagellum.; *J. Mol. Biol.*; **213** (4): 819–832.

[32] **Homma, M., Komeda, Y., Iino, T. and Macnab, R. M.** (1987); The *flaFIX* gene product of *Salmonella typhimurium* is a flagellar basal body component with a signal peptide for export.; *J. Bacteriol.*; **169** (4): 1493–1498.

[33] **Hueck, C.** (1998); Type III protein secretion systems in bacterial pathogens of animals and plants.; *Microbiol. Mol. Biol. Rev.*; **62** (2): 379–433.

[34] **Hughes, K. T., Gillen, K. L., Semon, M. J. and Karlinsey, J. E.** (1993); Sensing structural intermediates in bacterial flagellar assembly by export of a negative regulator.; *Science*; **262** (5137): 1277–1280.

[35] **Inoue, H., Nojima, H. and Okayama, H.** (1990); High efficiency transformation of *Escherichia coli* with plasmids.; *Gene*; **96** (1): 23–28.

[36] **Karlinsey, J. E., Tsui, H. C., Winkler, M. E. and Hughes, K. T.** (1998); Flk couples *flgM* translation to flagellar ring assembly in *Salmonella typhimurium*.; *J. Bacteriol.*; **180** (20): 5384–5397.

[37] **Kojima, S. and Blair, D. F.** (2004); The bacterial flagellar motor: structure and function of a complex molecular machine.; *Int. Rev. Cytol.*; **233**: 93–134.

[38] **Laemmli, U. K. and Favre, M.** (1973); Maturation of the head of bacteriophage T4. I. DNA packaging events.; *J Mol. Biol.*; **80** (4): 575–599.

[39] **Larsen, S. H., Reader, R. W., Kort, E. N., Tso, W. W. and Adler, J.** (1974); Change in direction of flagellar rotation is the basis of the chemotactic response in *Escherichia coli*.; *Nature*; **249** (452): 74–77.

[40] **Letellier, L., Howard, S. P. and Buckley, J. T.** (1997); Studies on the energetics of proaerolysin secretion across the outer membrane of *Aeromonas* species. Evidence for a requirement for both the protonmotive force and ATP.; *J. Biol. Chem.*; **272** (17): 11,109–11,113.

[41] **Lundin, A. and Thore, A.** (1975); Comparison of methods for extraction of bacterial adenine nucleotides determined by firefly assay.; *Appl. Microbiol.*; **30** (5): 713–721.

[42] **Lupas, A. N. and Martin, J.** (2002); AAA proteins.; *Curr. Opin. Struct. Biol.*; **12** (6): 746–753.

[43] **Macnab, R.** (2003); How bacteria assemble flagella.; *Annu. Rev. Microbiol.*; **57**: 77–100.

[44] **Macnab, R. M.**; Flagella and motility. In *Escherichia coli* and *Salmonella*: Cellular and Molecular biology.; vol. 1 (American Society for Microbiology, Washington, D.C., 1996); 2 ed.

[45] **Macnab, R. M.** (2004); Type III flagellar protein export and flagellar assembly.; *Biochim. Biophys. Acta.*; **1694** (1-3): 207–217.

[46] **Macnab, R. M. and Koshland, D. E. J.** (1972); The gradient-sensing mechanism in bacterial chemotaxis.; *Proc. Natl. Acad. Sci.*; **69** (9): 2509–2512.

[47] **Maloy, S. R. and Nunn, W. D.** (1981); Selection for loss of tetracycline resistance by *Escherichia coli*.; *J. Bacteriol.*; **145** (2): 1110–1111.

[48] **Maloy, S. R. and Roth, J. R.** (1983); Regulation of proline utilization in *Salmonella typhimurium*: characterization of *put*::Mu*d(Ap, lac)* operon fusions.; *J. Bacteriol.*; **154** (2): 561–568.

[49] **Manoil, C. and Bailey, J.** (1997); A simple screen for permissive sites in proteins: analysis of *Escherichia coli lac* permease.; *J Mol. Biol.*; **267** (2): 250–263.

[50] **Manson, M., Tedesco, P., Berg, H., Harold, F. and Van der Drift, C.** (1977); A protonmotive force drives bacterial flagella.; *Proc. Natl. Acad. Sci.*; **74** (7): 3060–3064.

[51] **Matsuura, A., Shioi, J. I. and Imae, Y.** (1977); Motility in *Bacillus subtilis* driven by an artificial protonmotive force.; *FEBS Lett.*; **82**: 187–190.

[52] **McClelland, M., Sanderson, K. E., Spieth, J., Clifton, S. W., Latreille, P., Courtney, L., Porwollik, S., Ali, J., Dante, M., Du, F., Hou, S., Layman, D., Leonard, S., Nguyen, C., Scott, K., Holmes, A., Grewal, N., Mulvaney, E., Ryan, E., Sun, H., Florea, L., Miller, W., Stoneking, T., Nhan, M., Waterston, R. and Wilson, R. K.** (2001); Complete genome sequence of *Salmonella enterica* serovar Typhimurium LT2.; *Nature*; **413** (6858): 852–856.

[53] **McMurry, J. L., Van Arnam, J. S., Kihara, M. and Macnab, R. M.** (2004); Analysis of the cytoplasmic domains of *Salmonella* FlhA and interactions with components of the flagellar export machinery.; *J. Bacteriol.*; **186** (22): 7586–7592.

[54] **Meynell, E. W.** (1961); A phage, $\phi\ \chi$, which attacks motile bacteria.; *J. Gen. Microbiol.*; **25**: 253–290.

[55] **Minamino, T., Imae, Y., Oosawa, F., Kobayashi, Y. and Oosawa, K.** (2003); Effect of intracellular pH on rotational speed of bacterial flagellar motors.; *J. Bacteriol.*; **185** (4): 1190–1194.

[56] **Minamino, T. and Macnab, R. M.** (1999); Components of the *Salmonella* flagellar export apparatus and classification of export substrates.; *J. Bacteriol.*; **181** (5): 1388–1394.

[57] **Minamino, T. and MacNab, R. M.** (2000); Interactions among components of the *Salmonella* flagellar export apparatus and its substrates.; *Mol. Microbiol.*; **35** (5): 1052–1064.

[58] **Minamino, T., Yamaguchi, S. and Macnab, R. M.** (2000); Interaction between FliE and FlgB, a proximal rod component of the flagellar basal body of *Salmonella*.; *J. Bacteriol.*; **182** (11): 3029–3036.

[59] **Nagai, T., Ibata, K., Park, E. S., Kubota, M., Mikoshiba, K. and Miyawaki, A.** (2002); A variant of yellow fluorescent protein with fast and efficient maturation for cell-biological applications.; *Nat. Biotechnol.*; **20** (1): 87–90.

[60] **Namba, K. and Vonderviszt, F.** (1997); Molecular architecture of bacterial flagellum.; *Q. Rev. Biophys.*; **30** (1): 1–65.

[61] **Ohnishi, K., Fan, F., Schoenhals, G. J., Kihara, M. and Macnab, R. M.** (1997); The FliO, FliP, FliQ, and FliR proteins of *Salmonella typhimurium*: putative components for flagellar assembly.; *J. Bacteriol.*; **179** (19): 6092–6099.

[62] **Patton, T. G., Yang, S.-J. and Bayles, K. W.** (2006); The role of proton motive force in expression of the *Staphylococcus aureus cid* and *lrg* operons.; *Mol. Microbiol.*; **59** (5): 1395–1404.

[63] **Rasband, W.**; ImageJ - http://rsb.info.nih.gov/ij/ (U. S. National Institutes of Health, Bethesda, Maryland, USA, 1997-2006).

[64] **Sambrook, J., Fritsch, E. and Maniatis, T.**; Molecular cloning: a laboratory manual, 2nd ed. (Cold Spring Harbor Laboratory Press, Cold Spring Harbor, New York, 1989).

[65] **Samuel, A. D., Pitta, T. P., Ryu, W. S., Danese, P. N., Leung, E. C. and Berg, H. C.** (1999); Flagellar determinants of bacterial sensitivity to χ-phage.; *Proc. Natl. Acad. Sci.*; **96** (17): 9863–9866.

[66] **Sanderson, K. E. and Roth, J. R.** (1983); Linkage map of *Salmonella typhimurium*, Edition VI.; *Microbiol. Rev.*; **47** (3): 410–453.

[67] **Schade, S. and Adler, J.** (1967); Purification and chemistry of bacteriophage χ.; *J. Virol.*; **1** (3): 591–598.

[68] **Schade, S. Z., Adler, J. and Ris, H.** (1967); How bacteriophage χ attacks motile bacteria.; *J. Virol.*; **1** (3): 599–609.

[69] **Schoenhals, G. J., Kihara, M. and Macnab, R. M.** (1998); Translation of the flagellar gene *fliO* of *Salmonella typhimurium* from putative tandem starts.; *J. Bacteriol.*; **180** (11): 2936–2942.

[70] **Sertic, V. and Boulgakov, N.** (1935); Classification et identification des typhiphages; *Compt. Rend. Soc. Biol.*; **119**: 1270–1272.

[71] **Sertic, V. and Boulgakov, N.** (1936); Bactériophages spécifiques pour des variétés bactériennes flagellées; *Compt. Rend. Soc. Biol.*; **123**: 887–888.

[72] **Silverman, M. and Simon, M.** (1973); Genetic analysis of flagellar mutants in *Escherichia coli*.; *J. Bacteriol.*; **113** (1): 105–113.

[73] **Silverman, M. and Simon, M.** (1974); Flagellar rotation and the mechanism of bacterial motility.; *Nature*; **249** (452): 73–74.

[74] **Sourjik, V. and Berg, H. C.** (2000); Localization of components of the chemotaxis machinery of *Escherichia coli* using fluorescent protein fusions.; *Mol Microbiol*; **37** (4): 740–751.

[75] **Stone, R.** (2002); Stalin's forgotten cure; *Science*; **298**: 728–731.

[76] **Summers, W.** (2001); Bacteriophage therapy.; *Annu. Rev. Microbiol.*; **55**: 437–451.

[77] **Thomas, J. D., Daniel, R. A., Errington, J. and Robinson, C.** (2001); Export of active green fluorescent protein to the periplasm by the twin-arginine translocase (Tat) pathway in *Escherichia coli*.; *Mol. Microbiol.*; **39** (1): 47–53.

[78] **Tomkiewicz, D., Nouwen, N., van Leeuwen, R., Tans, S. and Driessen, A. J. M.** (2006); SecA supports a constant rate of preprotein translocation.; *J Biol Chem*; **281** (23): 15,709–15,713.

[79] **Tusnady, G. E. and Simon, I.** (1998); Principles governing amino acid composition of integral membrane proteins: application to topology prediction.; *J Mol Biol*; **283** (2): 489–506.

[80] **Tusnady, G. E. and Simon, I.** (2001); The HMMTOP transmembrane topology prediction server.; *Bioinformatics*; **17** (9): 849–850.

[81] **Van Arnam, J. S., McMurry, J. L., Kihara, M. and Macnab, R. M.** (2004); Analysis of an engineered Salmonella flagellar fusion protein, FliR-FlhB.; *J. Bacteriol.*; **186** (8): 2495–2498.

[82] **van der Wolk, J. P., de Wit, J. G. and Driessen, A. J.** (1997); The catalytic cycle of the *Escherichia coli* SecA ATPase comprises two distinct preprotein translocation events.; *EMBO J.*; **16** (24): 7297–7304.

[83] **Vieira, J. and Messing, J.** (1982); The pUC plasmids, an M13mp7-derived system for insertion mutagenesis and sequencing with synthetic universal primers.; *Gene*; **19** (3): 259–268.

[84] **Vogel, H. J. and Bonner, D. M.** (1956); Acetylornithinase of *Escherichia coli*: partial purification and some properties.; *J. Biol. Chem.*; **218** (1): 97–106.

[85] **Vogler, A. P., Homma, M., Irikura, V. M. and Macnab, R. M.** (1991); *Salmonella typhimurium* mutants defective in flagellar filament regrowth and sequence similarity of FliI to F_0F_1, vacuolar, and archaebacterial ATPase subunits.; *J. Bacteriol.*; **173** (11): 3564–3572.

[86] **Wilharm, G., Lehmann, V., Krauss, K., Lehnert, B., Richter, S., Ruckdeschel, K., Heesemann, J. and Trulzsch, K.** (2004); *Yersinia enterocolitica* type III secretion depends on the proton motive force but not on the flagellar motor components MotA and MotB.; *Infect. Immun.*; **72** (7): 4004–4009.

[87] **Yonekura, K., Maki-Yonekura, S. and Namba, K.** (2003); Complete atomic model of the bacterial flagellar filament by electron cryomicroscopy.; *Nature*; **424** (6949): 643–650.

ERKLÄRUNG

Ich versichere hiermit, dass ich die vorliegende Arbeit mit dem Thema

„Genetic Structure and Function Analysis of the Conserved Integral Membrane Components (FliOPQR) of the Flagellar Type III Secretion Apparatus of *Salmonella enterica*“

selbständig verfasst und keine anderen Hilfsmittel als die angegebenen benutzt habe.

Die Stellen, die anderen Werken dem Wortlaut oder dem Sinne nach entnommen sind, habe ich in jedem einzelnen Falle durch Angabe der Quelle, auch der benutzten Sekundärliteratur, als Entlehnung kenntlich gemacht.

Ort, Datum

Unterschrift